Project X –Reference Design Report

V1.0
November 1, 2010

The Project X Collaboration:

Argonne National Laboratory
Brookhaven National Laboratory
Cornell University
Fermi National Accelerator Laboratory
Lawrence Berkeley National Laboratory
Oak Ridge National Laboratory/SNS
Michigan State University
Thomas Jefferson National Accelerator Facility
SLAC National Accelerator Laboratory
ILC/America's Regional Team

Bhabha Atomic Research Laboratory, Mumbai
Inter-University Accelerator Center, Delhi
Raja Ramanna Center for Advanced Technology, Indore
Variable Energy Cyclotron Center, Kolkota

RDR Version 1.0 Approval

_____

Stephen D. Holmes, Project Manager

Table of Contents

I Introduction (Steve) 3
- I.1 **Assumptions 4**
- I.2 **Facility Layout 5**

II Technical Goals (Steve) 6
- II.1 **Technical Goals 6**
- II.2 **Operational Scenario 6**

III Accelerator Facility Design 8
- III.1 **CW Linac (Steve) 8**
- III.1 **3-GeV Beam handling (Steve/DEJ) 19**
- III.2 **3-8 GeV Pulsed Linac (Sergei) 34**
- III.3 **8 GeV Transport Line (Steve/Dave) 37**
- III.4 **Recycler/Main Injector (Paul) 38**

IV Design Concepts of Major Subsystems 39
- IV.1 **CW Linac (Steve) 39**
- IV.2 **Collimators and Beam Dump (Steve/DEJ) 58**
- IV.3 **3-8 GeV Pulsed Linac (Sergei) 61**
- IV.4 **MI/RR (Paul) 62**
- IV.5 **Cryogenics (Paul) 64**
- IV.6 **Instrumentation (Paul) 67**
- IV.7 **Controls (Paul) 68**
- IV.8 **LLRF (Paul) 70**
- IV.9 **Safety and radiation shielding (Paul) 70**
- IV.10 **Conventional Facilities (Paul) 74**

V Appendix A: Longitudinal Beam Motion in a Flat-Bottom Potential Well 77

I Introduction

Project X is a high intensity proton facility being developed to support a world-leading program in neutrino and flavor physics over the next two decades at Fermilab. Project X is an integral part of the Fermilab Roadmap as described in the Fermilab Steering Group Report of August 2007 (http://www.fnal.gov/pub/directorate/steering/index.shtml) and of the Intensity Frontier science program described in the P5 report of May 2008 (http://www.er.doe.gov/hep/files/pdfs/P5_Report%2006022008.pdf).

The primary elements of that research program to be supported by Project X include:

- *A neutrino beam for long baseline neutrino oscillation experiments.*
  Based on proton beams of at least 2 megawatts delivered onto a neutrino production target at energies between 60 and 120 GeV.
- *Kaon and muon based precision experiments running simultaneously with the neutrino program.*
  Based on megawatt-class proton beams of ~3 GeV energy, with flexible capability for providing distinct beam formats to multiple users simultaneously.
- *A path toward a muon source for a possible future neutrino factory and, potentially, a muon collider at the Energy Frontier.*

These elements are expected to form the basis of the Mission Need statement as is required for Critical Decision 0 (CD-0*)*, and represent the fundamental design criteria for Project X.

The initial Project X goals and associated design concept[1] were primarily driven by the Project X synergy with the ILC and the 2-MW operation of the Main Injector for the long baseline neutrino program. This concept was based on an 8 GeV superconducting pulsed linac, paired with the existing Recycler and Main Injector rings. The details of operation with a slow extracted beam at 8 GeV were not considered in this first concept. While some enhancements were introduced in the Project X Initial Configuration Document-1 (ICD-1)[2] it still followed the same path as the initial Project X concept but with an increased beam current. The accelerator complex defined in ICD-1 could drive the long-baseline neutrino program, and provided enhanced capabilities in the muon-to-electron conversion experiment (mu2e); however, it did not provide a flexible platform to pursue a broader research program in rare muon and kaon processes based on high duty-factor beams. ICD-2[3] addressed the lack of flexibility in ICD-1 through the introduction of a 2 GeV CW (continuous wave) linac and a 2-8 GeV rapid cycling synchrotron, paired with the existing Recycler and Main Injector. The intent of ICD-2 was to strengthen the rare physics process program while preserving the 2 MW neutrino beam program from the Main Injector.

This document presents the Reference Design for Project X. The Reference Design is based on an evolution of the designs that were developed through ICD-1 and ICD-2. The Reference

[1] Project X-doc-79
[2] ICD-1, Project X-doc-83
[3] ICD-2, Project X-doc-230

Design remains based on a superconducting CW linac; however, the energy has been raised to 3 GeV, based on an understanding of the requirements for kaon production, and the selection of rf frequencies has been changed to provide more efficient acceleration. The 3 GeV linac operates at an average current of 1 mA, providing up to 3 MW of beam power to the rare processes program. Options considered for accelerating the beam from 3 GeV to the 8 GeV injection energy of the Recycler include a rapid cycling synchrotron (RCS) or a 3-8 GeV pulsed linac. The pulsed linac is the preferred configuration because of the flexibility it provides for future programs of interest to the U.S. High Energy Physics community, and has been selected for the Reference Design. The configuration of the Main Injector and Recycler remain as developed in the ICD-1 and ICD-2.

The Reference Design matches the Initial Configurations in its capability to support the long baseline neutrino program, but greatly exceeds the Initial Configurations in its ability to support a wide ranging rare processes program. It is anticipated that the final configuration and operating parameters of the complex will be refined through the R&D program in advance of CD-2.

I.1 Assumptions

The following assumptions are made in determining the Project X facility configuration that meets the mission elements defined above:

- Project X will be constructed on the Fermilab site and will utilize the upgraded Main Injector and Recycler for the generation of a long baseline neutrino beam.
- The long baseline neutrino program will require an initial capability of greater than or equal to 2 MW proton beam power on a neutrino production target at any energy within the range 60-120 GeV, and will eventually require additional beam power upgrades.
- The rare process program requires MW class proton beams, high duty factors, and flexible bunch patterns. This is best accomplished with a CW linac based on Superconducting RF (SRF) technology.
- The production yield curve of kaons vs. incident proton energy sets the minimum CW linac energy at ~ 3 GeV
- The neutrino and 3 GeV programs must operate simultaneously.
- The Recycler operates at a fixed energy of 8 GeV; the upgraded Main Injector will be capable of injection energies as low as 6 GeV.
- The NOvA Project will have upgraded the Main Injector to support a 1.2 second cycle time to 120 GeV and will have converted the Recycler to serve as a proton accumulator ring. Additional upgrades to the MI/RR will be needed for 2 MW operation.
- A neutrino beam-line directed towards LBNE will be operating with beam power on target of 700 kW, with shielding and infrastructure designed to accommodate up to 3 MW.

I.2 Facility Layout

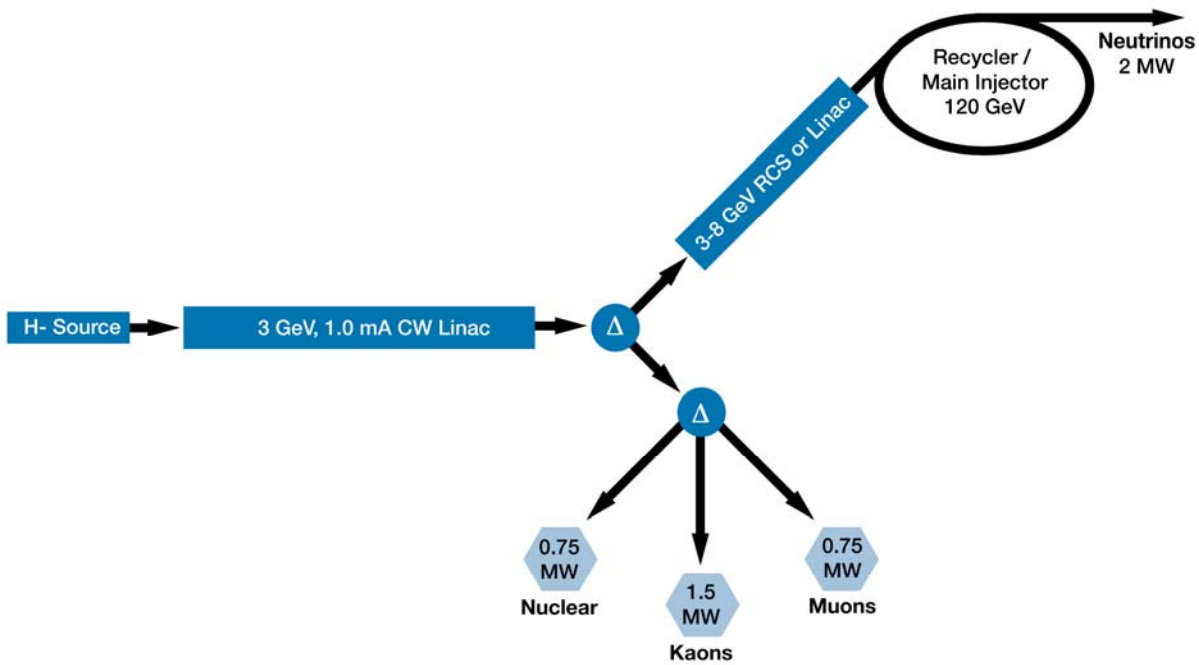

Figure I-1: A schematic layout of the Project X Reference Design accelerator complex.

Figure I-1 presents a schematic layout of Project X aligned with the mission needs and assumptions outlined above. The primary elements are:

- An H- source consisting of a 2.5 MeV RFQ, and Medium Energy Beam Transport (MEBT) augmented with a wideband chopper capable of accepting or rejecting bunches in arbitrary patterns at up to 325 MHz;
- A 3 GeV superconducting linac operating in CW mode, and capable of accelerating an average (averaged over >1 μsec) beam current of 1mA, and a peak beam current (averaged over <1 μsec) of 10 mA;
- A 3 to 8 GeV pulsed superconducting linac capable of accelerating an average current of 33 μA with a 1-5% duty cycle;
- A pulsed dipole that can split the 3 GeV beam between the neutrino program and the rare processes program;
- An rf beam splitter that can deliver the 3 GeV beam to multiple (at least three) experimental areas.

II Technical Goals

The overall goal of the Reference Design is to define a scope that will provide a basis for supporting the mission needs identified in Section I and for the cost estimate necessary as part of the Critical Decision 0 (CD-0) process – the first step in the critical decision tree mandated by DOE order 413.3. CD-0 requires a cost range and discussion of alternatives. The cost range will be established via variations of a number of assumptions inherent in the Reference Design, including:

- Substitution of a RCS for the pulsed linac for 3-8 GeV acceleration;
- Direct injection from the pulsed linac into the Main Injector at 6 GeV, reducing the length of the linac and eliminating the Recycler from the scope of Project X.

II.1 Technical Goals

The performance goals for Project X are defined through a Functional Requirements Specification (FRS)[4]. It is anticipated that the FRS will be approved by the Directors of DOE/OHEP and Fermilab as part of the CD-0 process. High level performance goals associated with the Project X Reference Design are listed in Table II-1.

The proposed experimental program determines the CW linac energy. The linac energy of 3 GeV has been determined to be sufficient to meet the requirements of both the muon conversion and a kaon programs.

Description	Req.	Unit
Linac Beam Power @ 3 GeV	3	MW
Main Injector Beam Power @60-120 GeV	>2	MW
3 GeV Average Beam Current	1	mA
3 GeV Bunch Pattern	Programmable	
Beam Power at 8 GeV	300	kW
3 GeV Availability	90	%
6-120 GeV Availability	85	%

Table II-1: Performance Goals for the Project X Accelerator Facility

II.2 Operational Scenario

In the operational scenario, the facility provides beam to an RF separator. The CW beam is delivered to three users simultaneously by way of selectively filling appropriate RF buckets at the front end of the linac and then RF separating them to three different target halls[5]. The design of target halls and the experimental apparatus is outside of the project scope. For the initial scenario we have used a muon conversion experiment and a rare kaon decay experiment as two

[4] Project X Functional Requirements Specification, Project X-doc-658

[5] In this document we consider 3 end users. However the number of users can be increased if required by installation of additional RF separators, serially to the existing one/ones.

of the three CW beam users. The third user is not yet determined at the time of this report writing, but possibilities include experiments related to nuclear physics and/or nuclear energy.

For the rare-decay program, the facility provides 1 mA (average) of H^- ions at 3 GeV with variable and adjustable bunch structures. For the Reference Design we have used beam requirements developed for the "Muon conversion" and "Kaon" experimental programs. Table II-2 presents these requirements.

	Train Frequency	Pulse Width (nanoseconds)	Inter-Pulse Extinction
Kaon experiments	20-30 MHz	0.1-0.2	10^{-3}
Muon conversion experiment	0.5-1.0 MHz	50	10^{-9}

Table II-2: Bunch train requirements for the kaon and muon rare decay programs

Several front end beam subsystems are employed to provide beam users with a variable bunch pattern concurrently. These subsystems are described in detail in the following sections; here we briefly touch upon the main considerations. For the optimal linac operation the power of the RF system should be matched to the required beam power. This minimizes the operational cost and, for constant beam intensity, it results in no energy variations related to the beam intensity. If the average beam intensity stays constant but the peak intensity varies with time so that the beam power (temporarily) exceeds the power of the RF system, the beam energy begins to droop. Fortunately, SC cavities have a comparatively large stored energy that strongly suppresses the energy variations if the beam intensity variations are sufficiently fast. For the accelerating gradient of 17 MV/m, suggested for the 1.3 GHz section of the CW linac, the stored energy in a Tesla-type cavity is ~30 J/cavity. This means that for an average beam current of 1 mA, any intensity redistribution within ~3 μs results in energy gain variation of less than 0.1%. All presently suggested experiments require significantly faster beam intensity variations (or bunching patterns) leading to these variations being "invisible" for the accelerating structures. In our configuration we are proposing to use a variable intensity DC ion source, capable of delivering 0-10 mA of H^- ions, accompanied by a wideband chopper that can allow population of 325 MHz buckets in an arbitrary pattern. After bunching in a 325MHz RFQ the beam is chopped (at 2.5 MeV) so that each experiment receives a desired beam pattern. The only limitations are that (1) the beam current, when averaged over time spans in excess of ~2 μs, should not exceed 1 mA, (2) all bunches (which are not chopped out) should have the same intensity, and (3) the pattern period for each experiment would not exceed a few microseconds.

As an example, Figure II-1 presents a possible beam structure to support a muon conversion experiment, a rare kaon experiment, and a third unspecified program. Using an RF separator running at five/fourths of the bunch frequency (406.25 MHz), every other pulse is available to the muon experiment, so a burst of 17 162.5-MHz bunches (~100 nsec) of 11×10^7 ppb can be provided. The other RF buckets are chopped and equally split between two other experiments to match the 20-30 MHz desired bunch spacing. In this example the CW linac provides 900 kW of 3 GeV H^- ions for the muon conversion experiment and 1050 kW to the two additional locations

simultaneously (at 325/16=20.3 MHz). In this example the H^- ion source delivers about 5.7 mA DC. The average current is then reduced to 1 mA by the wideband chopper.

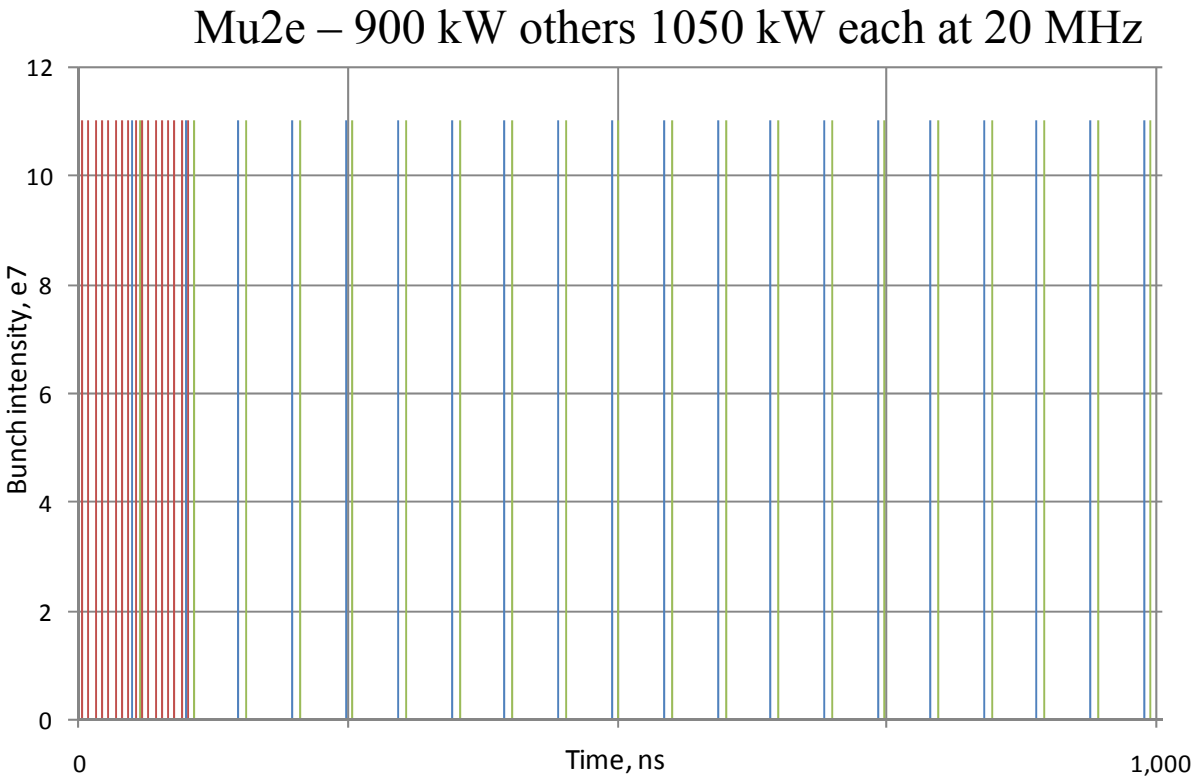

Figure II-1: A 1-μsec period in the CW linac, with red pulses for the muon conversion experiment, blue for rare kaon decay experiments, and green for other experiments. The integral bunch intensity is 11e7 with a 50 psec (FW) bunch length.

III Accelerator Facility Design

III.1 CW Linac

Figure III-1 shows the configuration of the CW linac. The CW linac accereates H- ions from an ion source to 3 GeV, at which point they are directed either towards the 3 GeV experimental areas or towards the 3-8 GeV pulsed linac. The average beam current is 1 mA, with transients of 10 mA accommodated for periods of less than 1 μsec. The entire CW linac as shown includes the following major elements:

(i) ion source,
(ii) RFQ,
(iii) medium energy beam transport (MEBT), including the chopper and bunching cavities

(iv) three accelerating sections based on 325 MHz Single-Spoke Resonators (SSR),
(v) two accelerating sections of 650 MHz elliptical cavities, and
(vi) one accelerating section of 1.3 GHz ILC-type cavities.

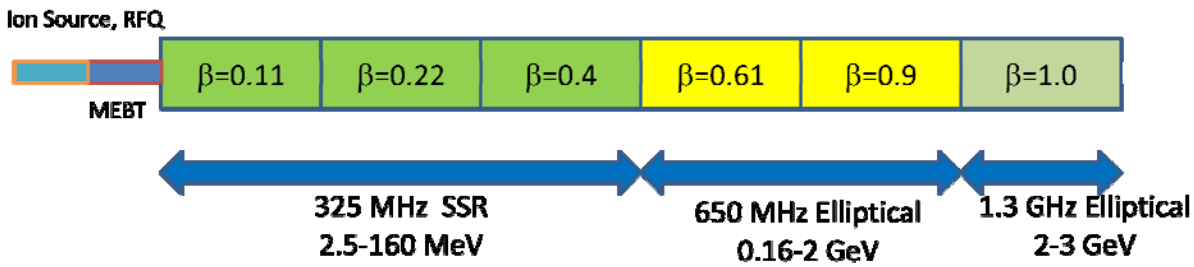

Figure III-1: 3 GeV CW linac

III.1.1 Ion Source, RFQ, and MEBT

The beam originates from a 1-10 mA DC H^- source. The beam is bunched and accelerated by a CW normal-conducting RFQ to 2.5 MeV and a chopper, following a pre-programmed timeline, formats the bunch pattern. Since the linac average beam current is 1 mA and the beam current at the ion source can be as high as 10 mA, up to 90% beam has to be removed by a chopper in the MEBT section. The power of removed beam is quite high, on order 25 kW, and thus it will require a dedicated beam dump. The beam energy of 2.5 MeV was chosen in part because it is below the neutron production threshold for most materials.

Figure III-2 shows the linac timeline schematically. There are two timeline periods: (1) the long time period associated with a 10-Hz injection rate to RCS and (2) the short time period (~ μs) associated with the rare-processes experiments (see Figure II-1). Six 2.2 msec pulses are provided at a rate of 10 Hz for acceleration in the pulsed linac and transfer to the Recycler/Main Injector in support of the long baseline neutrino program. The beam is directed into the pulsed linac by a pulsed dipole with a rise time of 0.5 msec. The linac average current during this pulse is 2 mA. For the duration of the ~95 msec between pulsed linac pulses the beam is directed toward the rare processes program with an average current of 1 mA.

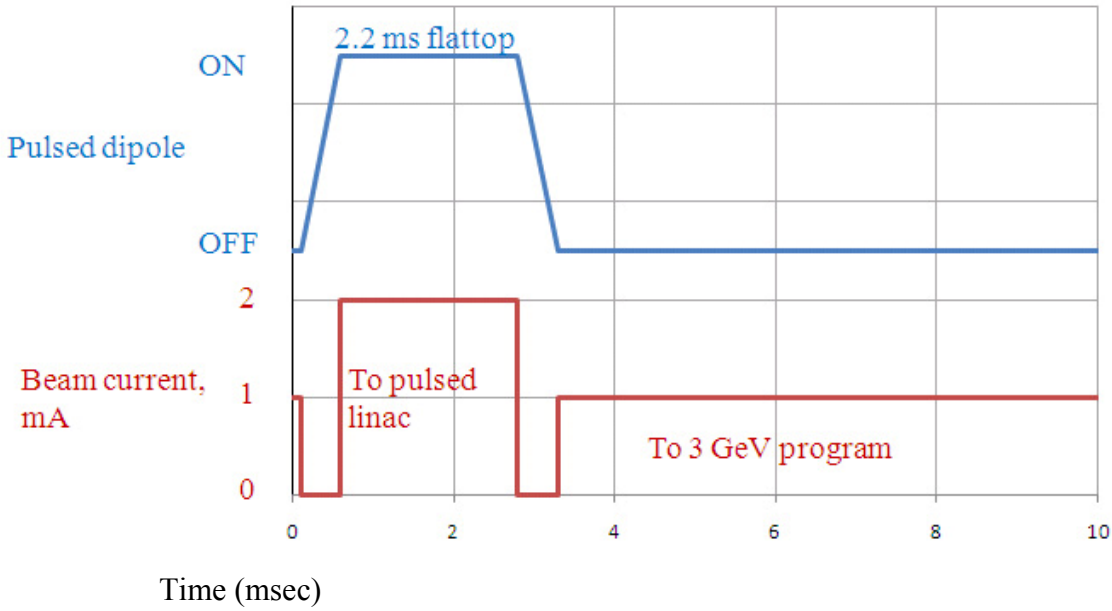

Figure III-2: A schematic timeline for linac beam current (first 10 ms of the 100 ms cycle). The pulsed magnet's rise and fall time is assumed to be 0.5 ms.

III.1.2 CW Linac – Accelerating Cavities

The selection of cavity frequencies and cell configuration is made to maximize acceleration efficiency for the different beam velocities present in the different parts of the linac, and to address other factors that will minimize beam loss. The primary efficiency factor is the transit time factor, which has a dependence on beam velocity (β) as shown in Figure III-3 as a function of the number of cells in a cavity. One can see that the range of betas over which beam can be efficiently accelerated increases as the number of cells goes down. On the other hand, providing too few cells decreases effective gradient and increases costs due to end effects.

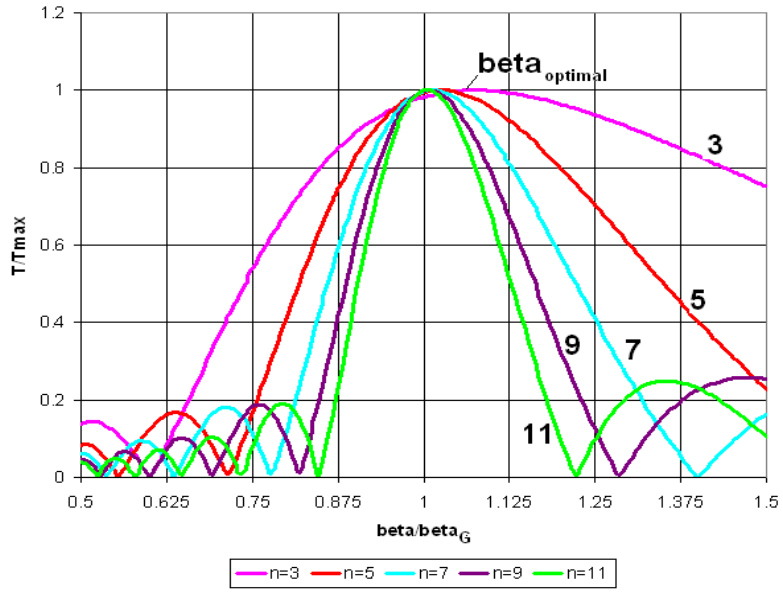

Figure III-3: **Transit time factor versus the ratio of the beta to the geometrical beta for different number of cells in a cavity n. Geometrical beta is a ratio of the cavity period to the half-wavelength (the cavity operates in CW π-mode).**

Based on these considerations we have selected three frequencies for the reference design, 325, 650, and 1300 MHz, with three types of spoke resonators in the 325 MHz section, two types of elliptical cavities in the 650 MHz section, and one type of elliptical cavity in the 1300 MHz section. At 650 MHz the cavities are 5-cell, and at 1300 MHz 9-cell. The primary benefits of this arrangement are as follows:

- It simplifies the beam dynamics: The Project X front end operates at 325 MHz, and the 2-fold frequency jumps at transition to the high energy stages for 650 MHz and 1300 MHz are relatively straightforward and should suffer little beam loss.
- The lower frequency sections provide sufficient aperture for maintaining uncontrolled beam loss at tolerable levels (0.1 - 0.2 W/m).
- Losses caused by intra-beam stripping will be minimized.
- The effects of acceleration cavities focusing will be benign.
- Higher Order Mode (HOM) impedances (transverse and longitudinal) are small in the lower energy portion of the linac, which may allow elimination of HOM dampers, which have been a source of problems in other proton accelerators.

However, there are trade-offs inherent in choosing the energy for transition between the 650 and 1300 MHz systems:

- Microphonics represent a more serious issue at lower frequencies.
- Cavities for 650 MHz are more expensive (more niobium) than at 1300 MHz, but the increase in price may be compensated by smaller number of the cavities and RF sources.

The operating gradient is chosen to provide a peak surface magnetic field that allows operation below high-field Q-slope; see Figure III-4 taken from [*Ciovati. "Review of high field Q*

slope", SRF2007]. For the frequency of 325 MHz the peak magnetic field should be not greater than ~60 mT, whereas at 650 MHz ~70 mT can be tolerated. On the other hand the peak surface electric field should be lower than 40 MV/m [see *Reschke, Analysis of the RF results of recent 9-cell cavities at DESY, TTC-Report 2009-01, Oct. 2009*] in order to avoid the risk of strong field emission. The 650 and 1300 MHz elliptical cavities are thus both designed to operate with peak surface magnetic fields of 70 mT.

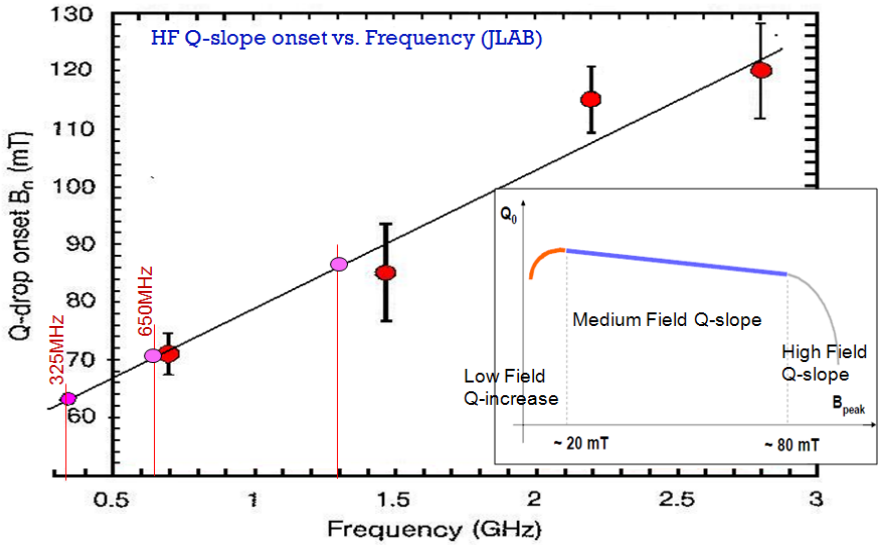

Figure III-4: High field Q-slope versus frequency.

The transition from the front-end operating at 325 MHz based on single-spoke cavities to the 650 MHz section based on elliptical cavities is chosen at the energy 160 MeV, because for lower energies elliptical cavities lose efficiency. For H^- acceleration above 2 GeV 1300 MHz, β=1 ILC-type cavities may be used, because the transit time factor for these energies is sufficiently high. It is inefficient to accelerate H^- from 160 MeV to 2 GeV using the same type of a cavity and two families of 650 MHz cavities should be used.

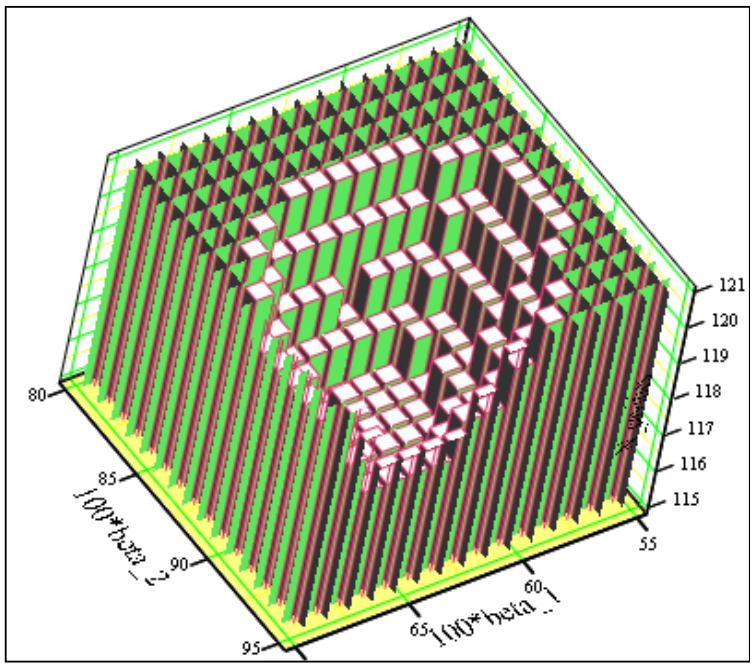

S

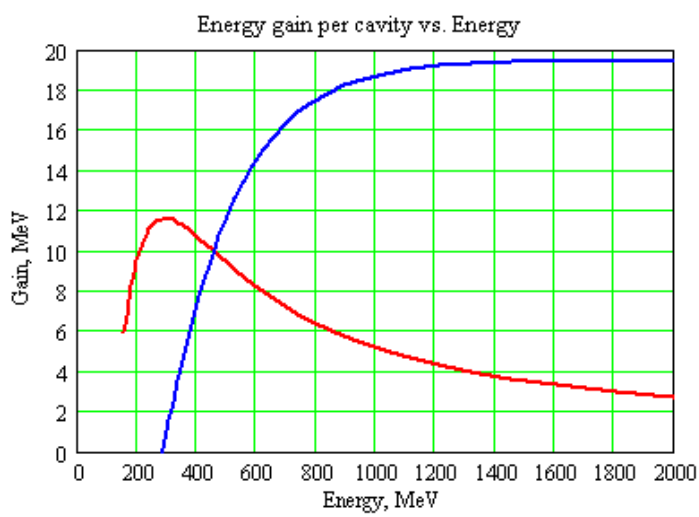

Figure III-5: Number of cavities versus betas in the two 650 MHz sections. first and second section (upper and middle figures). Gain per cavity versus the particle energy in both sections.

Figure III-5 demonstrates the optimization of the transition energy between the two families of 650 MHz cavities and their geometrical betas supposing the linear dependence of the field enhancement factors versus beta [*O. Brunner et.all, PRST- Acc.& Beams. 12, 070402, 2009*]. The upper figure shows the number of cavities required as a function of the betas of the two sections. The lower figure shows the energy gain per cavity vs. beam energy for β=0.64 cavities (red curve) and β=0.9 cavities (blue curve). The fully optimized geometrical betas for the two 650 MHz sections are 0.64 and 0.9 respectively (upper figure), and the optimal transition energy is 460 MeV (lower figure). The initial synchronous phase is -30°, and it increases with the as the

square root of the energy. More exact simulations taking into account realistic enhancement factors show optimal choice of betas of 0.61 and 0.9.

The resultant characteristics of the six cavities types identified for the Project X CW linac are summarized in Table III-1. The cavity Q_0's are based on an assumed operating temperature of 2K.

Section	β_G	Freq (MHz)	Type of cavities	Energy range (MeV)	Number of cavities	Accelerating Gradient (MV/m)	Q_0 (10^{10})
SSR0	0.114	325	Single spoke cavity	2.5-10	26	6	0.6
SSR1	0.215	325	Single spoke cavity	10-32	18	7	1.1
SSR2	0.42	325	Single spoke cavity	32-160	44	9	1.3
LE650	0.61	650	Elliptic cavity	160 - 500	42	16	1.7
HE650	0.9	650	Elliptic cavity	50 - 2000	96	19	1.7
ILC	1	1300	Elliptic cavity	2000-3000	72	17	1.5

Table III-1: Accelerating cavity requirements for the CW linac. β_G is cavity geometrical phase velocity

III.1.3 CW Linac – Cryomodules

Cavities and focusing elements are grouped within cryomodules. In the 325 MH section of the linac focusing is provided by solenoids. In the 650 MHz section a standard FD quadrupole doublet lattice is used, followed by a FODO lattice in the 1300 MHz section. All magnets are superconducting with built-in dipole correctors for beam steering. The arrangement by cryomodule type is shown in Table III-2.

Section	SSR-0	SSR-1	SSR-2	LE650	HE650	ILC1300
Focusing	SR	SR	SR^2	FDR^2 FDR^2	FDR^8	FR^8/DR^8

Table III-2: Disposition of accelerating cavities and focusing elements within a cryomodule: R – Resonator, S—solenoid, F and D – quadrupoles.

For beam diagnostics purposes each magnet package includes a beam position monitor (BPM). The linac also includes several warm sections between cryo-strings. These warm sections are used for additional diagnostics, such as bunch transverse and longitudinal profile monitors, beam loss monitors, etc. and collimation sections necessary to avoid uncontrolled beam loss and protect the SC cavities and quadrupoles. The disposition of warm insertions will be determined by requirements of safe and reliable operations, diagnostics, collimation, and cryogenic segmentation constraints.

Integrated estimates of RF power consumption and cryogenic losses for the CW linac are shown in Table III-3, and plotted by cavity in Figure III-6 andFigure III-7.

Section	Freq MHz	# of cavities	# of CMs	Total power, kW	Average power per CM	Total cryo losses, W	Average cryo losses per CM, W
SSR0	325	26	1	7.2	7.2	3.4	3.4
SSR1	325	18	2	21	10.5	16	8
SSR2	325	44	4	127	32	160	40
LE 650	650	42	7	372	53	858	123
HE 650	650	96	12	1441	120	2147	179
ILC	1300	72	9	1159	129	1557	173
Total		298	35	3100		4141	

Table III-3: Integrated RF power consumption and cryogenic losses.

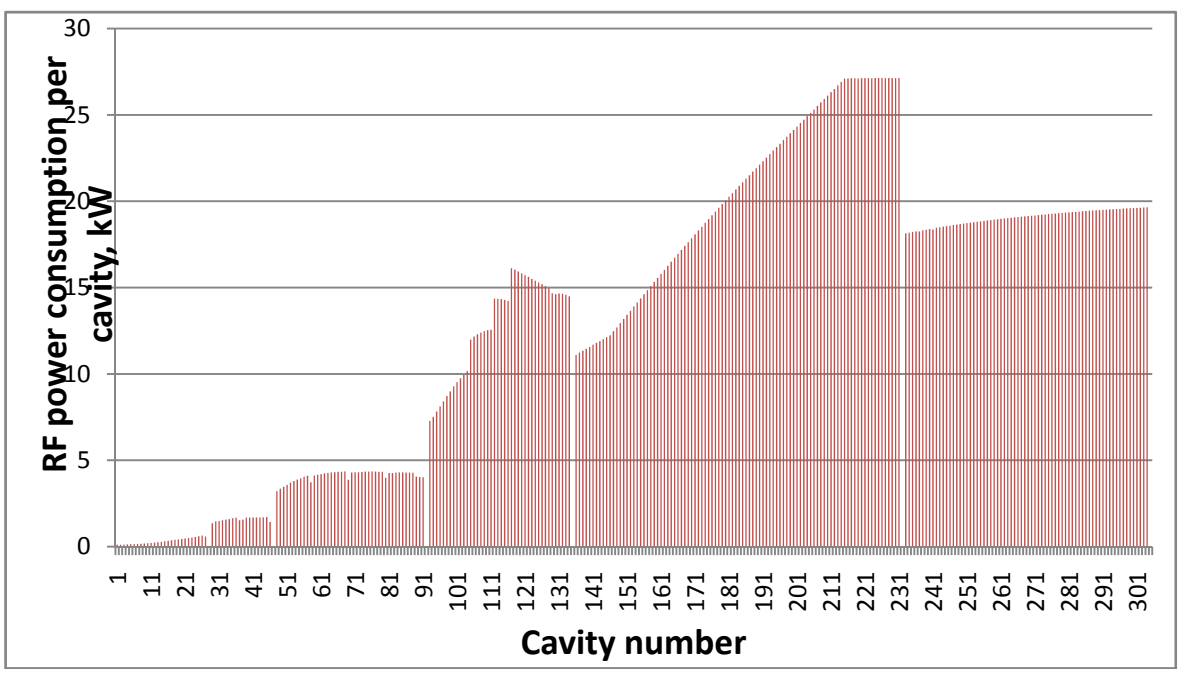

Figure III-6: Distribution of the RF power consumption per cavity in the linac.

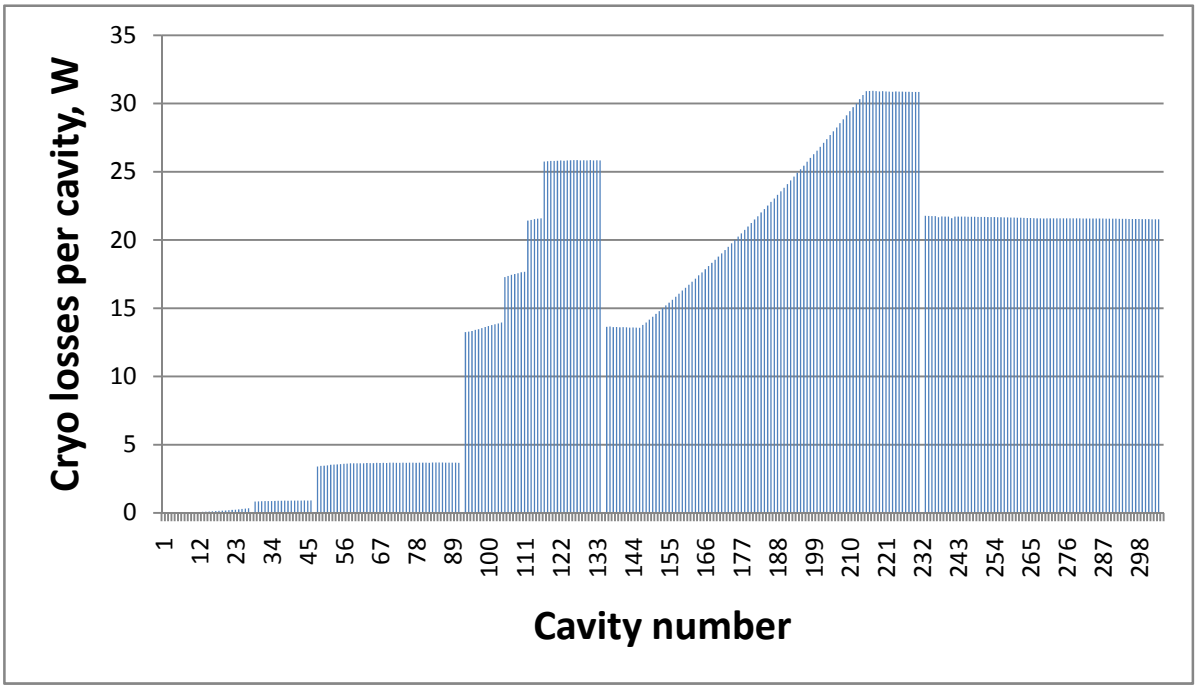

Figure III-7: Distribution of the cryogenic losses per cavity in the linac.

III.1.4 **CW Linac – Beam Dynamics**

The rms normalized beam emittance budget for the CW lina is established as: 0.25 mm-mrad at the ion source and 0.4 mm-mrad at the exit of the linac. The lattice design and the beam dynamics optimization are made utilizing the TRACK, TraceWin and GenLinWin codes. The results of the beam dynamics simulations are shown in Figure III-8. Figure III-8 a) shows the evolution of the one sigma beam envelopes through the CW linac. The top figure shows the two transverse dimensions and the bottom figure the bunch length. Figure III-8b) shows displays the evolution of longitudinal and transverse emittances through the linac. As shown, there is essentially no transverse and only modest longitudinal growth. Figure III-8 c) displays the actual particle density distribution through the linac. Figure III-8 d) shows the eveolution of beam energy through the linac. Finally, a calculation of beam power loss (W/m) due to intrbeam stripping of H- is given in Figure III-8 e). It is noted that losses due to this mechanism are everywhere below 0.1 W/m.

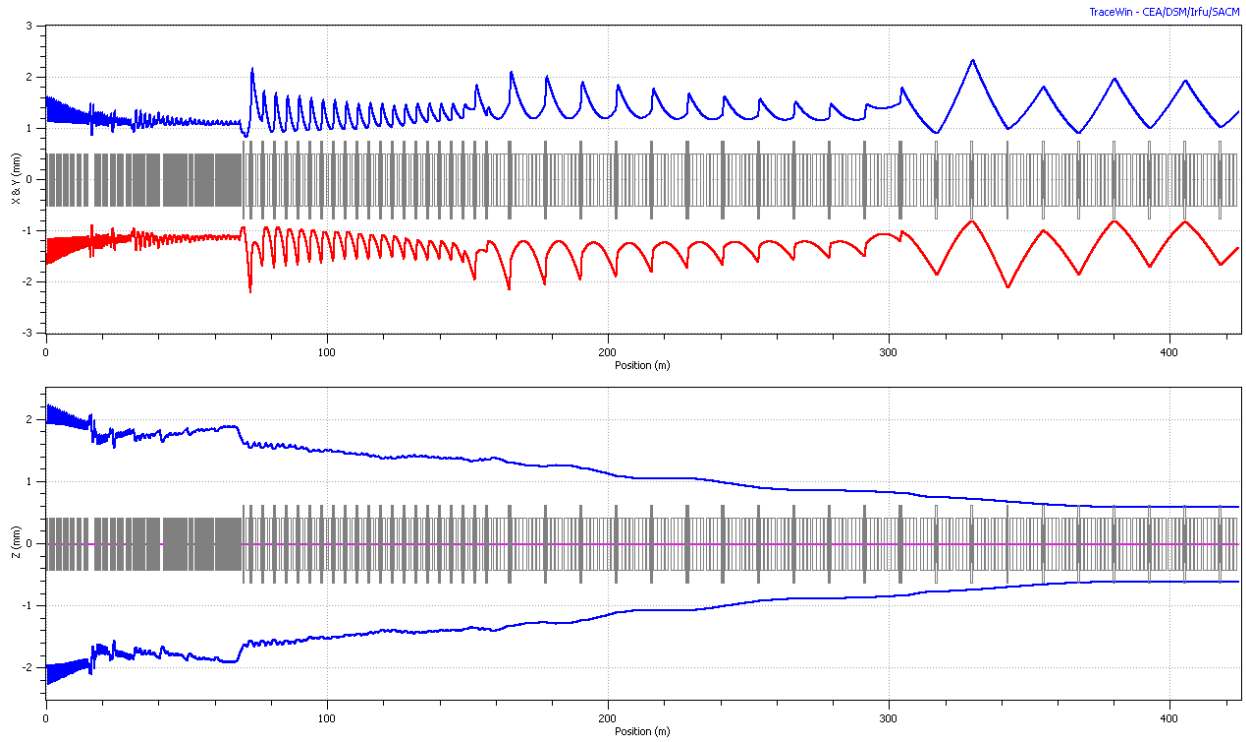

(a) Transverse one sigma x- and y – envelope (above) and longitudinal one sigma bunch size (below) along the linac.

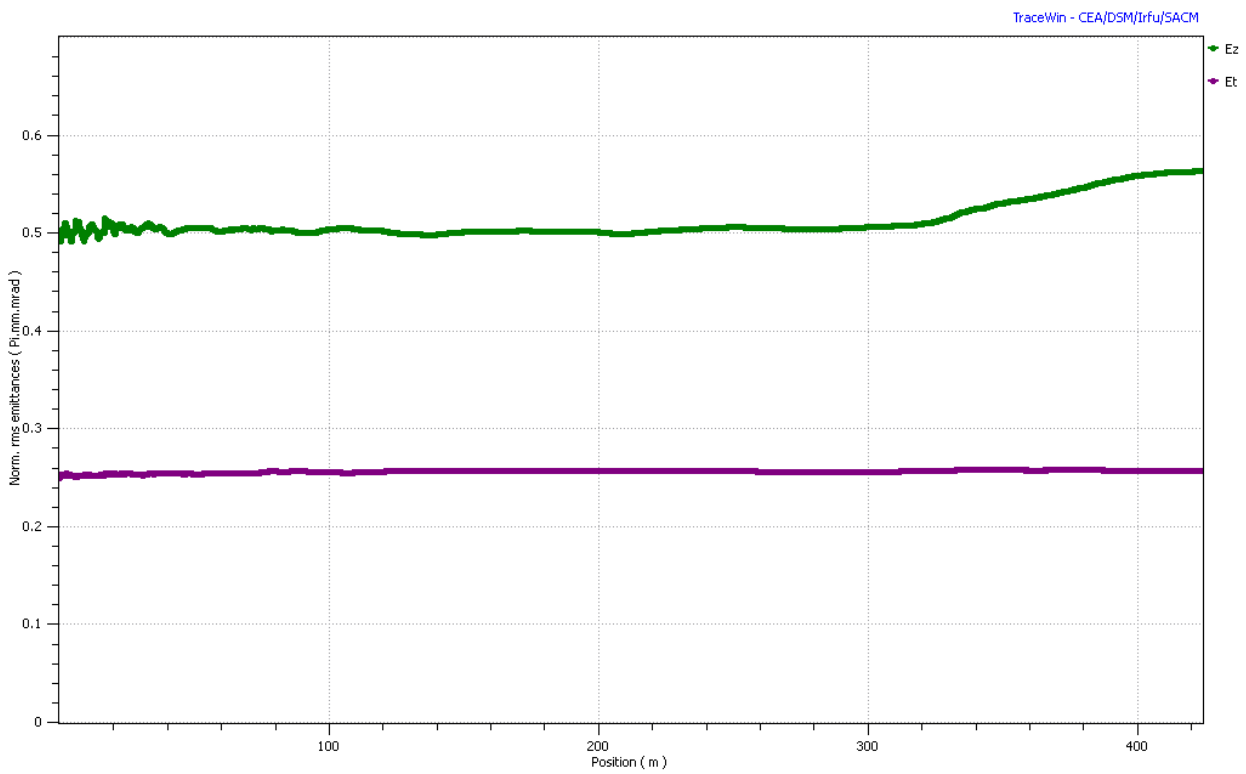

(b) Normalized transverse (magenta) and longitudinal (green) emittances along the linac, in mm-mrad. Longitudinal emittance corresponds to 1.6 keV*nsec.

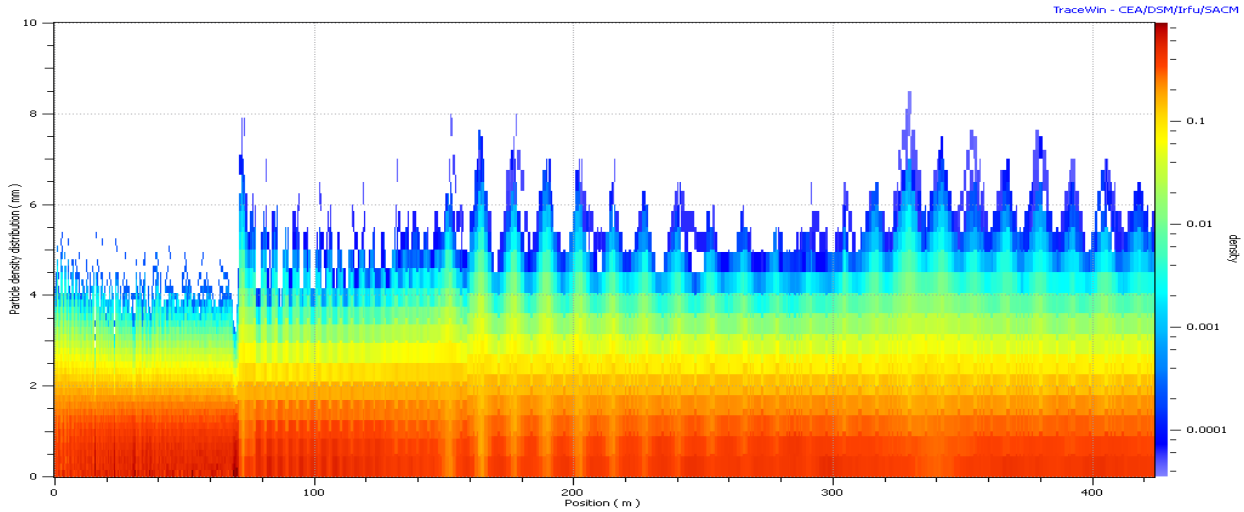

(c) Particle density distribution along the linac. 100k tracked by PARTRAN.

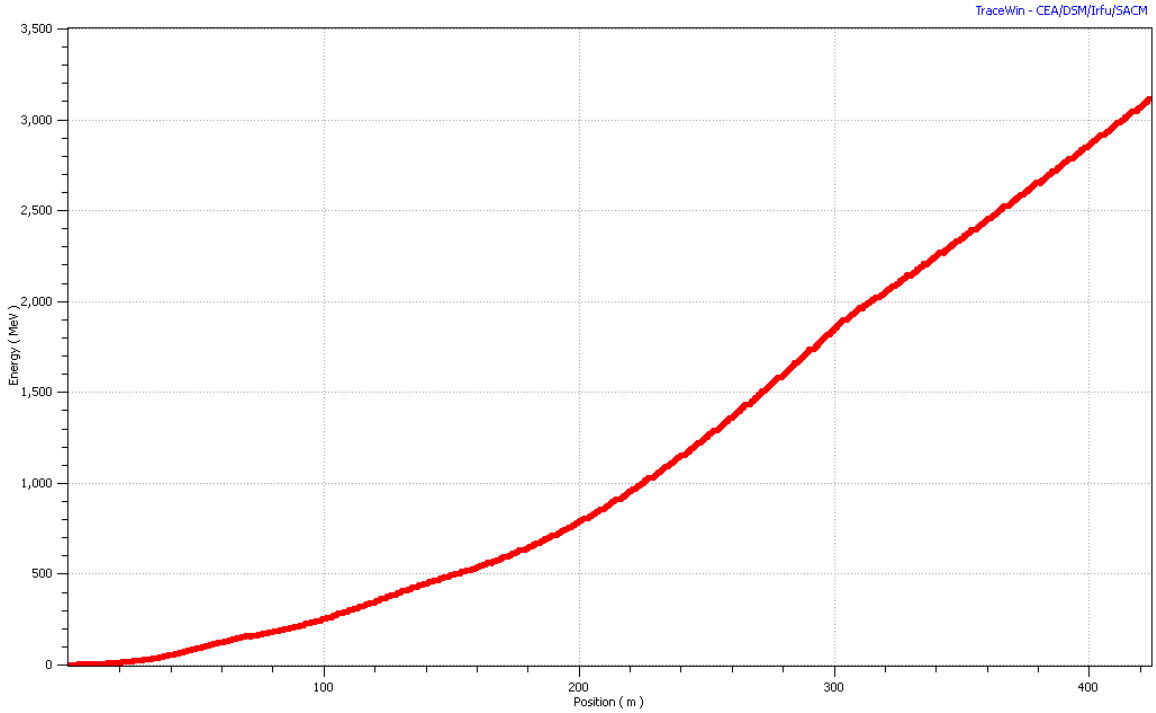

(d) Energy versus longitudinal coordinate.

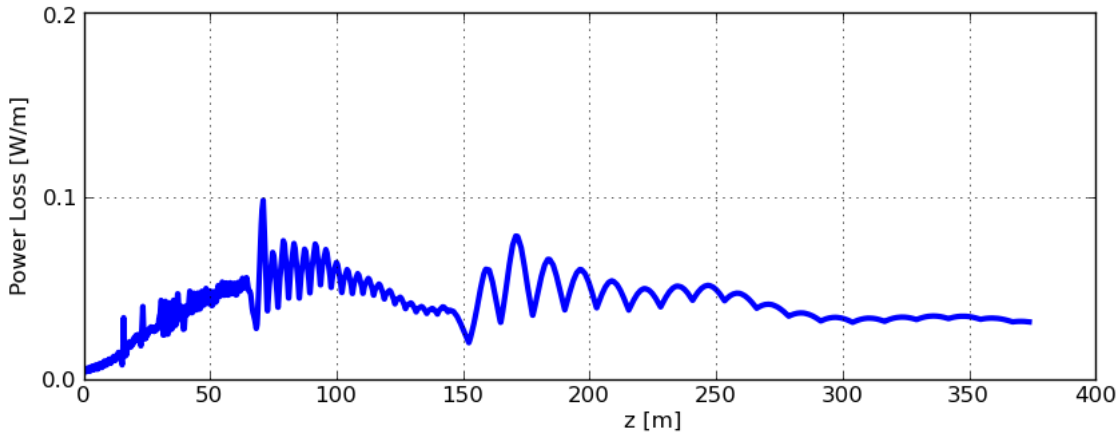

(e) The beam power losses per unit length caused by intra-beam stripping.

Figure III-8: Results of the lattice design and beam dynamics optimization.

III.1 **3-GeV Beam handling**

The CW linac accelerates H^- ions having the base bunch frequency of 325 MHz set by the RFQ. The beam may be steered toward the 3-8 GeV High Energy Linac (Pulsed Linac), to the experimental area, or to the Linac dump as shown in Figure III-9. The injection to the HE linac is controlled by switching on a pulsed switch magnet for ~2.2 ms. It is located immediately after the matching section between the linac and transfer line. With this pulsed magnet on, the beam is directed to the HE linac with a two dipole horizontal achromat with each dipole contributing approximately 2 degrees of bending. If this pulsed magnet is off and a DC selection magnet, one cell downstream, is energized the H^- will be transported to the Experimental Area for further distribution to the experiments. If both switch magnets are off, the beam goes to straight ahead the Linac dump. Beam line layouts are shown in Figure III-9. The basic cell structure and dipole bending is common in all three transport lines with the same cell length (12.6m) as in the 1.3 GHz section of the 3 GeV CW linac.

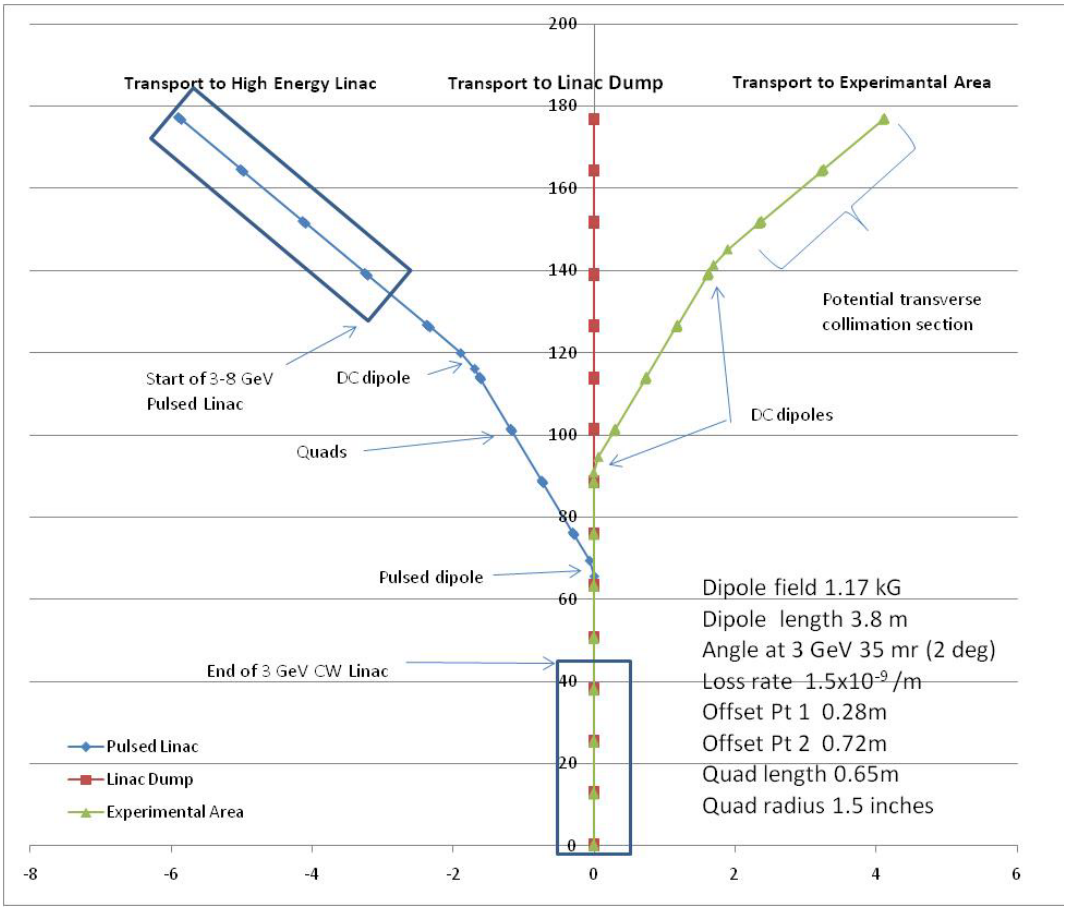

Figure III-9: Layout of the transport lines from the end of the linac to the High Energy Linac (blue), the 3 GeV Experimental Area (green), and the linac dump (red).

III.1.1 Beam Loss

The configuration of transport lines supports H^- beam transport both to the 3-8 GeV HE (Pulsed) Linac (135 kW) and to the Experimental Area (3 MW). The requirements to the fractional beam loss are dominated by the higher intensity beam transport to the Experimental Area.

The H^- transport should have sufficiently small loss to minimize residual radiation in the tunnel. It is highly desirable to keep residual radiation level well below 20 mRem/hr. Many facilities use the metric of 1 W/m as a limit for "hands on" maintaince, however, at 3 GeV, a 1W/m loss rate corresponds to a loss of $2.1\text{x}10^9$ p/m/s and produces a peak contact residual dose rate of ~150 mRem/hr on a bare beam pipe. This loss rate produces significantly lower residual activation on external surfaces of magnets due to shielding by the lamination steel. However, a main concern is the residual level at magnet interfaces and instrumentation locations. These levels are based upon MARS estimations and used for order of magnitude estimations. A more accurate estimation will be required once a detailed model of the transport line is available. Setting a desirable activation level to 10 mRem/hr results in a loss goal of ~0.07 W/m, and, consequently, fractional loss rate of $5.25\cdot10^{-7}$ m^{-1} and $2.25\cdot10^{-8}$ m^{-1} for 135 kW beam to the pulsed linac and 3 MW beam to the experiments, respectively.

The single particle mechanisms contributing to the beam loss are the Lorentz stripping in dipoles, the beam stripping in the residual gas, the photo detachment by blackbody radiation in the beam pipe, and loss due to intra-beam stripping.

Beam motion in a magnetic field excites an electric field in the beam frame. If this electric field is sufficiently strong, it can detach the weakly bound outer electron (Lorentz stripping). Figure III-10 shows the loss rate per meter of dipole field for a 3 GeV kinetic energy H^- as a function of magnetic field. One can see that a dipole field of 1.3 kG produces a fractional loss of 3.7×10^{-8} m^{-1}. As the dipoles occupy a comparatively small fraction of the beam line length, ~10m for the line to the pulsed linac and ~75m for the experimental line, one would like to select a field which produces negligible loss. The loss rate is a steep function of field: a field increase to 1.5 kG increases the fractional loss to 1.7×10^{-6} /m, while its decrease to 1.2 kG reduces the fractional loss to 3.4×10^{-9}/m.

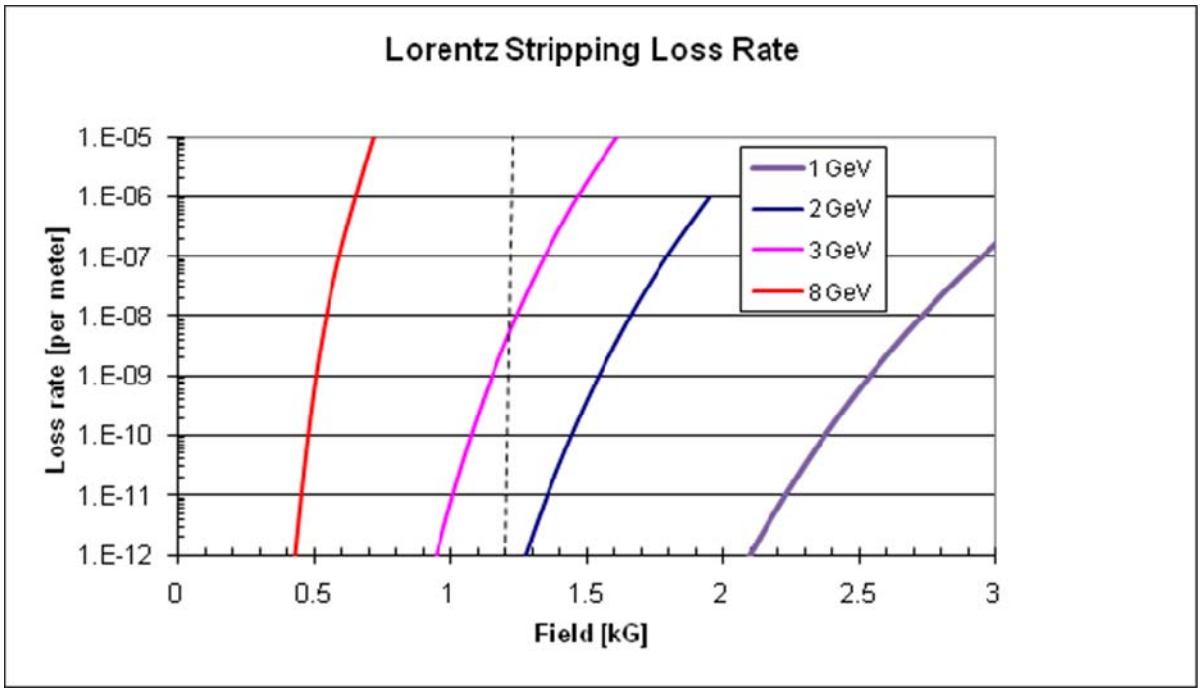

Figure III-10: Fractional loss for a 3 GeV H^- ion traveling in a dipole field. The dashed line marks a magnetic field of 1.2 kG.

The loss rate due to H^- scattering on the residual gas molecules is proportional to their density and the ionization cross section of the molecules present. The cross section decreases proportional to β^{-2}. An analysis carried out for the 8 GeV Proton Driver yielded that for a typical transport line pressures on the order 1×10^{-8} Torr or better can routinely be expected. The fractional loss at 3 GeV is expected to be about 1.3×10^{-8} m^{-1} at this pressure and room temperature. Dropping the pressure to 5×10^{-9} Torr reduces the loss rate to 6.9×10^{-9} m^{-1}. That sets a requirement to the desired vacuum to be $<10^{-8}$ Torr with a goal of 5×10^{-9} Torr.

The contribution from the blackbody photons at 3 GeV at room temperature is 1.3×10^{-7} m^{-1} as seen in Figure III-11. It is well within specifications for transport to the pulsed linac, where the beam power is limited to 130 kW at 3 GeV, however for transport of 3 MW beam power it is just outside the specs. Lowering the beam pipe temperature to just 150 degrees K reduces the fractional loss to 5×10^{-10} m^{-1}

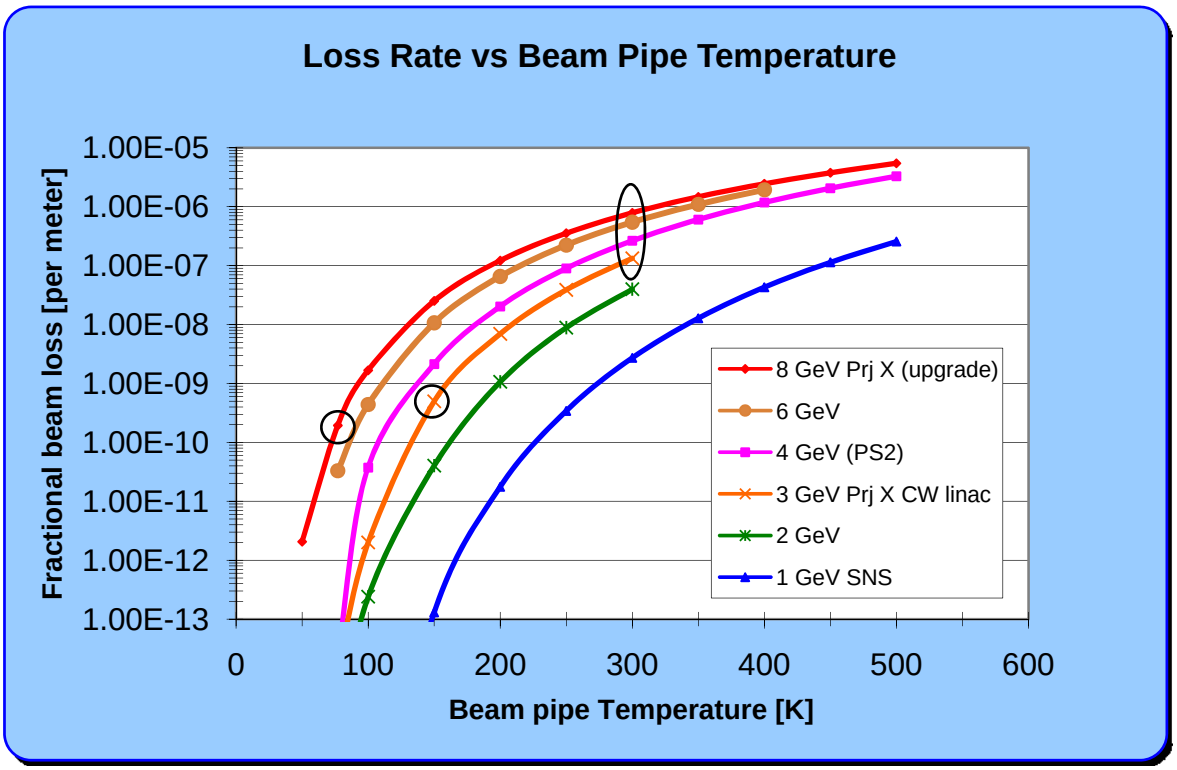

Figure III-11:Loss rate [m^{-1}] due to the interaction of blackbody photons as a function of internal beam pipe surface temperature for several values of H^- kinetic energy.

At room temperature, one can see that the black body radiation is expected to make a major contribution.

Estimation of loss due to intra-beam stripping has been carried out for the entire CW linac. The loss depends on the local transverse velocity of the ions and proportional to the lattice functions. The transport line utilizes the same FODO structure as the 1.3 GHz linac so the contribution due to intra-beam stripping should be comparable to that calculated for the end of the CW linac, namely ~30 mW/m.

Table III-4 summarizes the contributions of the four single particle loss mechanisms discussed above. Note that the value for the intra-beam stripping contains only an estimated lost beam power where the value was taken from the CW Linac estimates. For the HE linac transport line the loss rate due to Lorentz stripping, with the selection of the dipole field of 1.4 kG, is comparable to that for intra-beam stripping, but it's still at an acceptable level at ~86 mW/m with an expected residual activation of ~13 mrem/hr on a bare beam pipe. Lowering the dipole field to 1.2 kG (equivalent of reducing the bend from 2.4^o to 2° per bend) would drop the loss to ~50 mW/m with an expected bare beam pipe residual activation of ~ 7 mrem/hr. Using the same parameters (vacuum level, dipole field, and beam pipe temperature) in the experimental line as in the transport to the HE linac leads to beam loss of on the order of 1.3 W/m, clearly unacceptable.

Simply reducing the dipole field to 1.2 kG lowers this rate to ~ 0.5 W/m (still producing a residuat activation on bare beam pipe on nearly 70 mrem/hr). Lowering the beam tube internal surface temperature with a beam screen to gaseous nitrogen temperature, 150°K, and improving the vacuum to 5x10^{-9} Torr (not an unreasonable value) lowers the beam loss to ~ 60 mW/m and expected residual activation on a bare beam pipe of ~ 10 mrem/hr.

Table III-4: 3 GeV Beam loss summary

Loss Mechanism	CW to P Linac125 kW			Experimental 3 MW w/o shield			Experimental 3 MW w/ shield		
	Value	loss/m	W/m	value	loss/m	W/m	value	loss/m	w/m
Vacuum	1x10^{-8}	1.30E-08	0.002	1x10^{-8}	1.30E-08	0.039	5x10^{-9}	6.90E-09	0.021
Lorentz	1.4 kG	2.90E-07	0.037	1.2 kG	3.40E-09	0.010	1.2 kG	3.40E-09	0.010
Black body	300°K	1.30E-07	0.017	300°K	1.30E-07	0.387	150°K	5.00E-10	0.001
Intra-beam	NA	NA	0.030	NA	NA	0.030	NA	NA	0.030
Total		4.33E-07	0.056		1.46E-07	0.466		1.08E-08	0.062
Residual activation bare beam pipe [mrem/hr]			8.351			69.857			9.321

III.1.2 Transport line functionality

The 3 GeV transport line must be able to select the destination upon clock event. Figure III-12 shows the upstream end of the 3 GeV beam handling and the common components. The blue quads represent the last four quads in the 1.3 GHz cryo-modules of the CW linac. These will be used to match into the upstream end of the transport line. The figure shows common quads in the transport line in yellow. The upper red ellipses indicate the pulsed selection dipole for the HE linac transfer while the lower is the DC selection dipole for the Experimental Area. If both switch dipoles are off the beam goes to the linac Dump.

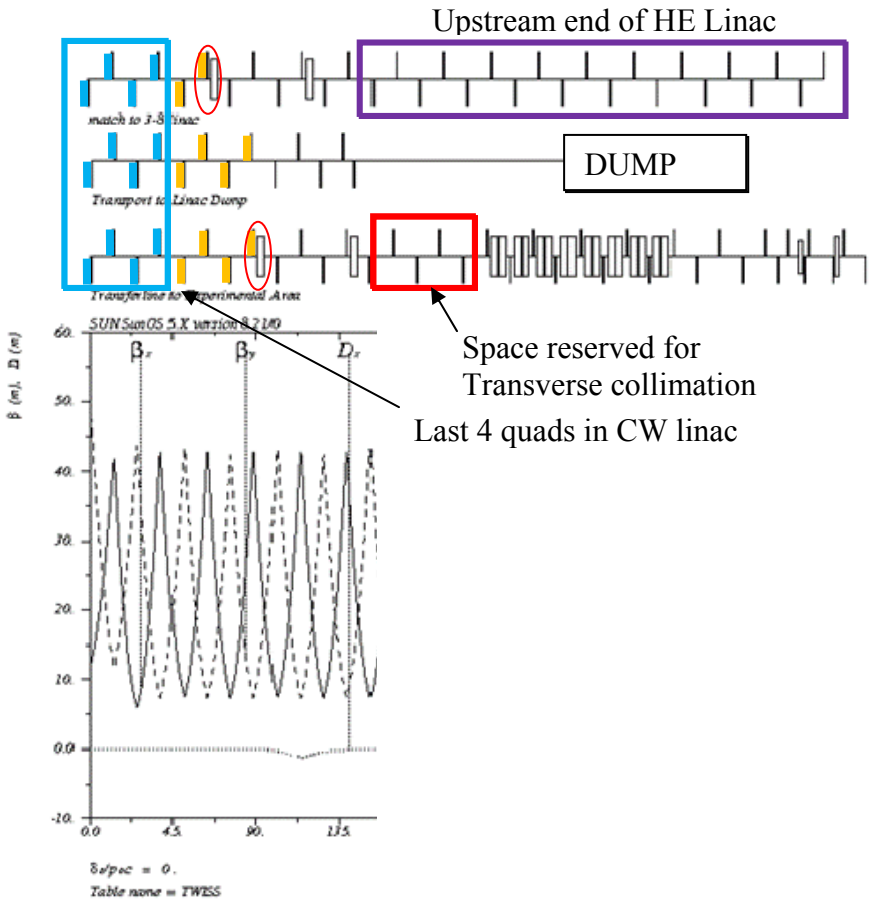

Figure III-12: Basic lattice of the transfer line from the end of the linac through the switch magnets for HE Linac line (top) and the Experimental Area line (lower).

In addition to controlling the single particle loss the transport line should provide a mechanism for controlling loss from large amplitude particles, linac energy errors, and alignment/ power supply errors.

Based upon experience from SNS, a two stage transverse collimation system is considered for installation in the upstream end of the 3 MW Experimental Area transfer line, after the transfer switch achromat dipoles, but before the arc dipoles (see red box in figure III-12). A decision on the installation of a collimation system will be based upon planned detailed error simulation in the CW linac and estimation of halo formation in the linac. If the decision is made to eliminate collimation the geometry can be re-evaluated to potentially shorten the line. If

collimation is deemed prudent, it will consist of a movable thick carbon foil (100% stripping efficiency) upstream of a transport line quad and an absorber downstream of the quad to intercept the large amplitude protons generated from H^- passing through the foil. With an expected 90˚ cell structure of the transport line, two horizontal and two vertical systems would be required for all phase coverage. Although only the largest amplitude particles will be intercepted, a prudent design will size the capacity for the system at 4% of 3MW or ~1% (30 kW on each system) due to the uncertainty of halo production in the CW linac. Obviously, the determination on ultimate capacity of the collimation system will wait till a final design of the CW linac and more extensive modeling including errors has been performed. Due to the differing beam power requirements of the HE linac and Experimental Area transport lines the collimation system has been placed only in the Experimental Area transport line.

To protect the Experimental Area from errant beam energies, a momentum collimation system will be considered for installation at the dispersion peak of the achromatic horizontal bend module. A detailed aperture analysis and error analysis to be carried out will determine if momentum collimation system is necessary, and if so, it's requirements and parameters.. The concept of this system, similar to the transverse, uses a thick movable foil placed between the central arc quad and the downstream dipoles. The foil will convert H^- with wrong energy to protons, which will be swept out of the transport line to a momentum dump by the following dipoles. This implies that these two dipoles need to be of a c-magnet design with an open side-leg. Requirements for the Experimental Area are to be reviewed to determine if momentum collimation is required.

Typical alignment errors achieved during accelerator and transport line installation are 0.25mm transverse and 0.5mr roll. It is expected that these tolerances will be adopted for the installation tolerances in this project. A dipole corrector system will be utilized to correct any orbit distortions caused by misalignments. These will likely be new correctors, similar in design to existing beam line trims. Experience has showed that these correctors are able to correct alignment errors an still provide ample orbit control within the aperture.

III.1.3 H^- Linac Dump

A straight-ahead beam dump is provided for tune up. The transport line to the dump is the same FODO lattice used in the linac-to-Experimental Area transport line. At an appropriate distance a lattice quad is moved upstream 1/2 cell length and tuned (~120% of arc quad gradient) to produce a round beam at the face of the dump. The beam dump is located in a separate enclosure at a distance of approximately 150 to 160 meters from the end of the linac. A buried beam pipe connects the beam-line enclosure to the beam dump enclosure. The lattice is shown in Figure III-. For a linac RMS emittance of 0.25 π-mm-mr, the spot size on the face of the dump with a beta of 250 m is about 25 mm.

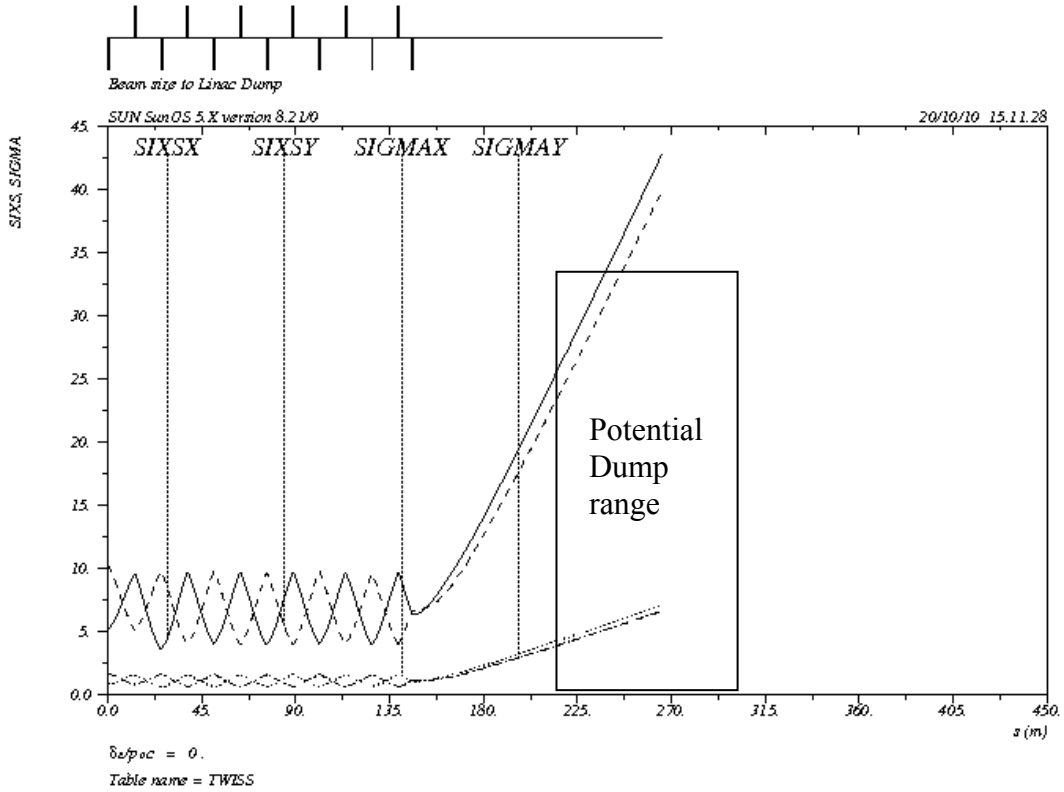

Figure III-13: Beam envelope for the linac straight ahead dump line. First four quads are in the end of the CW linac.

Since the cell structure for the 3 GeV transport lines approximates that of the end of the CW linac, this initial design assumed quads with the same approximate effective length as those in the 1.3 GHz cryo-modules, but of different design. The pole tip diameter is assumed to be 3”. The exterior dimensions of the quad are assumed 0.254m on a side to allow identical FODO channels in each of the three transport lines. The design of these could follow from those designed for the RCS with the maximum gradient about 11% of that in the RCS design. Table III-5 lists the quad parameters for the linac dump line.

Table III-5 Quad parameters for Linac Dump line

Quad	Number	Max gradient [kG/m]
Common BL	4	23.2
Dump quads	4	22.38
Quarter wave	1	26
Quad length	0.65 m	
Pole-tip radius	0.0375 m	

III.1.4 H^- Transport to Pulsed Linac

To fill the Recycler, the chopper will create notches in the CW beam at 2.5 MeV for the rise and fall time of a pulsed switch magnet with a ~2 ms flattop to divert 2.7×10^{13} particles into the HE pulsed linac. In addition, the chopper will need to create the micro-bunch structure to fill 540 out of the 588 53 MHz Recycler RF buckets and to remove approximately 2 out of every 6 linac bunches which do not completely fit into the Recycler RF buckets.

Running at the full 10 Hz rep rate corresponds to 2.7×10^{14} particles/sec for a maximum beam power of 130kW at 3 GeV (345 kW at 8 GeV). Since only 6 of the 10Hz cycles are used to fill the Recycler for each MI cycle, the average beam power can be reduced depending on the flattop energy of the MI, its cycle time, and beam requests from the 8 GeV program. For a 120 GeV MI cycle, with a cycle time of 1.2 sec, the average beam power at 3 GeV is 64 kW (170 kW at 8 GeV). For the 60 GeV MI cycle, with a cycle time of 0.75 sec, the average beam power at 3 GeV is 102 kW (273 kW at 8 GeV). The four cycles not used for the MI neutrino program are available for an 8 GeV program off the Recycler. For beam loss specifications, we will use the maximum beam power.

III.1.4.1 Initial 3 GeV Transfer line layout

An initial layout for the 3 GeV H^- transfer line that captures the requirements discussed above is shown in **Error! Reference source not found.**. The selection dipoles also have a bend angle of 2 degrees and are configured in a horizontal achromat. The achromat is formed by inserting 2 dipoles with the same bend angle 180° apart within the 90° FODO structure. The first dipole will be pulsed and the second dipole is DC. The dipole field is 1.2 kG and has a length of 3.8 m. It is assumed that a notch of approximately 500 μsec will be generated in the beam structure at the head and tail of the HE linac pulse to allow for the rise time for the pulsed dipole. The flattop for the pulsed dipole is assumed to be roughly 2.2 sec. (see figure III-2 depicts dipole waveform). Since the field of the pulsed dipole is less than 2 kG, a detail design of the magnet and power supply could yield to a much shorter ramp time and notch in the beam. All quads in the transport line are 0.65 meters in length and have a pole-tip radius of 37.5mm. transport line**.**

Table III-5 gives a summary of the dipole parameters used in the transport line and Table III-6 provides quad parameters. The initial transport line lattice designed with MAD (shown in Figure III-14) is inserted into the WINTRACE for matching.

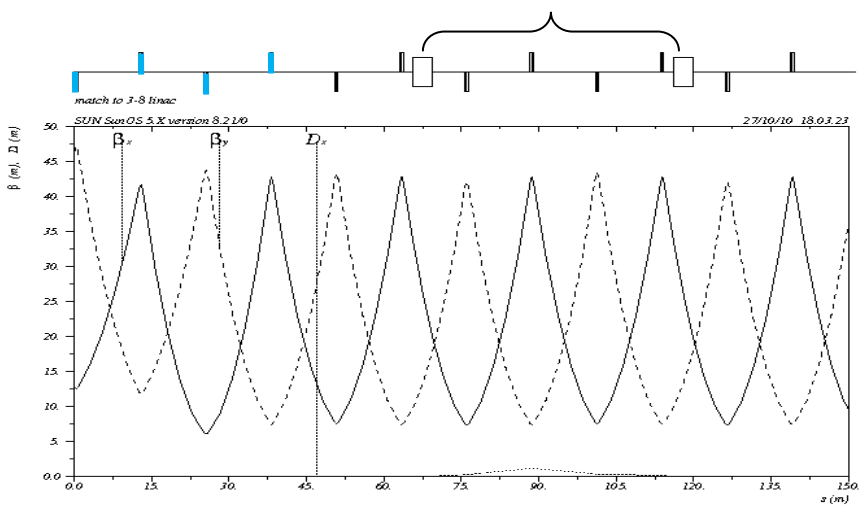

Figure III-14 Initial lattice to transport beam between the CW and Pulsed linac. The last four quads in the cryo-modules of the CW linac are shown in blue and are used to match into the transport line.

Table III-5: Dipole parameters for the CW to Pulsed Linac transport line

Number of Dipoles	2 total
selection Pulsed	1
selection DC	1
Field	1.17 kG
Bend Angle	35 mr
Length	3.8 m
Gap	0.050 m
Pole tip width	0.100 m

Table III-6: Quadrupole counts for the CW to Pulsed Linac transport line

Quad	Nunber	Max gradient [kG/m]
Linac Match	3	32
Arc quads	21	33.31
RCS Match	4	75
Quad length	0.5 m	
Pole-tip radius	0.0375 m	

III.1.5 H^- Transport to Experimental Area

If the pulsed HE linac switch magnet is off and the DC Experimental Area switch magnet is on, the 3 GeV CW linac H^- beam will be directed toward the Experimental Area. The beam power in this transport line is up to 3 MW. It is critical to minimize single particle losses, provide sufficient aperture, and provide collimation to remove large amplitude particles that could become lost in unprotected areas.

III.1.5.1 Initial Transport Line Configuration

Immediately after splitting off the dump line via a horizontal 2 dipole achromat, a section of the FODO lattice is reserved for a potential collimation system for the H^- . Since this transport line the beam power handling capability is significantly larger, thus requiring significantly larger absorbers and cooled beam screen for reduction of losses due to black body radiation if H- ions were to be transported the entire length of the transport line. As discussed below the initial concept of an RF separator/Lambertson combination may require an upstream stripping station to convert 100% of the 3 MW beam into protons.

Currently, the dipoles and quads for this line are of the same design used in the linac-RCS and the linac dump line, although a new design will be investigated. The transport line will have the usual complement on instrumentation (BPMs, profile monitors, loss monitors, and beam current monitors) and well as dipole correctors.

The beam may be directed toward any one of three experimental areas utilizing and RF separator to give bunches arriving at the separator (separated in time, see Figure III-14) either a positive, negative, zero vertical kick (depending on their arrival phase) and a downstream three way Lambertson to separate the beams horizontally. The location of this facility is depicted at the end of the transport line in Figure III-13. The three transport lines after the Lambertson are not shown, but expected to be similar FODO channels and the early part of the transfer line. Based upon the current design, the required dipole field in the Lambertson to produce significant separation between the three downstream beam lines will require a stripping station to be located upstream of the separator/Lambertson combination to convert the H- ions into protons. Optimization of this configuration will be discussed in section III.1.7.

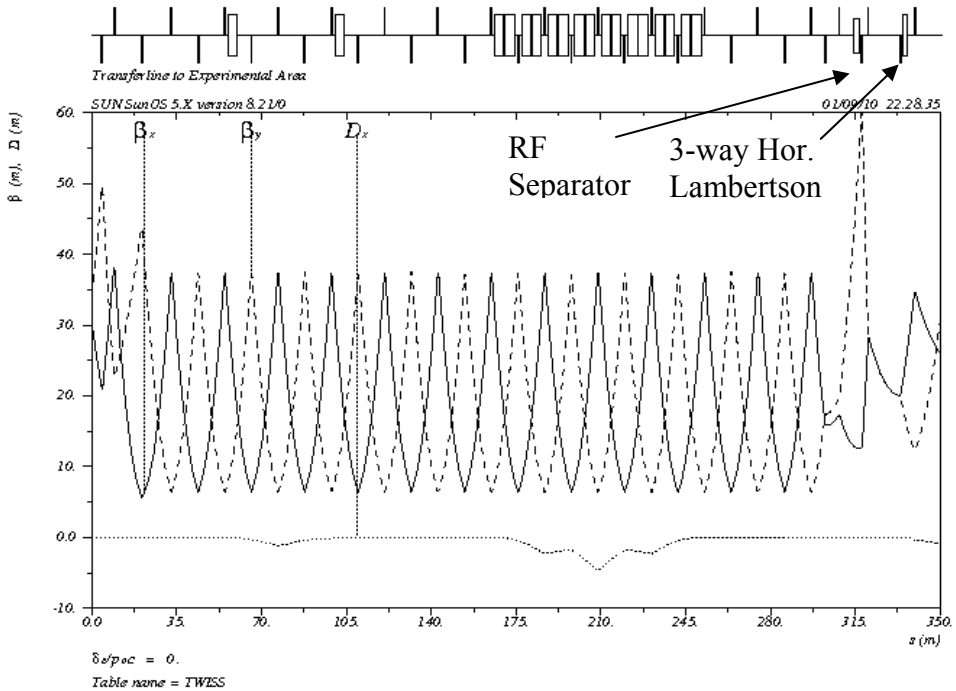

Figure III-13: Lattice functions for the Experimental Area transport line.

III.1.6 **RF Beam Separation for 3 GeV Experimental Program**

To reduce the power required for the RF beam separation in CW regime a SRF structure with the deflecting TM_{110} mode is assumed. The structure should operate at the frequency $f_0(m\pm1/4)$, where f_0 is the bunch sequence frequency (f_0=325 MHz). In the 3.9 GHz deflecting structure developed at FNAL[6], the deflection strength is 7 MeV/m. To reduce the emittance growth related to different kicks applied to the bunch tail and head we choose lower frequency of 406.25 MHz (m=1). Figure III-14 presents a schematic of bunch RF separation. For the deflection strength of 10 MeV a deflection angle is ±2.5 mrad. Assuming a 20 m long drift space, the beam separation is ±50 mm.

[6] L. Bellantoni, *et al*., FERMILAB-Conf-01/103-E July 2001.

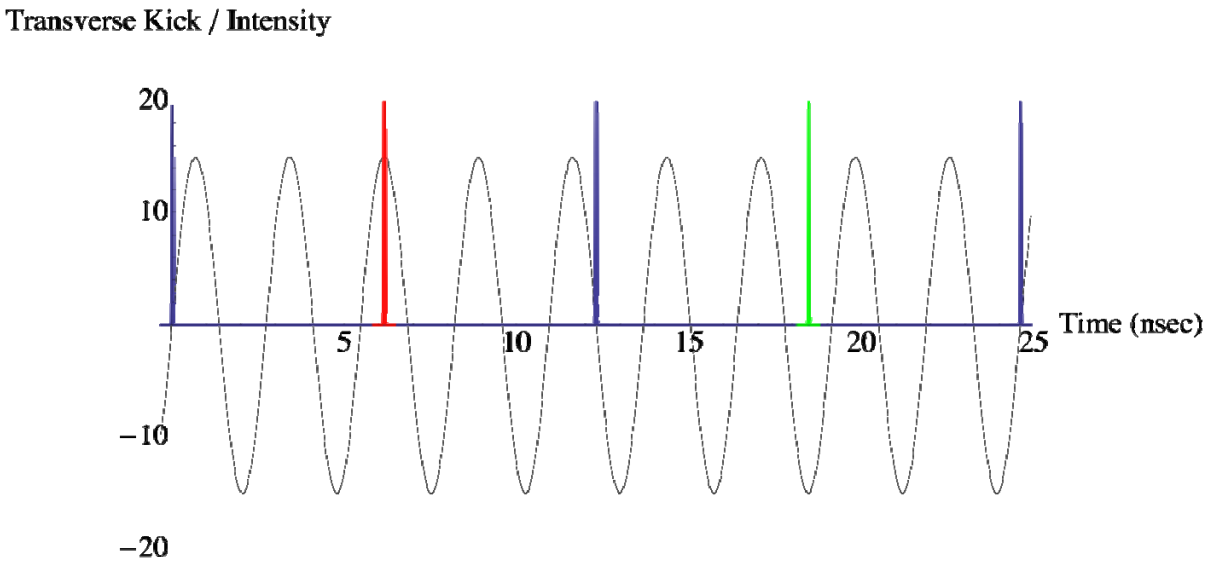

Figure III-14: Transverse deflecting kick at 406.25 Mhz. The blue pulses are not deflected, the red pulse is deflected to the right, and the green pulse is deflected to the left.

KEK-B utilizes a 500 MHz crab cavity with a squashed-cell shape and has achieved a separating gradient of 30 MV/m at 4.2 K. The cavity operates at 21 MV/m (a kick voltage of 1.44 MV). Scaling to a cavity of 406.25 MHz, the operating parameters in Table III-7 appear feasible. Three cavities with a kick of 3.1-3.4 MeV are needed for a total kick of 10 MeV over a total length of approximately 3.5 m. The surface magnetic field for this gradient is 60-65 mT. Figure III-15 shows a representative drawing of the separator cavities, including input power couplers and mode couplers.

Parameters	
E (surface field) MV/m	**29.3**
B (surface) mT	**72**
R/Q (Ohm)	**27**
Longitudinal size (mm)	**440**

Vertical size (mm)	**865**
Horizontal size (mm)	**962**
Operating Frequency (MHz)	**406.25**
Power (W)/cavity	**260**
Transverse kick/cavity (MeV)	**3.75**

Table III-7: Operating parameters of separator cavity at 406.25 MHz. 3 cavities for a total transverse kick of 10 MeV are required.

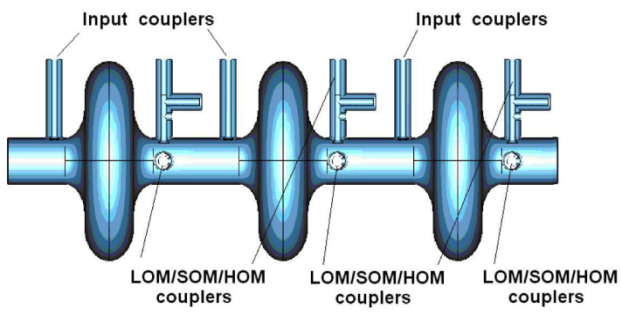

Figure III-15: Representative drawing of a separator cavity section, including power and mode couplers.

The total power load in the cavity is a combination of the power necessary to maintain the RF field, power necessary to overcome beam loading from misalignments, and power necessary to handle microphonic detuning. With an assumed Q_0 of 10^9, the power load is dominated by the microphonics contribution (20 kW/cavity), followed by beam loading compensation (9 kW/cavity). The field is maintained with 200 W/cavity. In total, the separator cavity will need approximately 60 kW at 406.25 MHz.

III.1.7 Separator/Lambertson Optics

To minimize the required vertical deflection angle, a 3-way Lambertson is installed approximately 20 m downstream of the RF separator. The total deflection from the RF separator is dependent on the position and vertical aperture of the Lambertson. Figure III-16 shows the beam envelope assuming a rms emittance of 0.25 π. The aperture to beam envelope in the separator is almost a factor of 20. This leaves significant room for optimization on the location of the Lambertson and the number and strength of the RF cavities. A small vertically focusing quadrupole is located just in from of the Lambertson to reduce the vertical angle from the separator. Three beam lines emerge from the Lambertson and there needs to be enough horizontal separation between the beam lines to install quadrupoles in each line. The optimal optical situation is all three lines are optically identical. Utilizing H^- as the primary particle through the RF separator limits the magnitude of the field in the Lambertson to ~1.3 kG and

requires approximately 10 meters of Lambertson. On the other hand stripping the H^- to protons prior to the splitting removes the maximum field limit on the Lambertson. A Lambertson with a field of 6.4 kG and length of 2 meters produces a 100 mr bend and 370 mm separation at the downstream quadrupoles. Optimization of the Lambertson field and geometry will proceed as the downstream experimental area requirements develop. Figure III-17 shows a cross section of the 3-way Lambertson concept (a magnet of this design is currently in use in the FNAL switchyard). Here the field is noted as 6.4 kG. A reduction of this field only makes the leakage field in the central aperture smaller.

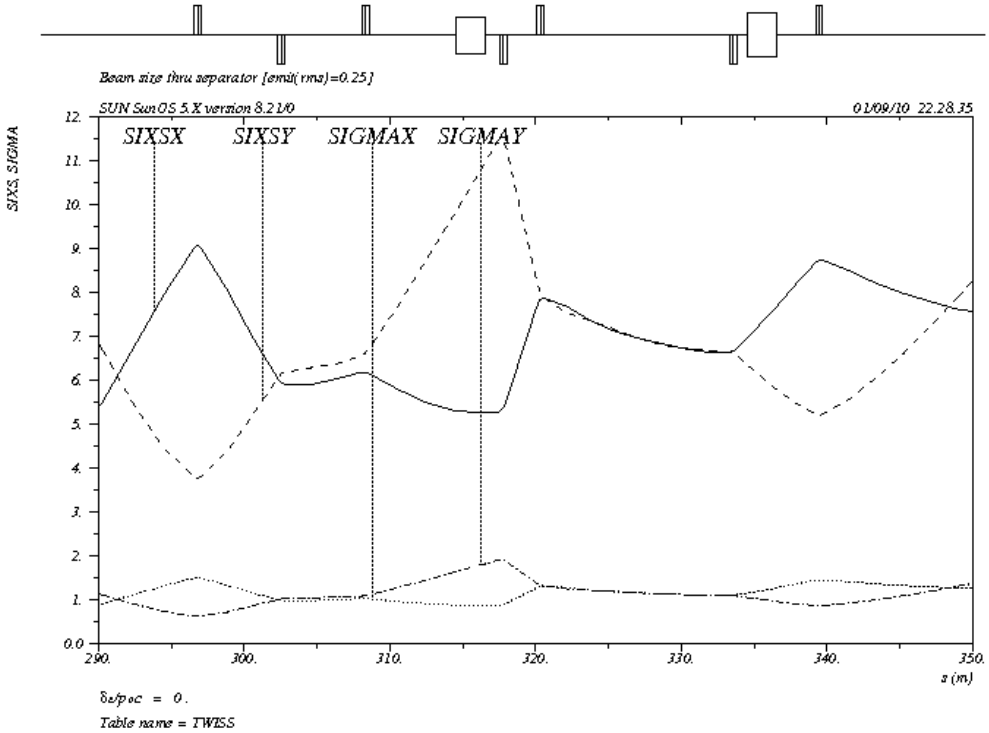

Figure III-16: Beam sizes through the initial concept of the RF separator and Lambertson.

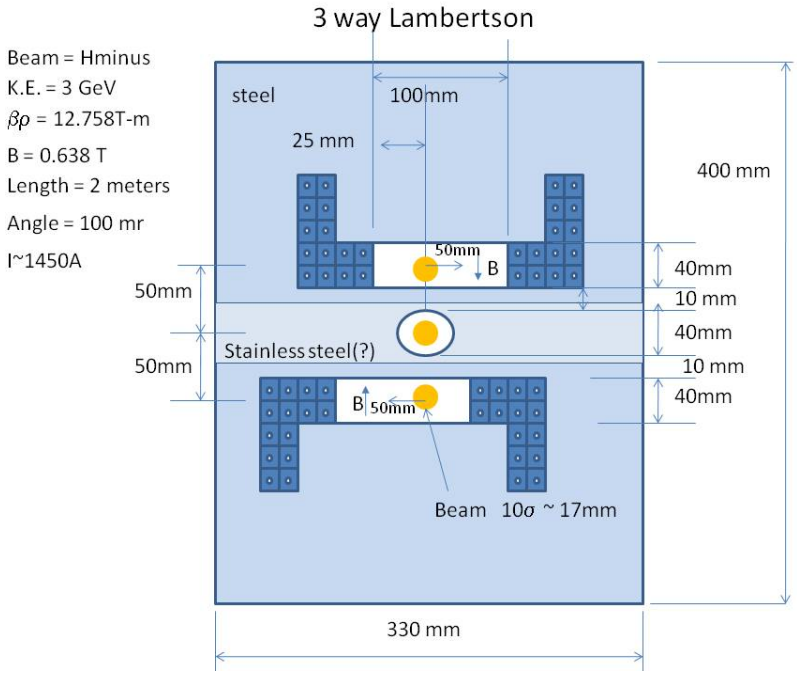

Figure III-17: Concept for 3-way Lambertson.

III.2 3-8 GeV Pulsed Linac

III.2.1 Linac Parameters

The 3-8 GeV pulsed linac is a superconducting linac that can support a beam current of 2 mA, a pulse length of 2.2 msec, and a repetition rate of 10 Hz to an energy of 8 GeV. Figure III-18 shows the linac timeline schematically. Six 2.2 msec pulses are provided at a rate of 10 Hz for acceleration in the pulsed linac and transfer to the Recycler/Main Injector in support of the long baseline neutrino program. The beam is directed into the pulsed linac by a pulsed dipole with a rise time of 0.5 msec. The pulsed dipole and the beam line transporting the beam from the 3-GeV cw linac to the 3-8 GeV pulsed linac are described in the 3-GeV Beam Handling section.

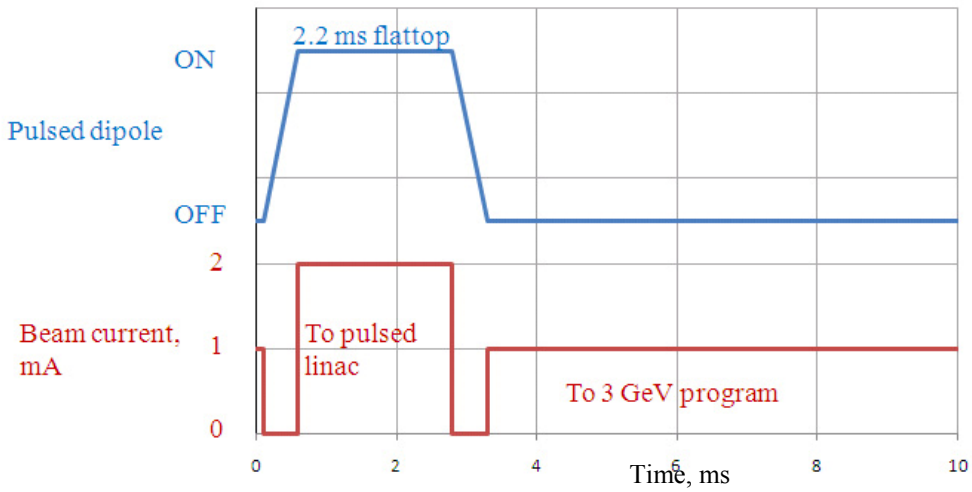

Figure III-18: A schematic timeline for linac beam current (first 10 ms of the 100 ms cycle). The pulsed magnet's rise and fall time is assumed to be 0.5 ms.

Table III-8 presents the basic parameters of the pulsed linac.

Parameter	Quantity	Unit
Particle Species	H- ion	
Input Beam Energy	3.0	GeV (kinetic)
Output Beam Energy	8.0	GeV (kinetic)
Pulse Repetition Rate	10	Hz
Beam Pulse Length	2.2	msec
Average Pulse Beam Current	2	mA
8-GeV Transverse Emittance	0.4	mm-mrad (rms norm)
8-GeV Long Emittance	1.6	keV-nsec
8-GeV Bunch Length	1.0	psec (rms)

Table III-8: Linac Parameters

III.2.2 Accelerating Cavities and Cryomodules

The linac is based on 1.3-GHz 9-cell cavities (Figure III-19) optimized for $\beta = 1$ and ILC-type cryomodules, providing a FODO focusing structure (Figure III-20).

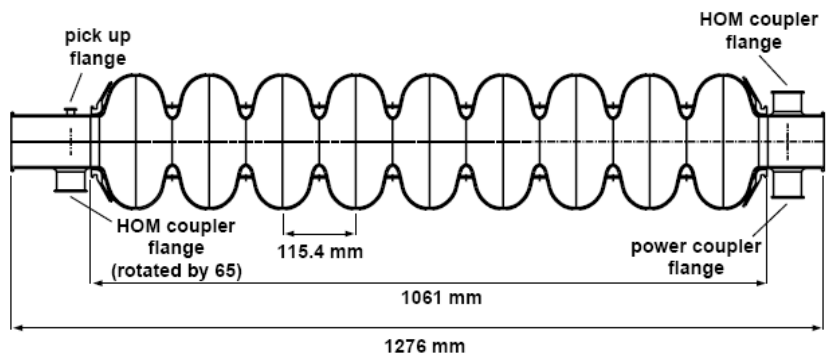

Figure III-19: Schematic of a 9-cell 1.3-GHz cavity

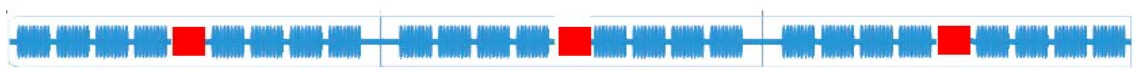

Figure III-20: Schematic of the linac focusing structure (red – quadrupoles, blue – SCRF cavities)

We choose a cavity gradient of 25 MV/m, which is readily achievable with current superconducting RF (SCRF) technology. At this gradient the number of cavities (cryomodules) required for such a linac is 224 (28). The total length of the linac is 353 m.

III.2.3 Pulsed Linac – Beam dynamics

The lattice design and the beam dynamics optimization are made utilizing the TRACK and TraceWin codes. Figure III-21 shows the simulated beam envelopes along the linac. Figure III-22 displays the actual particle density distribution through the linac.

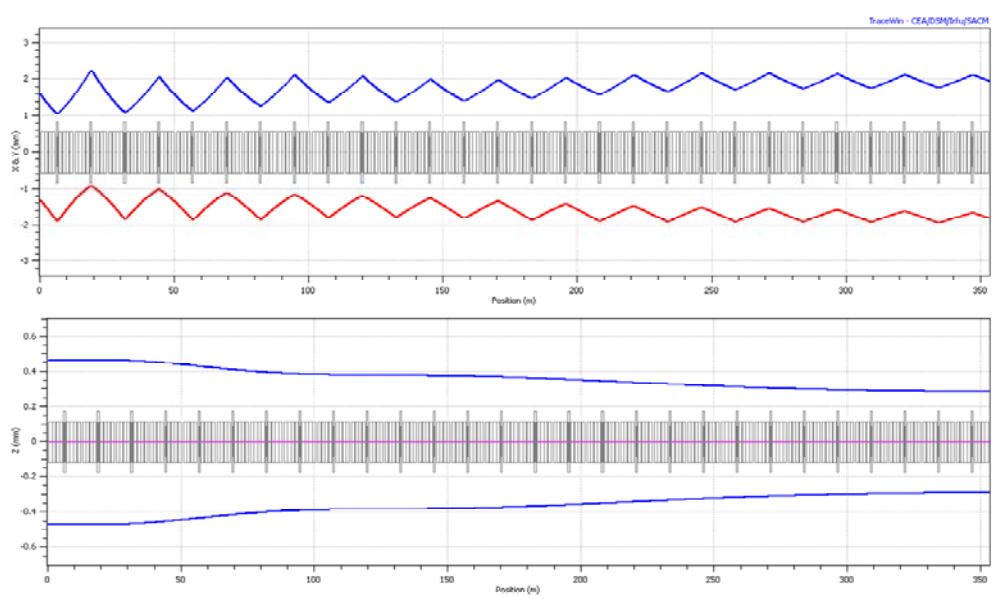

Figure III-21: Simulated rms beam envelopes in the pulsed linac: transeverse (top) and longitudinal (bottom).

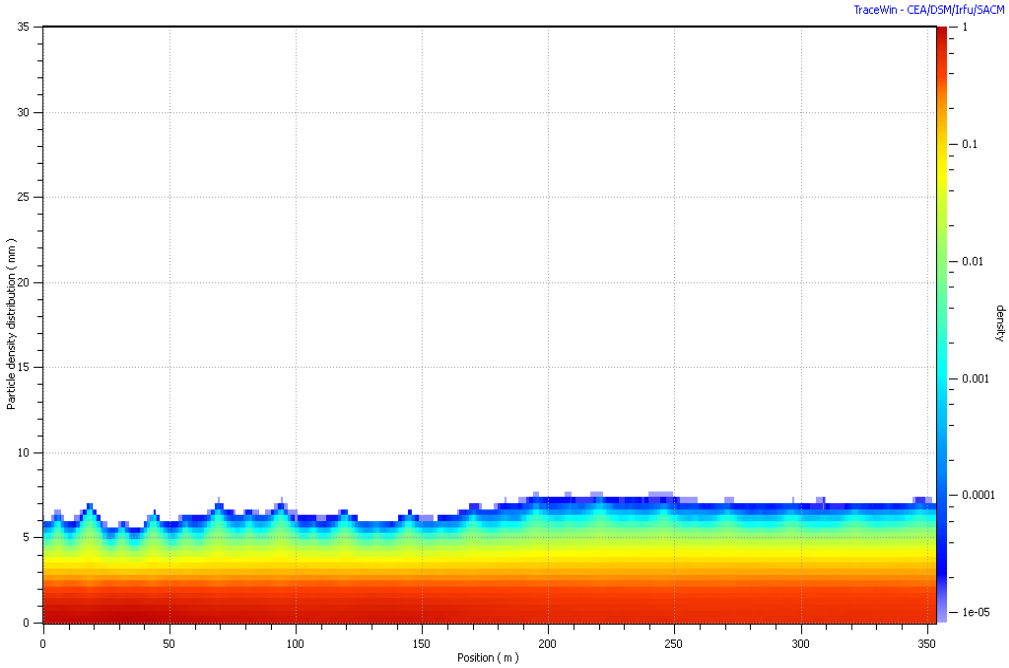

Figure III-22: Particle density distribution along the linac. 100k tracked by PARTRAN.

III.3 8 GeV Transport Line

The length of the transport line has previously been determined to be approximately 1 km due to the siting of the linac inside the Tevatron ring, the limited dipole field of ~ 500G to prevent the stripping of the weakly bound outer H- electron, and the drift necessary to place a phase rotator cavity. To mitigate blackbody radiation stripping of the H-, we include a liquid nitrogren cryogenic shield around the beam pipe for the full 1 km length. The transport line includes a transverse collimation scheme for capturing large amplitude particles, a momentum collimation system for the protection of off energy particles, and a passive phase rotator cavity to compensate for energy jitter.

With 60° per half cell, we need ~80 dipoles and ~60 quadrupoles for the transport line. Since the linac will be injecting into a fixed energy permanent magnet ring , permanent magnets will be utilized for the bending and focusing magnetic elements of the transport line. This choice is consistent with the existing permanent magnet 8 GeV transport line between the Booster and Main Injector.

The elevation at the end of the transport line is matched to the elevation of the Recycler Ring at 720.4 ft. The elevation of the transport line enclosure at the interface to the existing 8 GeV line/Main Injector tunnel is matched the MI tunnel floor elevation at 713.5'. Keeping this enclosure elevation throughout the transport line and linac provides adequate shielding and avoids elevation interferences with existing underground enclosures.

We use a thin carbon foil as the default stripping system at injection. We plan on investigating the laser stripping process that has been demonstrated at SNS for 1 GeV H-.

The injection process itself consists of both transverse and longitudinal phase space painting to create a "KV-like" distribution and minimize space-charge tune shift in the Recycler. We use a combination of horizontal painting and vertical injection steering to minimize the required vertical aperture and reduce the complexity of painting in the ring in both dimensions to produce a uniform transverse distribution in x and y.

III.4 **Recycler/Main Injector**

The Fermilab Recycler Ring is a fixed energy 8 GeV storage ring using strontium ferrite permanent magnets in the Main Injector (MI) tunnel. For the NOνA program, the Recycler will be converted from an antiproton storage ring to a proton accumulator for single turn injection into the Main Injector. The Recycler will operate as a stripping ring, using boxcar stacking of 6 pulses from the linac, capturing in 53 MHz RF buckets, and performing a single turn extraction into the MI. The MI will receive 1.6×10^{14} protons from the Recycler in a single turn and will accelerate them to 120 GeV in 1.2 seconds. In general, the Recycler and Main Injector operate in a similar mode to the NOνA operation[7].

III.4.1 **Recycler Modifications**

With a new injection insert in the Recycler, we anticipate the need for more flexibility in the lattice design. The Recycler is built with permanent magnet quadrupoles, permanent magnet combined function devices, powered dipole correctors, and a tune trombone of powered quadrupoles. The installation of new powered quad elements in the injection region allows for lattice flexibility.

III.4.2 **Main Injector Modifications**

In the present Main Injector, the injection energy is 8 GeV and maximum energy 120 GeV. Transition crossing is at $\gamma_t = 21.6$ GeV. Simulation shows that emittance dilution and beam loss will occur at high intensities. Furthermore, from experience at other machines (e.g., the AGS at BNL, the CERN PS, and the KEK PS), transition crossing could become a severe bottleneck in high intensity operation.

The design being considered is first-order system employing local dispersion inserts at dispersion-free straight sections. The normal ramp rate of the MI is 240 GeV/s. In order to have an effective γ_t-jump, the jump rate should be at least an order of magnitude higher. The system was chosen to provide a $\Delta\gamma_t$ from +1 to -1 within 0.5 ms, a jump rate of 4000 GeV/s, about 17 times faster than the normal ramp rate. Details can be found in the Proton Driver Design study document[8].

---

[7] D.S. Ayres *et al.*, NOνA Technical Design Report, Fermilab-Design-2007-1, (October 2007). Chapter 8 discusses the accelerator.

[8] G.W.Foster, W. Chou, and E. Malamud (ed), "Proton Driver Study II", Fermilab-TM-2169, (May 2002). The γ-t jump system is described in Chapter 16.

III.4.3 Electron Cloud Mitigation

Electron cloud induced instabilities in either the Recycler or the MI could be an important limitation to the maximum proton flux. Ongoing studies in the Main Injector are investigating the generation of electron clouds and the performace of beam pipe coatings (e.g., TiN) in reducing the secondary electron yield. Simulations are being benchmarked to measurements[9]. Based on the measurements and simulations, it appears that a combination of beam pipe coating and instability damper upgrades will be enough to mitigate electron cloud instabilities.

III.4.4 RF System Modifications

Upgraded RF systems are required in both the Recycler and the Main Injector. The Recycler RF system is used solely for capture of the injected beam. With the higher intensity, the Main Injector needs more power than is currently available to accelerate the beam at 240 GeV/s. To minimize changes to the existing instrumentation (specifically BPM systems), the RF will operate at the same harmonic number of 588.

The peak beam current in the Main Injector is 2.25 A and 2.7 MV/turn are necessary to reach the desired acceleration rate. With a synchronous phase angle $\phi_s = 36^\circ$, 240 kV per cavity are required. From injection energy (8 GeV) to flattop (120 GeV), the frequency sweep is from 52.811 MHz to 53.104 MHz. A cavity design is under development, to be used in both the Recycler and the Main Injector.

To mitigate possible space charge effects, an increased bunching factor is desired. A frequency mismatch between the capture RF and the linac RF induces a parasitic longitudinal painting[10] but that is not enough. Studies have shown that a 2nd RF system operating at the 2nd harmonic and at ½ the voltage increase the bunching factor to ~0.35, within the desired range to mitigate space charge effects[10].

IV Design Concepts of Major Subsystems

IV.1 CW Linac

IV.1.1 Ion sources, RFQ and MEBT

The front end system operates at 325 MHz, however not all of the RF buckets will contain bunches. There are two principal time structures needed for the linac operation (see Figure II-1): (1)a pulsed ~2.2 ms structure at 10 Hz; and (2)a CW structure with bunch variations at the microseconds level. These time structures are required to provide 2.2 ms long trains of bunches at 10 Hz for the injection into the pulsed linac, interleaved with beam delivery to the 3 GeV experimental areas. The bunch structure feeding the pulsed linac must incorporate the Recycler

---

[9] COMPASS SciDAC Collaboration (Paul L.G. Lebrun *et al.*), FERMILAB-CONF-10-091-CD, May 2010.

[10] P.S. Yoon, D.E. Johnson, W. Chou, "The Modeling of MicroBunch Injection into the Main Injector", FERMILAB-TM-2398-AD-APC, (January 2008).

RF bucket frequency (52.8 MHz) structure to facilitate pseudo bunch-to-bucket transfer (Figure IV-1) and also the Recycler revolution frequency (90.3 kHz) structure to provide a 200-ns extraction gap in the Recycler. This results in the removal of ~33% of bunches during the 2.2 ms period, which in turn requires for the ion source to provide 2.7 mA of beam current. The CW bunch structure is determined by rare decay experiments, an example is shown in Figure II-1. Figure IV-1 shows the chopping pattern required during the 2.2 msec pulse destined for the Recycler via the pulsed linac. Figure IV-2 shows the ion source current as a function of time corresponding to the full linac timeline presented in Figure III-2. In summary, the beam bunches can occupy arbitrary RF buckets as long as the average linac current does not exceed 1 mA for periods greater than ~1 μsec portion of the timeline associated with the 3 GeV program, or 2 mA during the portion of the timeline (2.2 msec) dedicated to filling of the Recycler . It is likely that such a time structure will be provided by two choppers, the first one (a pre-chopper) immediately after the ion source and the second in the MEBT section after the beam acceleration in the RFQ.

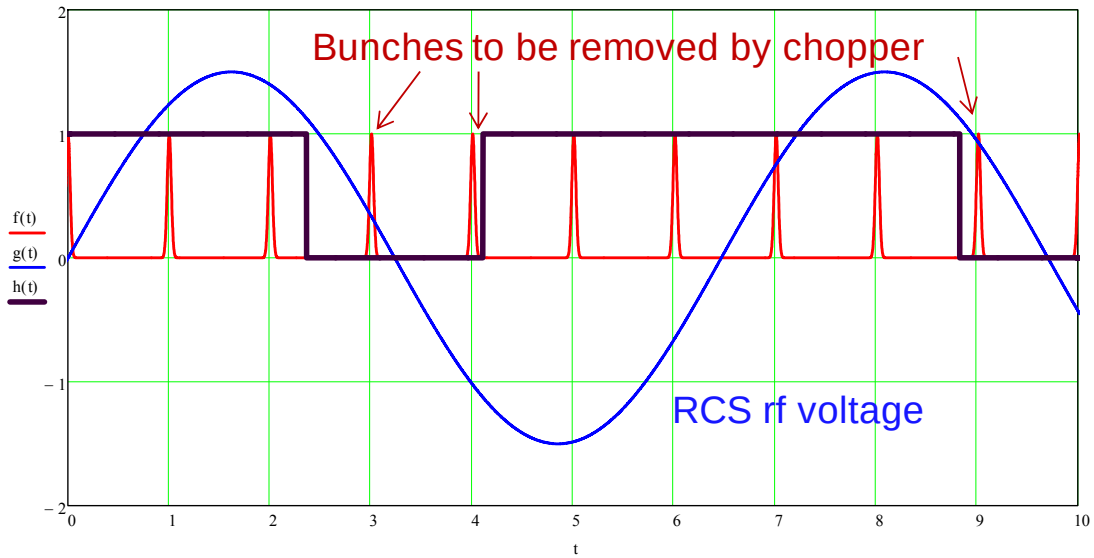

Figure IV-1: An example of the bunch chopping pattern for the RCS injection. The horizontal axis is the linac bunch period (1/325 MHz), the vertical axis has an arbitrary scale. The bunch repetition rate is 325 MHz (red), while the RCS RF cavity voltage frequency is 51.58 MHz (blue). Bunches outside of the ±7.3-ns long gate (black) are to be removed by the chopper.

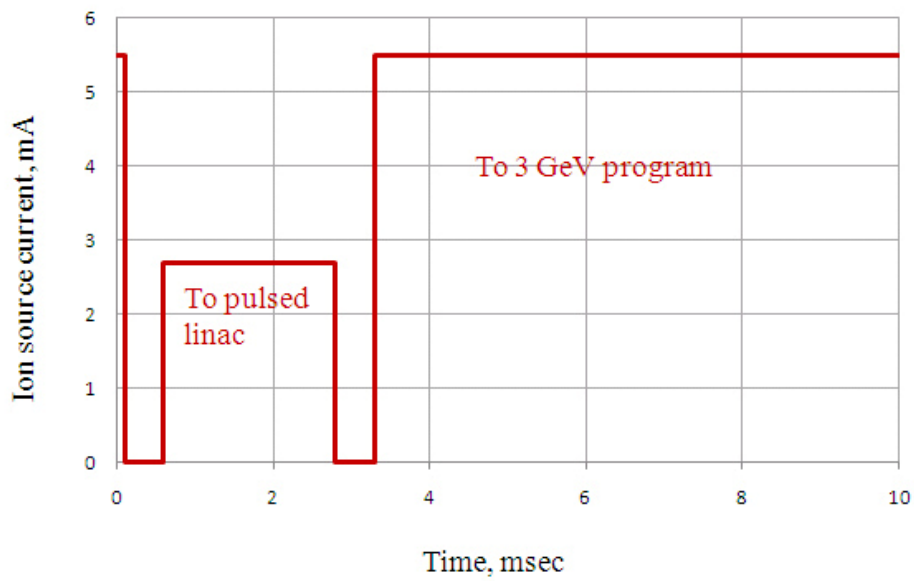

Figure IV-2: The ion source current as a function of time.

The H^- ion source is specified to provide 10mA DC current. The transverse emittance is required to be about 0.25 mm-mrad (rms normalized) and beam halo must be controlled to prevent unacceptable resultant beam losses at high energies.

The CW RFQ section provides bunching of the beam at 325 MHz and acceleration to 2.5 MeV. There are a number of CW RFQs operating at room temperature for beam currents of up to 100 mA and energies of up to ~7 MeV. These are summarized in Table IV-1, including possible designs for Project X at 162.5 and 325 MHz. The LBNL group has conducted preliminary CW RFQ studies based on their experience with the SNS front end system.

The RFQ is an electrostatically focused FDFD strong-focusing lattice with accelerating field (E_z) added as a perturbation. The energy bandwidth of the focusing lattice allows unaccelerated beam to be transported to the exit. About 90% of the beam is typically captured and accelerated to full energy. However, there is a low-energy tail that needs to be removed in the MEBT prior to injection into the SRF linac, possibly by a dipole magnet-based energy selector. The output longitudinal beam emittance is somewhat dependent on the beam current and can increase at lower currents. Two RFQs were studied, 162.5 MHz and 325 MHz. The requirements for both were 2.5 MeV, 10 mA beam current, and 0.25 mm-mrad emittance (RMS, normalized). The design was optimized to meet both beam requirements and thermal management requirements. The thermal management is critical because of high wall power density, which can lead to material stresses and geometric deformations, difficulties with maintaining frequency, and field distribution. It is also important to manage "hot spots" in the RF structure. This can be accomplished by a careful selection of cooling fluid passages configuration.

The RFQs are based on the so-called kick-bunching principle[11], which has several advantages for the low-current designs. This design approach is used in the IUCF RFQ. Table IV-1 presents several representative RFQs. Two last columns show RFQ parameters for this concept.

[11] Staples, Linac94

	CRITS	KOMAC	LEDA	IUCF	Proj-X 162	Proj-X 325	
Frequency	267	350	350	213	162.5	325	MHz
Injection Energy	50	50	75	20	35	30	keV
Output Energy	1270	3000	6700	700	2500	2500	keV
Current	86	23	110	1	10	10	mA
Length	147	324	800	118	385	287	cm
Length/Lambda	1.3	3.8	9.3	0.8	2.1	3.1	
Vane-Vane Voltage	78	100	102	35	90.8	64.2	kV
Peak E-field	28.8	33.1	33.6	13.8	20.7	27.6	MV/m
E-field/Kilpatrick	1.75	1.8	1.83	0.91	1.52	1.55	
Cavity Power	159	350*/417	1200	8.4*/12	155*	149*	kW
Power/Length	107	108	150	7.1	40	52	kW/m
Avg Wall Power Density	4.6	13	11.4	0.7	2.1	5.2	W/cm^2
Max Wall Power Density	116.7		65				W/cm^2
r_0 (transverse vane tip radius)				0.31	0.61	0.31	cm
minimum longitudinal radius				0.52	1.2	0.69	cm
Output rms Momentum Spread					0.15	0.15	percent
Output Longitudinal Emittance		0.246	0.174	0.024	0.056	0.046	MeV-Degree
Output Transverse Emittance		0.023	0.022	0.010	0.031	0.028	cm-mrad
Transmission			90	85	94	90	percent

*=Calculated
Thanks: Dale Schrage for CRITS, LEDA

Table IV-1: The RFQ parameters

Both concepts have similar power requirements and could meet the needs of Project X. The 325 MHz RFQ is selected for the Reference Design as it provides more preferable beam dynamics in the 325 MHz linac. RF sources for a CW RFQ of up to ~1 MW power are available at both 162.5 MHz and 325 MHz.

We assume that the chopper is capable of removing individual bunches or groups of bunches in an arbitrarily specified pattern. Such a chopper may be made of a single or multiple kickers. Preliminary simulations of the RFQ shows that the 100% bunch length is 1 ns while the spacing between bunches is 3 ns. The chopper pulse should deflect the bunch by about 10 mrad. In order to absorb the deflected beam, the beam displacement should be at least 4 RMS beam sizes at the absorber location. The pulse flattop should be 0.8 ns or more. Such a scheme requires a wide band chopper with bandwidth of ~1 GHz. A possible design can be based on a meander line proposed for the SPL in CERN[12]. The development of a chopper with these capabilities is a major focus of the Project X R&D program.

The MEBT section will contain the above mentioned chopper, several 325 MHz room temperature (RT) bunching cavities operating in CW mode in order to condition the beam for injecting it into the SRF 325-MHz linac section, and instrumentation for beam diagnostics. The cavity design is shown in Figure IV-3 and performance parameters are shown in Table IV-2.

[12] T. Kroyer, F. Caspers, E. Mahner, "The CERN SPL Chopper Structure: A Status Report", CARE-Report-06-033-HIPPI, Geneva, Switzerland, October 2006

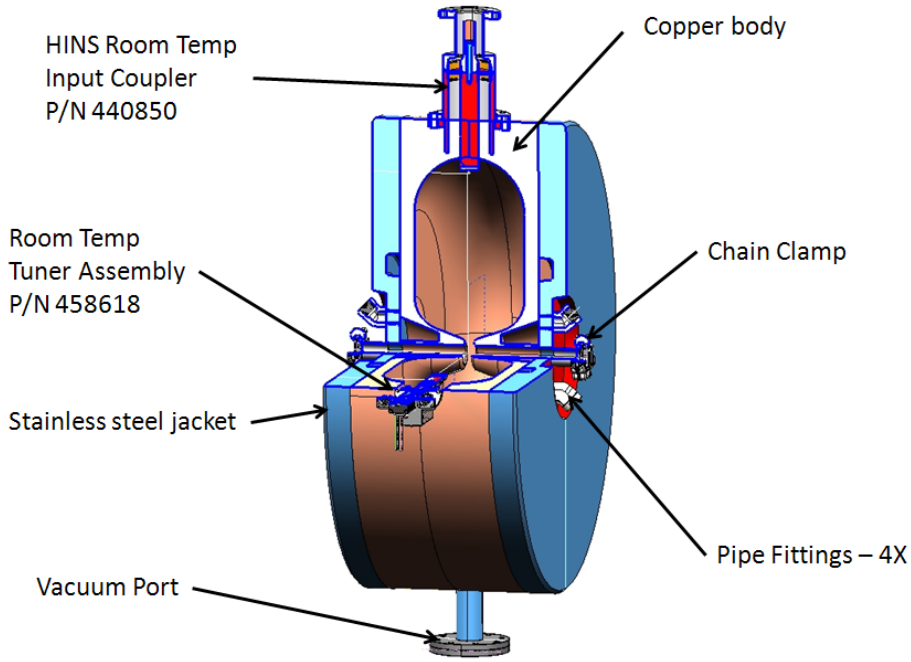

Figure IV-3: Layout of 325 MHz CW room temperature bunching cavity.

Parameter	
Frequency, MHz	325
Q factor	28468
Aperture radius, mm	15
Gap, mm	13
Particle energy, MeV	2.5
Effect. shunt impedance, MOhm	2.31
Max. energy gain, keV	75
Power , kW	2.43
Max. electric surface field, MV/m	16.8

Table IV-2: Parameters of room temperature bunching cavity

IV.1.2 **Low-beta section (2.5-160 MeV, 325 MHz)**

Three cavity types are required to get from 2.5 to 160 MeV (β=0.07 to 0.52). The general requirements on these cavities are listed in Table III-1. All cavities are of the single spoke resonator (SSR) type. During the R&D phase studies will be completed comparing the relative benefits of these and other possible low beta configurations.

Acceleration from 2.5 to 10 MeV utilizes superconducting SSR cavities (SSR0) with β_G=0.114. The cavity shape has been optimized , with the results shown in Table IV-3. The transit time factors versus β and the field patterns are shown in Figure IV-4.

F(MHz)	325	MHz
Aperture	30	mm
β_G	0.114	
R/Q	108	Ω
G	50	Ω
E_{max}/E_{acc}	5.63	
H_{max}/E_{acc})	6.93	mT/(MV/m)
$D_{eff}=(2\beta_G\lambda/2)$	105	mm

Table IV-3: Parameters of the low-beta spoke cavities (SSR0)

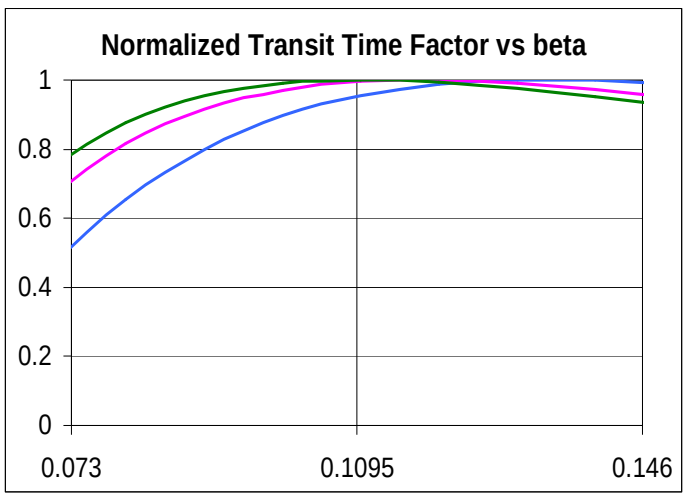

a)

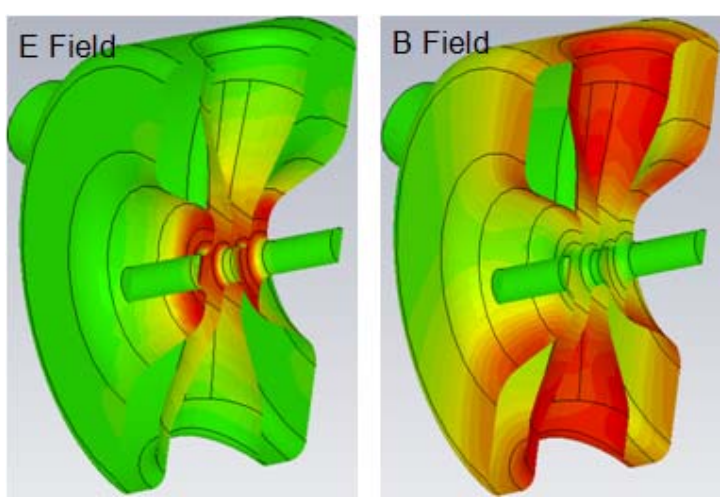

b)

Figure IV-4: The transit time factor vs. proton beta for three different cavities having β_G=0.135 (blue), β_G=0.114 (pink), and β_G=0.11 (green) (a); and cavity layout with field pattern for compromise cavity with β_G=0.114 (b). One can see that the surface magnetic field is distributed homogeneously on the spoke surface.

Acceleration from 2.5 to 10 MeV utilizes superconducting SSR cavities (SSR0) with β_G=0.114. The cavity shape has been optimized , with the results shown in Table IV-3. The transit time factors versus β and the field patterns are shown in Figure IV-4.

Mechanical design of the SSR0 cavity and layout of a focusing period, including one cavity and one SC solenioid, are shown in Figure IV-5. The ribs provide resonant frequency sensitivity versus the pressure fluctuations small enough in order to mitigate the problems with microphonics.

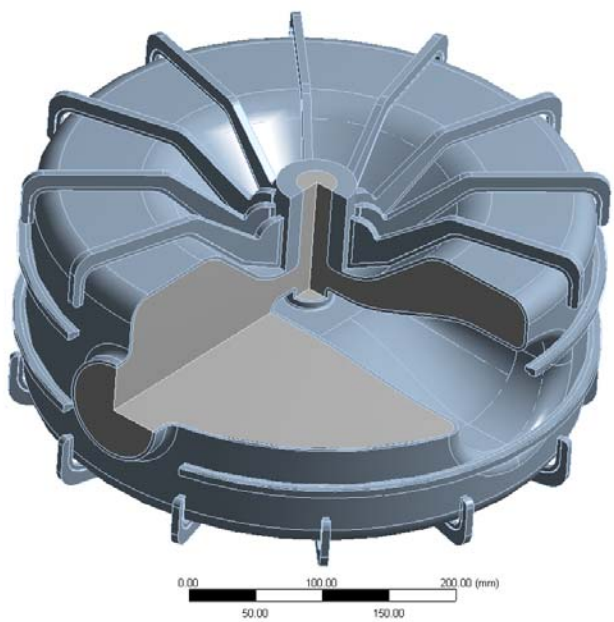

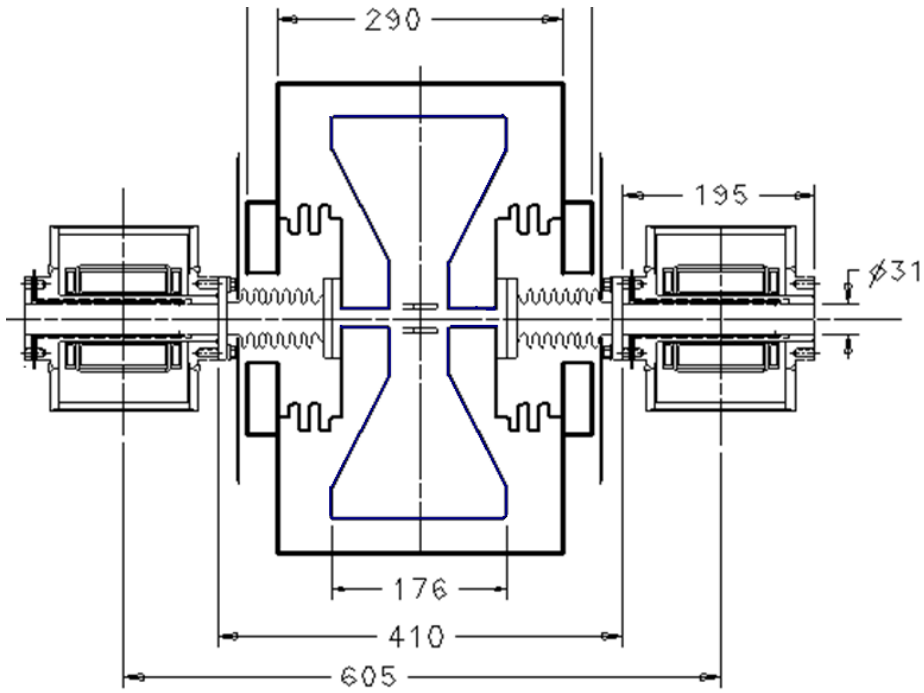

Figure IV-5: Preliminary mechanical design of the SSR0 cavity and one period layout (below)/ Note, dimensions are in mm.

Acceleration from 10 to 32 MeV utilizes superconducting SSR cavities with β_G=0.215 (SSR1). The cavity shape has been optimized with results shown in Table IV-4 . A SSR1 cavity matching these requirements has been designed, fabricated, and tested with rf power as part of the HINS program. The mechanical design, including focusing elements, is displayed in Figure IV-6.

F(MHz)	325	MHz
Aperture	30	mm
β_G	0.215	
R/Q	242	Ω
G	84	Ω
E_{max}/E_{acc}	3.84	
H_{max}/E_{acc}	5.81	mT/(MV/m)
$D_{eff}=(2\beta_G\lambda/2)$	198.5	mm

Table IV-4: Parameters of the low-beta spoke cavities (SSR1-02)

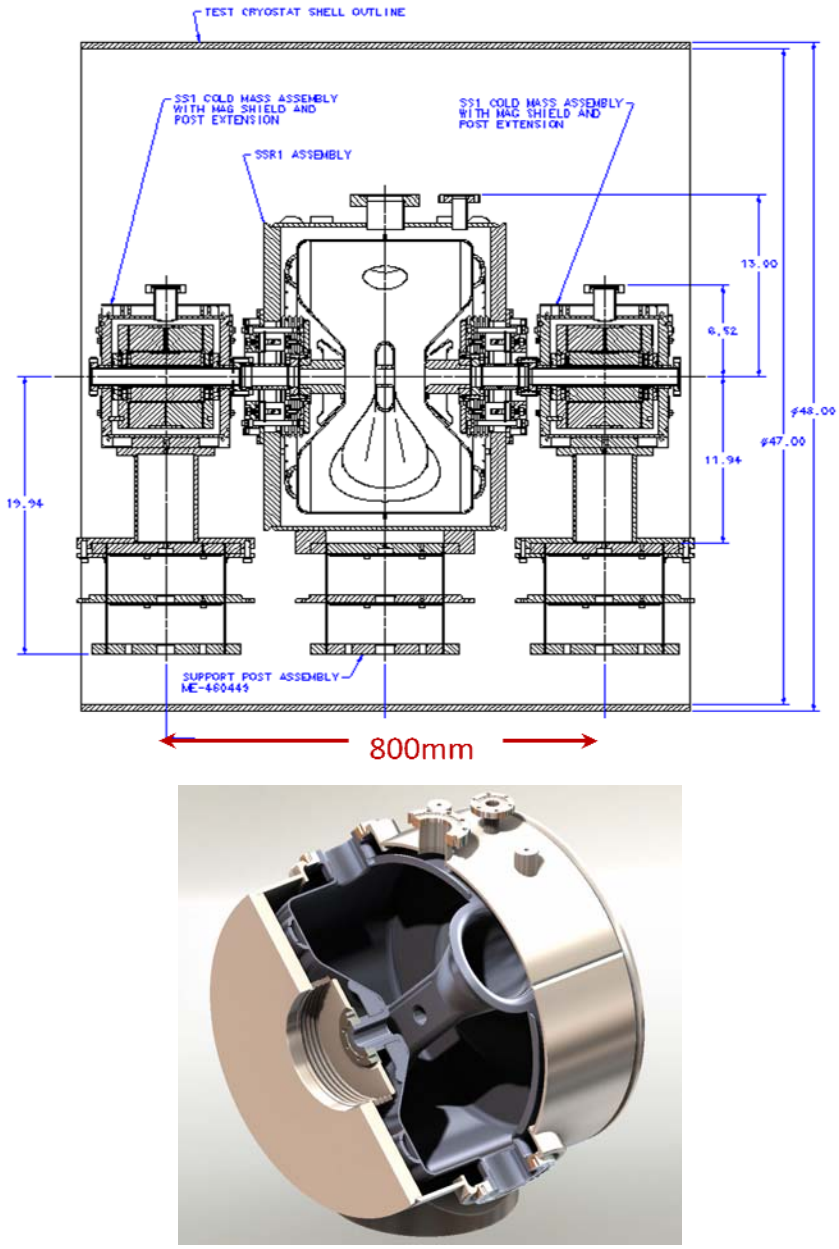

Figure IV-6: SSR1 cavity mechanical design and cutaway view.

Figure IV-7 shows the first(SSR1-02) cavity fabricated as part of the HINS program. The left photograph shows the bare cavity, the left a "dressed" cavity encased in its He jacket with ancillary slow and fast (piezo) tuners. The measured performance of the bare cavity in a vertical test is displayed in Figure IV-8. Measurements at both 4K and 2K are presented. This cavity shows an accelerating gradient of 16 MV/m at a Q_0 of 1.1×10^{10} at the 2K operating point, well above the required 7 MV/m. Conversely, the cavity shows a Q_0 of 1.8×10^{10} at an accelerating

gradient of 7 MV/m. The measured surface resistance of this cavity as a function of temperature is shown in Figure IV-9.

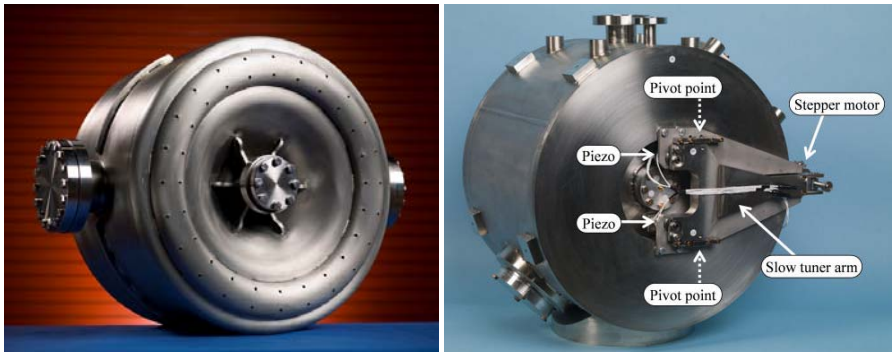

Figure IV-7: Photograph the bare and dressed prototype SSR1 cavity

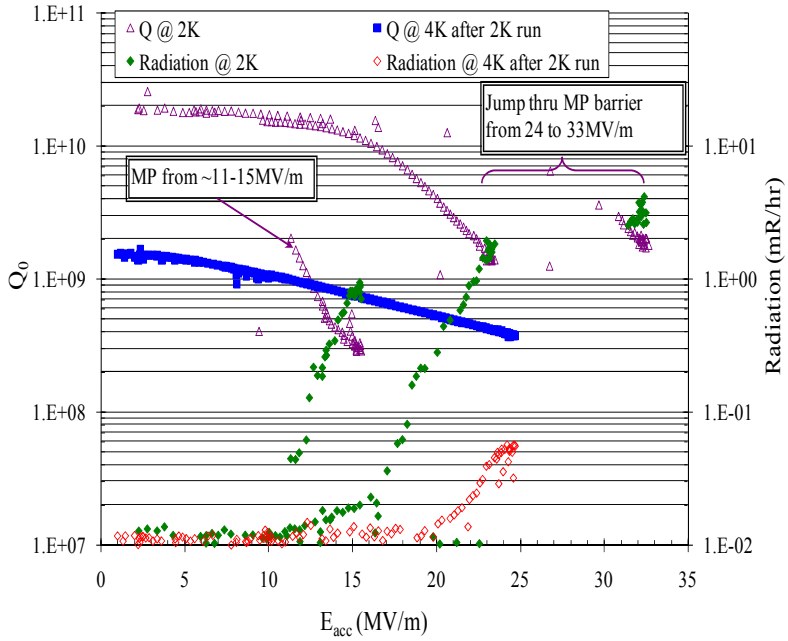

Figure IV-8: Q_0 vs. acceleration gradient from the first cold test of the SSR1-02 single-spoke cavity ($\beta = 0.22$). Note that acceleration gradient was determined as the energy gain per cavity over the cavity effective length, taken of $2/3\beta\lambda = 132$ mm. Magenta points present the quality versus the gradient shown on different stages of the cavity conditioning at 2 K. In blue the quality vs. the gradient is shown at 4 K after 2K run. Maximal gain is 3.3 MeV @ 4K; 4.4 MeV @ 2K.

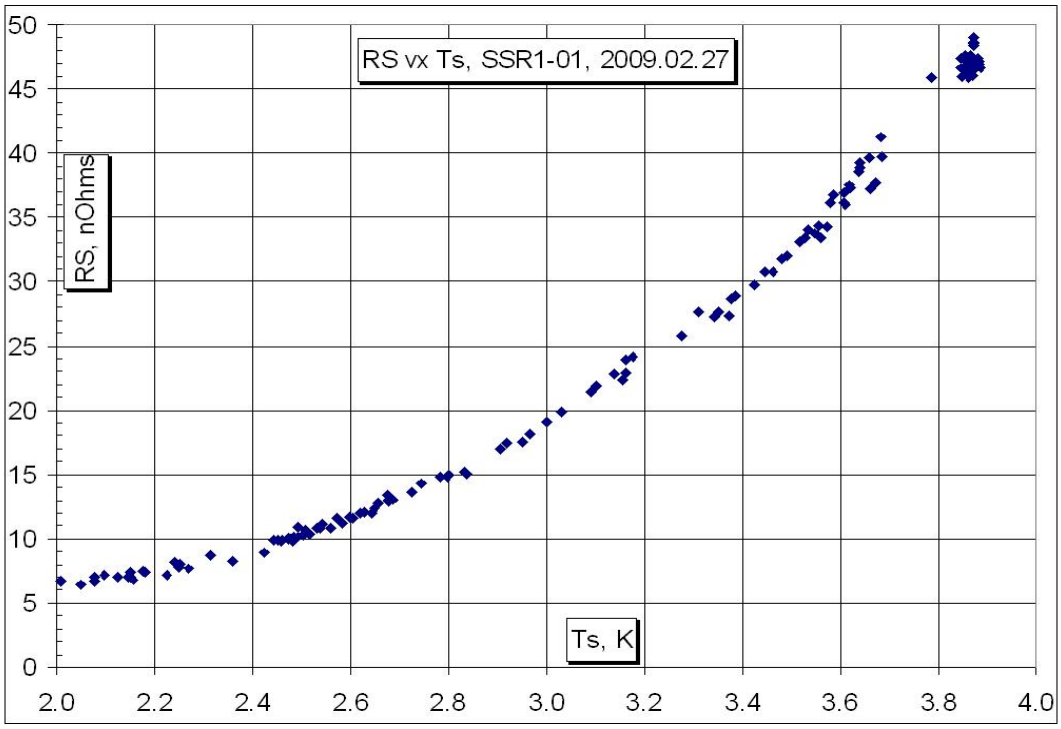

Figure IV-9: Temperature dependence of the surface resistance for SSR1 cavity.

Acceleration from 32 to 160 MeV utilizes superconducting SSR cavities with β_G=0.42 (SSR2). The cavity requirements are listed in Table IV-5. A mechanical design for this cavity has Table IV-5: Parameters of the low-beta spoke cavities (SSR2)also been developed by the HINS programl. The cavity layout is shown in the Figure IV-10. The electromagnetic optimization as well as mechanical design was completed including a piezo tuner and a helium vessel.

F(MHz)	325	MHz
Aperture	40	mm
β_G	0.42	
R/Q	292	Ω
G	109	Ω
E_{max}/E_{acc}	3.67	
H_{max}/E_{acc})	6.93	mT/(MV/m)
$D_{eff}=(2\beta_G\lambda/2)$	386.5	mm

Table IV-5: Parameters of the low-beta spoke cavities (SSR2)

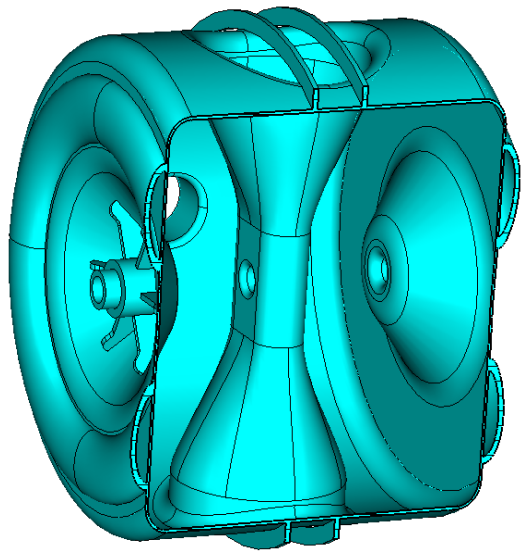

Figure IV-10: SSR2 cavity layout.

F(MHz)	325	MHz
Aperture	40	mm
β_G	0.42	
R/Q	292	Ω
G	109	Ω
E_{max}/E_{acc}	3.67	
H_{max}/E_{acc})	6.93	mT/(MV/m)
$D_{eff}=(2\beta_G\lambda/2)$	386.5	mm

Table IV-6: Parameters of the low-beta spoke cavities (SSR2)

Parameters of the three families of 325 MHz cavities, corresponding to the requirements displayed in Table III-1, are summarized in Table IV-7. We assume a surface resistance ~6 nOhm at 2 K (see Figure IV-9) and 30% of medium-field Q-slope for 60 mT of the magnetic surface field. Each cavity of SSR0, SSR1 and SSR2 types will be powered by a separate RF source. Inductive output tubes (IOTs) or solid state amplifiers are feasible for the required power consumption at 325 MHz.

cavity type	β_G	Freq MHz	$U_{acc,\,max}$ MeV	E_{max} MV/m	B_{max} mT	R/Q, Ω	G, Ω	$Q_{0,2K}$ $\times 10^9$	$P_{max,2K}$ W
SSR0	β=0.114	325	0.6	32	39	108	50	6.5	0.5
SSR1	β=0.215	325	1.47	28	43	242	84	11.0	0.8
SSR2	β=0.42	325	3.34	32	60	292	109	13.0	2.9

Table IV-7: Parameters of 325 MHz accelerating cavities.

IV.1.3 **Medium-beta section (160 – 2000 MeV, 650 MHz)**

Acceleration from 160 MeV to 2 GeV will be provided by two families of the 5-cell elliptical cavities operating at 650 MHz and designed to β_G =0.61 and β_G =0.9. The cavity shape is optimized to decrease the field enhancement factors (magnetic and electric) in order to improve the interaction between the beam and the cavities. In order to do this, the cavity aperture should be as small as possible subject to the following considerations:

- field flatness,
- beam losses,
- mechanical stability,
- reliable surface processing.

The working gradient is chosen to provide the peak surface magnetic field that allows operation below high-field Q-slope, see Figure III-4. For a frequency of 650 MHz the peak magnetic field should be not greater than ~70 mT. In addition we require that the peak surface electric field be lower than 40 MV/m in order to avoid the risk of strong field emission.

For a given relative error in the frequencies of the cavity cells field flatness is determined mainly by the distance between the operating frequency and the frequency of the neighbouring mode $\pi(n-1)/n$, as follows from the linear perturbation theory, or by the coupling k between the cavity cells and the number of cells:

$$\delta E/E \sim f_\pi/|f_\pi - f_{\pi(n-1)/n}| \equiv f_\pi/\delta f \approx 1/kn^2.$$

Thus, for a required field flatness $k \sim 1/n^2$, and a cavity with a smaller number of cells allows smaller coupling k. For 9-cell ILC cavity one has $\delta f/f_\pi$ of 6e-4 (k=1.87%). For a 5-cell cavity one can take the same $\delta f/f_\pi$ at least, that gives $k > 0.6\%$. For comparison, the cavity aperture for the 805 MHz high-energy part of the SNS proton linac, that is close to Project-X linac in average current, is 83 mm for low-beta part and 100 mm in high-beta part. Thus, it appears plausible that such an aperture would be consistent with tolerable beam losses. It appears that these apertures also allow the required surface processing.

However, 650 MHz cavities require the walls thicker than at 1.3 GHz. In Figure IV-11 the results are shown of a simulation of the cavity sag caused by its weight. The maximal sag of the ILC cavity is 120 μm for 2.8 mm wall thickness. In order to have the same sag for 650 MHz cavity having 100 mm aperture, the wall thickness is to be ~4 mm. Note that a small cavity wall slope (designated by α in Figure IV-12) gives more freedom to decrease the field enhancement factors. However, the slope is limited by surface processing and mechanical stability requirements. For beta=0.9 we select a slope of 5°. For beta=0.61 the slope is reduced to 2°, in order to maintain an acceptably low field enhancement with this shape.

Optimization of the two 650 MHz cavity shapes was done based on the constraints discussed above. Cavity performance parameters are summarized in Table IV-8. The physical description of the cavity shapes is displayed in Figure IV-12 and Table IV-8.

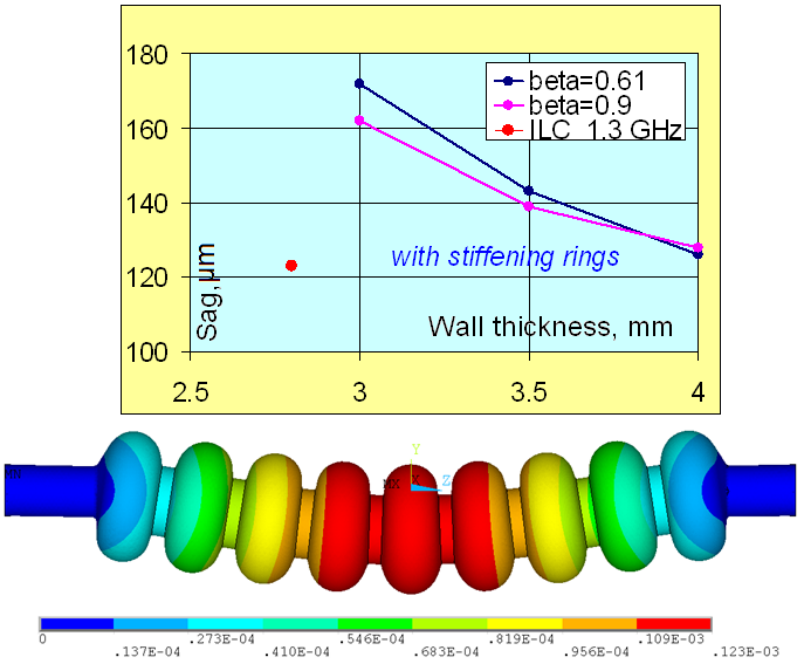

Figure IV-11: The cavity sag versus the wall thickness.

Beta	0.61	0.9
R/Q, Ohm	378	638
G-factor, Ohm	191	255
Max. gain per cavity, MeV(on crest)	11.3	19.9
Gradient, MeV/m	16.1	19.2
Max. Surfae electric field, MV/m	36.4	37.3
E_{pk}/E_{acc}	2.26	2
Max surf magnetic field, mT	68	72
B_{pk}/E_{acc}	4.21	3.75

Table IV-8: RF parameters of the 650 MHz cavities.

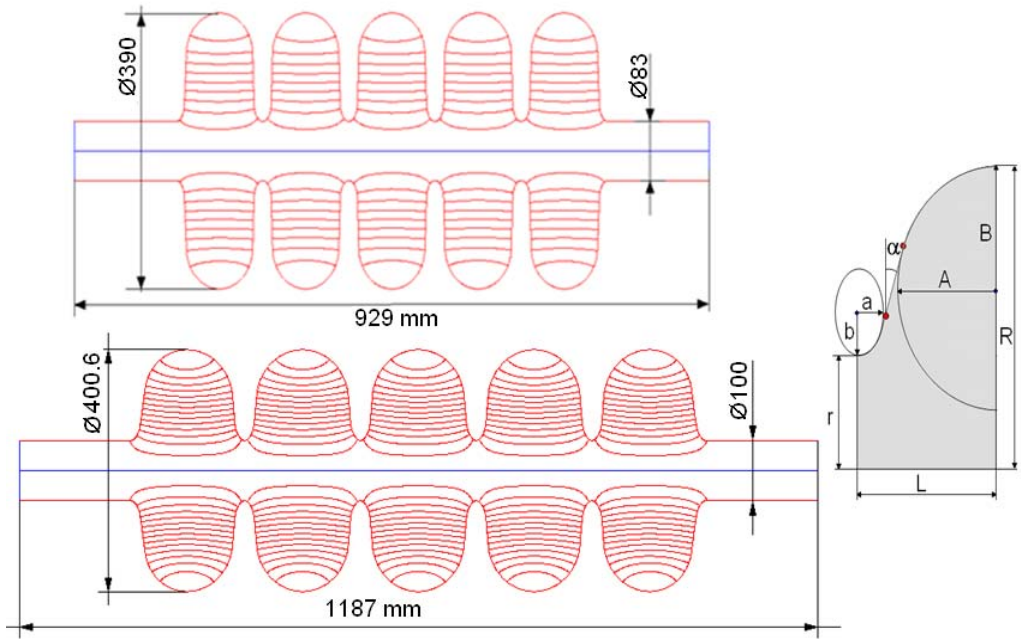

Figure IV-12: Layout of 650 MHz cavities. Beta=0.61(top) and beta=0.9 (bottom).

Dimension	Beta=0.61		Beta=0.9	
	Regular cell	End cell	Regular cell	End cell
r, mm	41.5	41.5	50	50
R, mm	195	195	200.3	200.3
L, mm	70.3	71.4	103.8	107.0
A, mm	54	54	82.5	82.5
B, mm	58	58	84	84.5
a, mm	14	14	18	20
b, mm	25	25	38	39.5
α,°	2	2.7	5.2	7

Table IV-9: Dimensions of the 650 MHz cavities.

Cryogenic losses in the cavities are determined by the R/Q value, G-factor and surface resistance. The surface resistance is in turn is a sum of residual resistance and BCS resistance. Modern surface processing technology may provide a residual resistance of ~5 nΩ (see, for example, *N. Solyak and V. Yakovlev, "Assumption about Q values in CW linac", http://projectx-docdb.fnal.gov/*). BCS resistance as a function of the frequency *f* and temperature *T* may be estimated using formula

$$R_{BCS} = 2.10^{-4}\frac{1}{T}\left(\frac{f}{1.5}\right)^2 e^{-17.67/T}$$

which gives an average value of the resistance among results achieved for different cavities. For 650 MHz one has ~3 nΩ for BCS and, thus, ~8 nΩ total. Assuming a medium field Q-slope at the peak field of 70 mT is about 30%, that gives the target for Q_0 value of the 650 MHz cavity of ~2×10^{10}, and losses at the operating gradient (18.7 MeV/m) of ~30 W/cavity, or < 250

W/cryomodule. The preliminary mechanical design of the beta=0.9 cavity is shown in Figure IV-13.

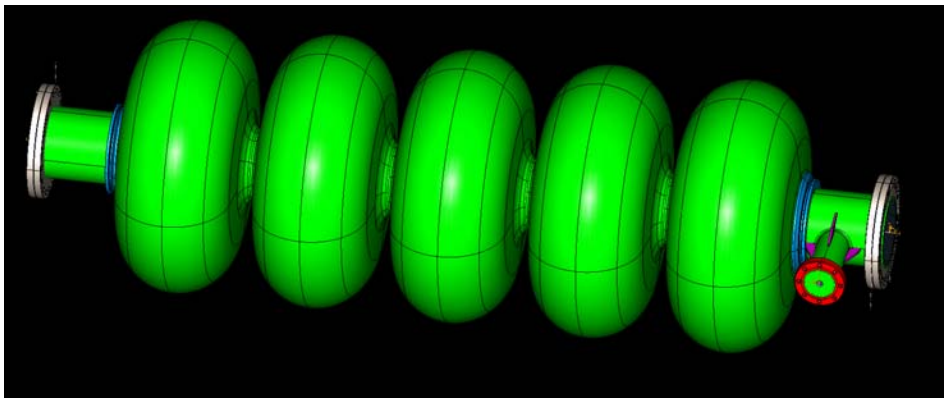

Figure IV-13: Preliminary mechanical design of the beta=0.9 cavity.

IV.1.4 High-beta section (2000-3000 MeV, 1300 MHz)

Acceleration from 2000 to 3000 MeV is provided by a β=1.0, 9-call cavity operating at 1300 MHz. The configuration is based on ILC-type 9-cell cavities and the ILC type-4 cryomodule is used. The gradient is chosen to be 16.4 MeV/m, corresponding to a surface magnetic field of 70 mT. For this gradient we expect a Q_0 that is at least 1.5×10^{10} – see Figure IV-14 where the test results for various TESLA 9-cell cavities are summarized. A photograph of the ILC 9-cell cavity is given in Figure IV-15. Performance requirements for the 1300 MHz cavities are summarized in Table IV-10.

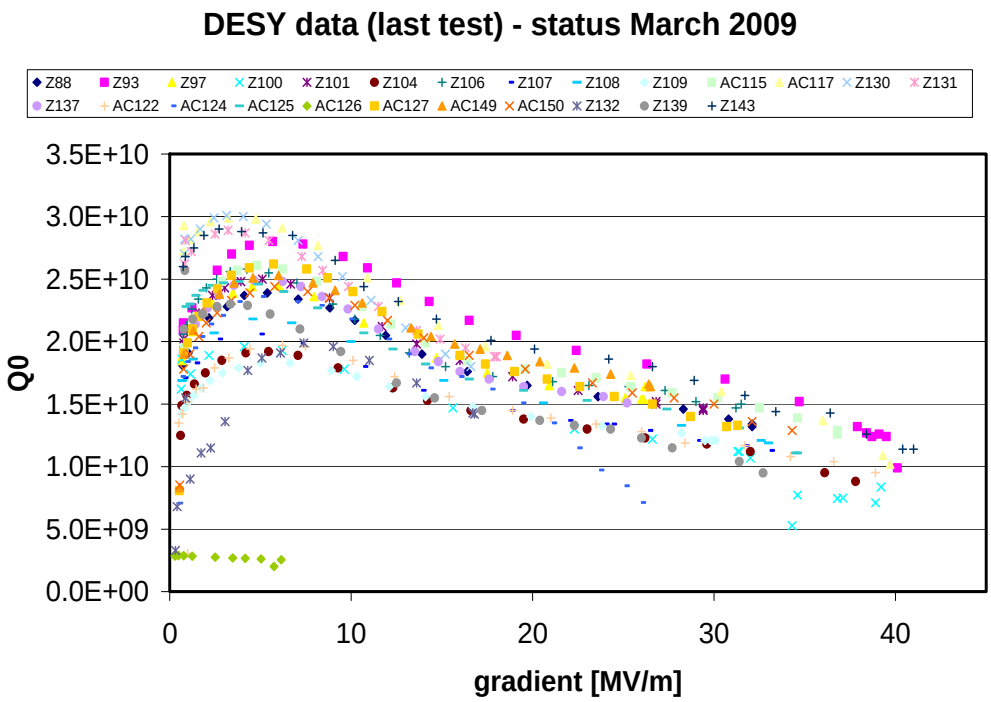

Figure IV-14: Q-factor versus acceleration gradient for 9-cell standard TESLA cavities (lower figure).

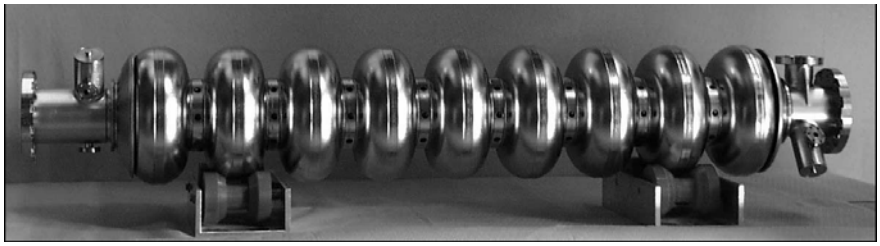

Figure IV-15: ILC 1300 MHz accelerating cavity

Beta	1
R/Q, Ohm	1036
G-factor, Ohm	270
Max. gain per cavity, MeV(on crest)	17
Gradient, MV/m	16.4
Max. surface electric field, MV/m	33
E_{pk}/E_{acc}	2
Max surface magnetic field, mT	70
B_{pk}/E_{acc}	4.26
Quality factor	1.5e10
Power losses at 2K, W	19

Table IV-10: RF parameters of the ILC-type 1.3 GHz cavities.

A total of 72 cavities are required in the 1300 MHz section. These cavities are contained within 9 cryomodules. Each cryomodule contains 8 accelerating cavities and one focusing element. Figure IV-16 shows the ILC Type-4 cryomdoule schematically accompanied by the disposition of focusing elements within neighboring cryomodules.

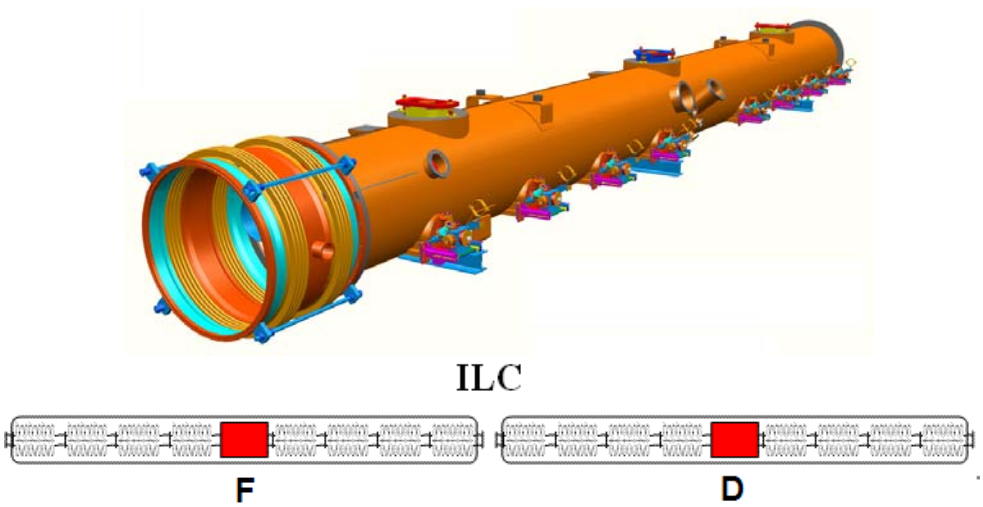

Figure IV-16: Type-4 ILC cryomodule (upper) and focusing schematics (lower).

IV.1.5 CW Accelerating Structures Summary

The physical parameters associated with all accelerating structures within the CW linac are summarized in Table IV-11. The average energy gain per cavity throughout the CW linac is given in Figure IV-17. Power consumption, tolerable microphonic amplitude, loaded Q and cavity bandwidth are shown in Table IV-12 (see also Figure III-6 for RF power consumption in the linac cavities).

	SSR0	SSR1	SSR2	LE	HE	ILC
# Cavities	26	18	44	42	96	72
# Solenoids	26	18	24	0	0	0
# Quadrupoles	0	0	1	42	24	9
# Cryomodules	1	2	4	7	12	9
Length, m	16.26	15.2	39.1	88.2	151.71	113.55

Position, m	0	16.26	31.46	70.56	158.76	310.47
Period Length, m	0.61	0.8	1.6	4.2	12.64	25.23
#Periods	26	18	24	18	18	9
Transition Energy, MeV	9.77	30.9	158.5	530.6	1964	3117
Transition β	0.143	0.251	0.518	0.769	0.946	0.973

Table IV-11: Linac components.

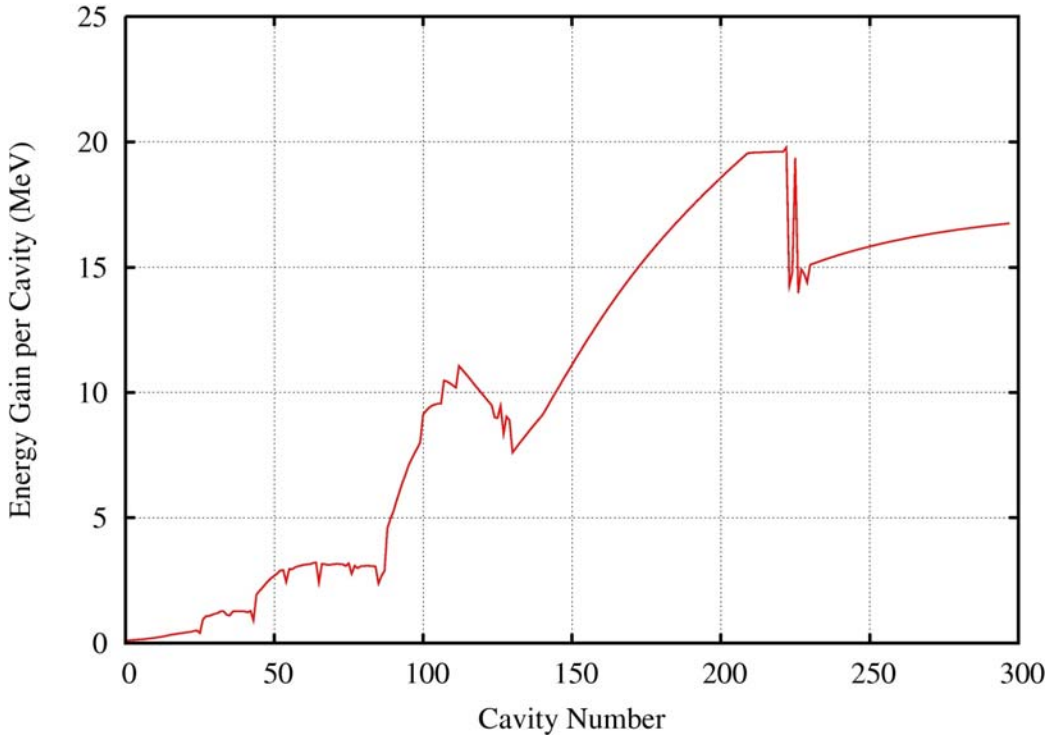

Figure IV-17: The energy gain per cavity. Cavities 1-88 are 325 MHz, 89-226 are 650 MHz, and 227-298 are 1.3 GHz.

Section	Freq MHz	Microphonic amplitude Hz	Minimal bandwidth Hz	Maximal loaded Q	Max power per cavity kW
SSR0	325	30	72	4.5e6	0.65
SSR1	325	30	68	5e6	1.7
SSR2	325	20	44	7.5e6	4.3
LE 650	650	15	33	2e7	16
HE 650	650	15	35	2e7	27
ILC	1300	30	85	1.5e7	20

Table IV-12: Maximal power consumption per cavity, tolerable microphonic amplitude, loaded Q and bandwidth.

IV.1.6 **RF power**

A klystron capable of 500 kW to 1 MW will be necessary to drive the RFQ at 325 MHz. Klystrons close to this frequency and at these power levels operate CW at the APS at Argonne National Lab.

RF requirements for the individual accelerating cavities are defined in Figure III-6 and in Table IV-12. Each of the cavities in the CW Linac will be powered by an independent RF system similar to what was done at SNS in Oakridge, TN. Power levels vary from a few hundred watts to 30 kW. Solid-state amplifiers have been chosen for the 325 MHz section of the linac. At 650 MHz inductive output tube amplifiers (IOT) have are utilized. IOTs have efficiencies approaching 60% and excellent saturation characteristics. However, IOTs also have inherently low gain and thus require a drive amplifier capable of several hundred watts. A 200 W solid-state amplifier will be utilized. For the 1300 MHz system the reference design is based on IOT's, but with solid state amplifiers and klystrons remaining under active considerations within the R&D program. In all SRF systems, a circulator will be used to isolate the cavity from the power amplifier (PA).

IV.2 **Collimators and Beam Dump**

IV.2.1 **Collimators**

There are a large number of beam collimators and beam dumps in the complex. It is assumed that beam collimation will start in the LEBT and continue in MEBT, where the beam chopper is located. Specific designs of these systems have not been done. Design guidance from systems at existing facilities, such as SNS and JPARC, for these systems will be utilized. Although specific locations have not been identified, it is assumed that a few transverse collimators will be strategically placed in the linac. A transverse and momentum collimation system will be located in the upstream end of the 8 GeV transport line to the Recycler. Currently under consideration is a transverse collimation system for the 3 GeV Experimental line. Final determination on the necessity and design of such system must wait for further linac tracking and modeling. The transport line collimation systems will typically be two stage systems similar to those at SNS (see section III-2-2). There are two beam dumps: the linac beam dump and the Recycler injection absorber. Table IV-13 lists requirements for high energy collimators, absorbers and beam dumps.

Table IV-13: Collimators, Absorbers, and Beam Dumps

Energy [GeV]	Function	Species	Beam fraction [%]	Beam Power [kW]	Survive (peak)
3	Linac Dump	H^-	10	300	Full int. 10 min
3	*Trans. Collimation*	*H^-*	*2*	*60*	*2 pulses full int.*
8	Trans. Collimation	H-	5	18	
8	Mom. Collimation	H-	5	18	
8	Injection Absorber	H^+	10	35	Full int 10 pulses

IV.2.2 **Recycler Injection beam absorber**

Energy deposition calculations for the initial conceptual Recycler injection absorber were performed with the MARS code. The absorber is designed to localize the beam loss at injection and meet the requirements of the Fermilab Radiological Control Manual (FRCM). The following issues were addressed: (i) surface water activation; (ii) residual activation; (iii) survival of the magnets around the absorber; (iv) cooling; and (v) stresses within the absorber core.

Current design of the absorber is based upon a preliminary design of an injection absorber for the Main Injector carried out for an earlier version of Project X. The essential features are a water cooled core made up of graphite and carbon disks in an inert atmosphere, similar to the Main Injector core, surrounded by a combination of tungsten, steel, concrete, and marble. The plan and elevation view are shown in **Error! Reference source not found.**. The current concept is to locate the absorber within the existing or an expanded MI-10 alcove. The absorber is shown at the Recycler elevation in the figure. Although the current location meets the radiological requirements, it is anticipated further optimization will be performed.

The beam intensity is 2.67×10^{13} 8-GeV proton/pulse at the repetition rate of 10 Hz, which corresponds to the beam power of 345 kW. It is anticipated that 2% of the beam will be sent to the absorber, but the thermal and shielding is designed for 10%.

Figure III-19 shows the star density at the shower max of a previous preliminary design where the expected static intensity was 10% of 1 MW or 100 kW. At this power the star density was at the allowable concentration limit. The current expectation is a maximum injected beam power of 345 kW. Although we expect 2% (7 kW) of the injected beam to go to the absorber, it is designed for a static beam power of 35 kW (10%). This reduces the star density in the soil down to ~30% of the concentration limit. Further optimization of the design will be carried out.

A preliminary thermal and stress analysis was also carried out for the absorber core. Several cases were analyzed, including, 36 kW and 100 kW static load and fault cases for cooling water failure and full beam power into the absorber. Figure IV-20 shows the

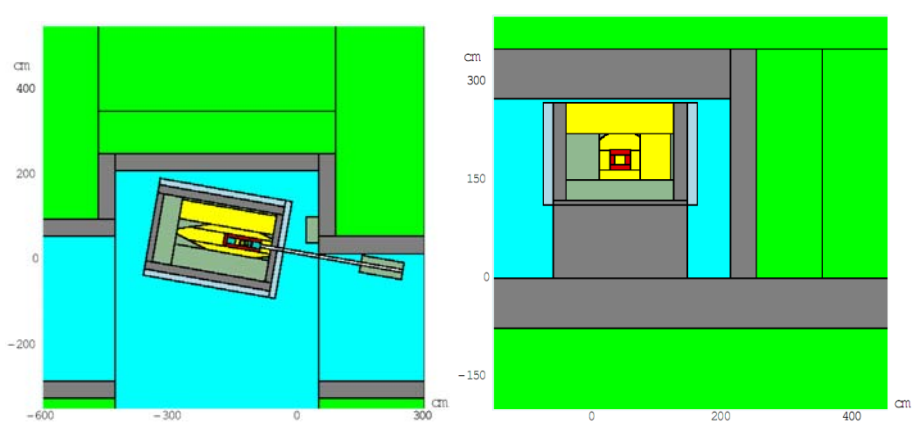

Figure IV-18: Plan view (left) and cross section (right) of the injection absorber in the tunnel.

temperatures within the core for 36 kW static heat load due to the energy deposition predicted from MARS. The temperature and stress values were OK for both static loads considered and the 36 kW case can sustain 10 minutes with no cooling. Even the 36 kW case is a factor of 5 over expected continuous beam load. The design of the absorber core and shielding and its location relative to the injection point will be further optimized for the current project configuration.

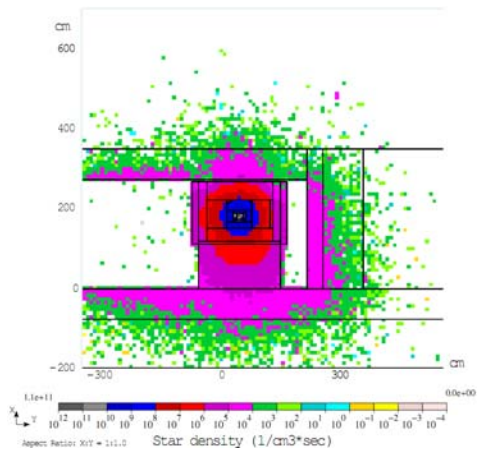

Figure IV-19: Calculated star density at the shower maximum.

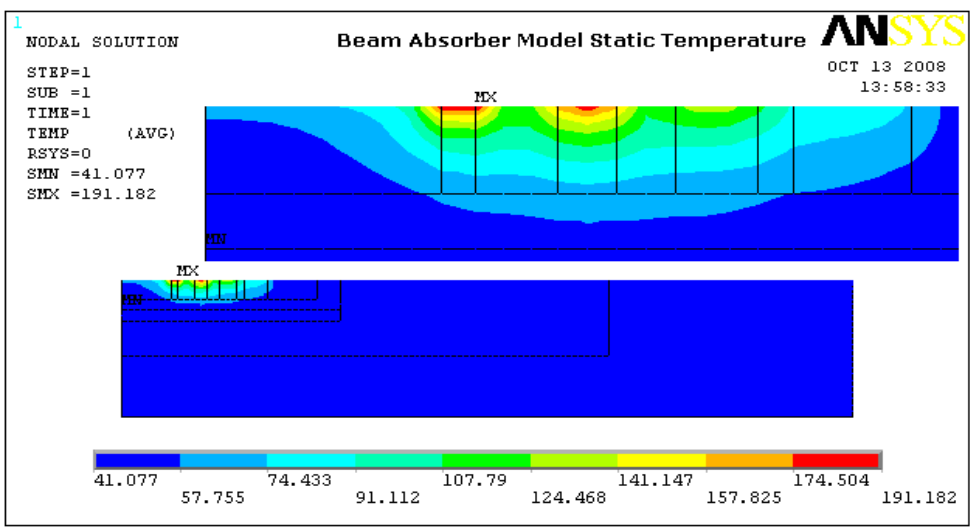

Figure IV-20: Model of water cooled core temperature with a 36 kW static heat load showing the graphite and tungsten sandwich core design. The maximum temperature in the Aluminum water cooled jacket is under 58 degrees C.

IV.3 **3-8 GeV Pulsed Linac**

IV.3.1 **Accelerating Structures**

Acceleration from 3 to 8 geV is provided by a β=1.0, 9-call cavity operating at 1300 MHz. The configuration is based on ILC-type 9-cell cavities and the ILC type-4 cryomodule is used. The gradient is chosen to be 25 MeV/m. Performance requirements for the 1300 MHz cavities are summarized in Table IV-1014.

Beta	1
R/Q, Ohm	1036
G-factor, Ohm	270
Gradient, MV/m	25
Max. surface electric field, MV/m	50
E_{pk}/E_{acc}	2
Quality factor	1e10

Table IV-14: RF parameters of the ILC-type 1.3 GHz cavities.

A total of 224 cavities are required in the 1300 MHz section. These cavities are contained within 28 cryomodules. Each cryomodule contains 8 accelerating cavities and one focusing element. Figure IV-21 shows the ILC Type-4 cryomdoule schematically accompanied by the disposition of focusing elements within neighboring cryomodules.

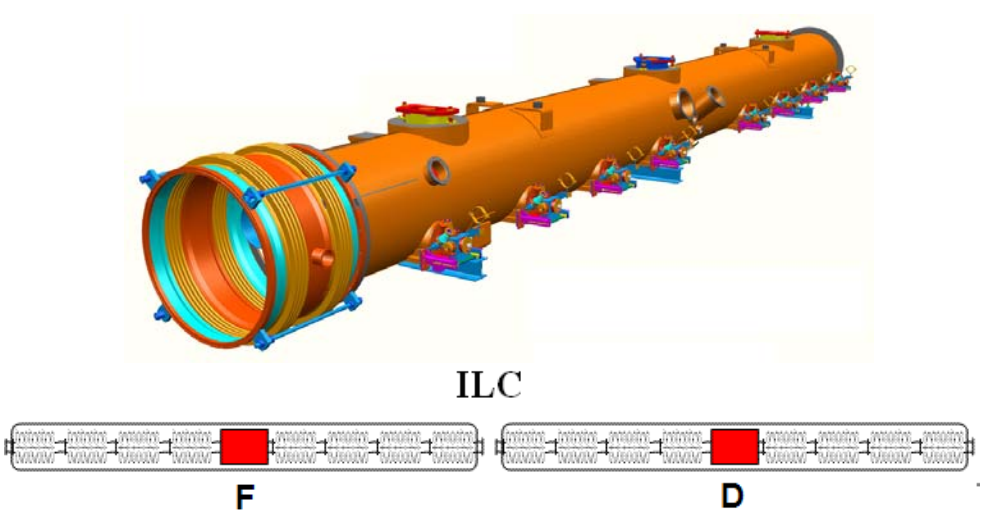

Figure IV-21: Type-4 ILC cryomodule (upper) and focusing schematics (lower).

IV.3.2 **RF Power**

We plan to use 1 Klystron per two cryomodules. The rf power distribution scheme would be very similar to that of the XFEL, with a vector-sum feed-back control providing both phase and amplitude control. The required Klystron needs to provide 1.6 MW in 5-ms pulses at 10 Hz repetition rate.

IV.4 **MI/RR**

As discussed in section **Error! Reference source not found.**, there are several areas of the Recycler and Main Injector that need upgrades to handle the proton intensity. Configuration details are discussed below.

IV.4.1 **Main Injector γ_t jump**

Designs for such a jump have been studied for the last 15 years. Details can be found in the Proton Driver Design Report[8]. A brief summary is included here. The system consists of 8 sets of pulsed quadrupole triplets. Each triplet has two quads in the arc and one of twice integrated strength in the straight section, with a phase advance of between each quadrupole. The perturbation to the original lattice is localized. In particular, the dispersion increase during the jump is small (ΔD_{max} H 1 m), which is the main advantage of a first-order jump system. Each triplet is optically independent from the others and provides roughly 1/8 of the total required jump amplitude (i.e., $\Delta\gamma_t$ H 0.25 per triplet). The power supply uses a GTO as the fast switch and a resonant circuit with a 1 kHz resonant frequency. The beam pipe is elliptical and made of Inconel 718. It has low electrical conductivity $\int$ and high mechanical strength so eddy current effects are relatively small. The eddy current effects scale as $\int d$, where d is the pipe wall thickness. The $\int d$ value of Inconel 718 is about four times lower than that of stainless steel.

The 8 pulsed triplet locations are summarized in Table IV-15. Since the original study was done, there have been changes to the Main Injector and these locations need to be revisited. A set of magnet design parameters has been developed and modeled (see Table IV-16).

Pulsed Triplet	Quad Locations
1	104, 108, 112
2	226, 230, 302
3	322, 326, 330
4	334, 338, 400
5	404, 408, 412
6	526, 530, 602
7	622, 626, 630
8	634, 638, 100

Table IV-15: Proposed γ_t quad triplet locations

Integrated Gradient	0.85 T
Vacuum pipe cross section (elliptical)	2.4 x 1.125 in
Field Quality, 1 inch radius	2%

Maximum length	17 in
Maximum Current	200 A
Maximum Voltage	As low as possible

Table IV-16: Pulsed quadrupole magnet parameters

IV.4.2 Electron Cloud Mitigation

Electron cloud generation could be a possible instability source for the intensities in the Recycler and Main Injector.

The best approach is to mitigate the generation of the cloud itself. There have been a series of measurements in the Main Injector, looking at secondary electron yield and cloud generation. A dedicated measurement setup now exists at MI-52, with newly developed RFA detectors. Both TiN and C coated beam pipes have been installed and measurements made. Both coatings show significant reductions in secondary electron generation when compared to an uncoated stainless steel pipe. VORPAL simulations are being benchmarked against these measurements.

Research continues into the coating process. The Main Injector beam pipe is captured in the dipole magnets, so coating needs to take place in situ. A test stand for in situ coating in a Main Injector dipole is under construction.

IV.4.3 RF Systems

The Recycler and Main Injector need new 1st and 2nd harmonic RF cavities. The same cavities will be used in both machines. A cavity design has been developed, with perpendicular biased tuners and and R/Q ~ 60 Ω. A mechanical drawing of the cavity is in Figure IV-22. Design of the 2nd harmonic cavity has not yet begun.

The power source needs to provide greater than 550 kVA of total power and 4.65 A of current. To simplify operation and maintenace, the source should have enough bandwidth to power both the 1st and 2nd harmonic cavities. The EIMAC 8973 power tetrode amplifier has a maximum operating frequency of 110 MHz, output power capabilities greater than 1 MW, and plate dissipation of 1 MW. An 8973 tube has been purchased and a power test stand is being developed.

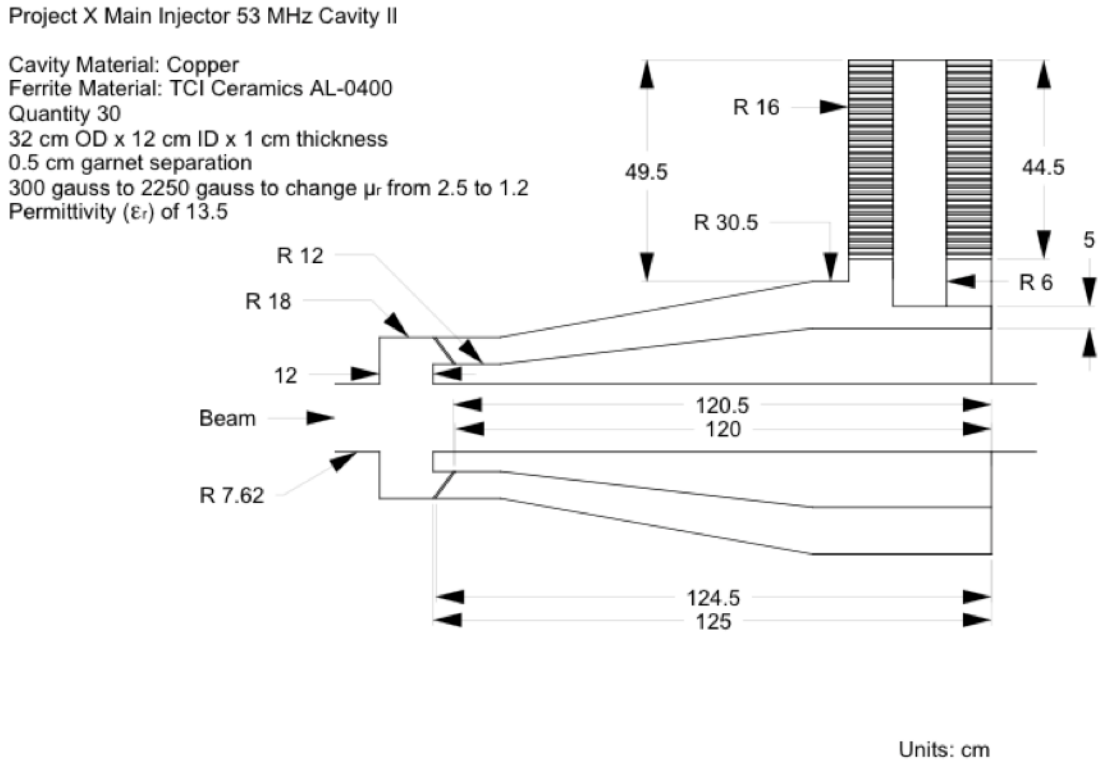

Figure IV-22: Mechanical drawing of proposed 53 MHz cavity.

IV.5 **Cryogenics**

The cryogenic system scope for Project X includes a new cryogenic plant, a cryogenic distribution system, and the necessary ancillary systems (purification system, cryogenic storage, etc.) to support the plant. A conceptual layout for the cryogenic system is shown in Figure IV-23.

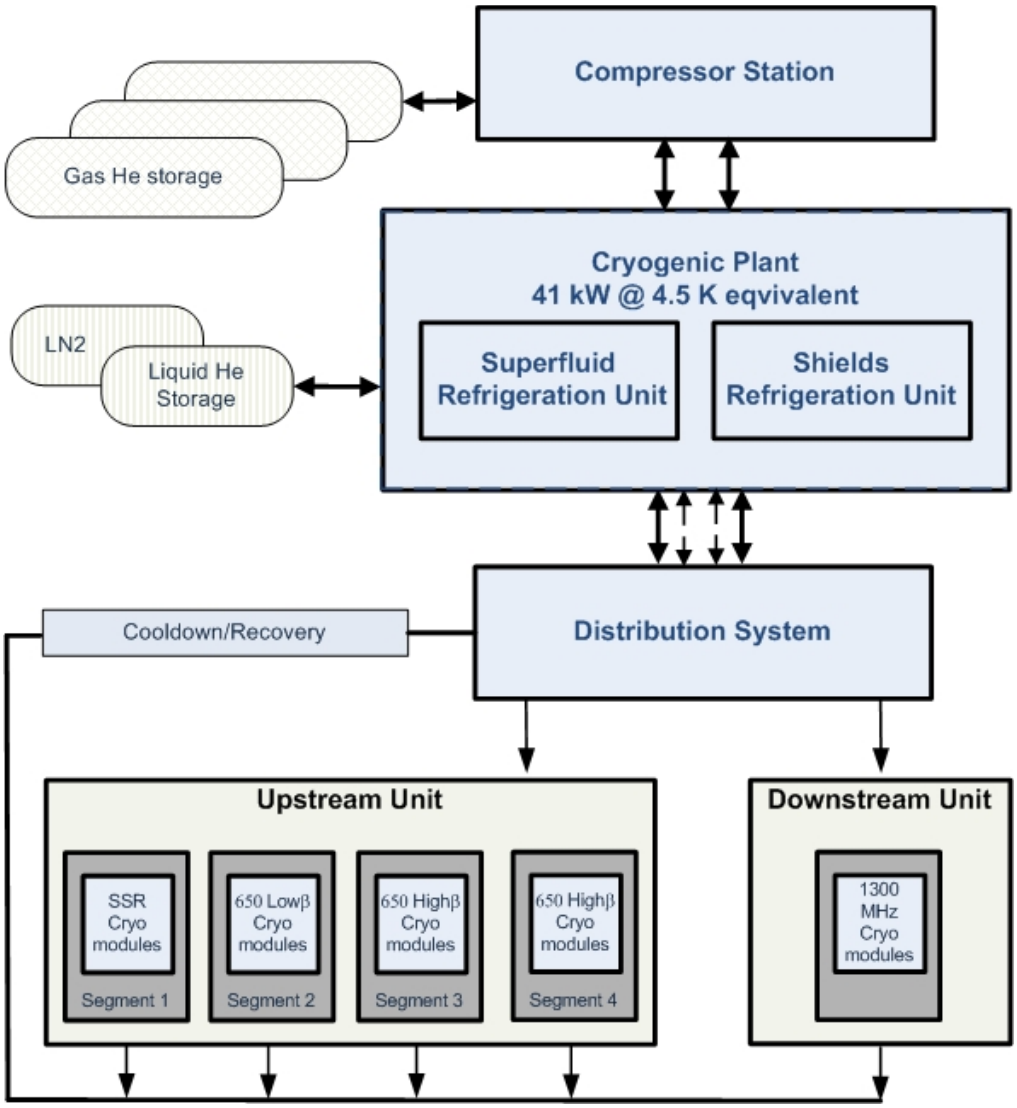

Figure IV-23: Conceptual Layout for the Project X Cryogenic System

The cryogenic distribution system accommodates a range of steady state and transient operating modes including RF on/RF off, cool down, and warm-up and fault scenarios. The system includes feed boxes, cryogenic transfer lines, bayonet cans, feed and end caps, string connecting and segmentation boxes, gas headers, etc. It will be capable of supporting operation of the linac within cool down and warm-up rate limits and other constraints imposed by accelerating SRF components. Protecting the superconducting RF cavities from over pressurization beyond the component's maximum allowable working pressure during fault conditions will be accommodated by the cryomodules and cryogenic distribution system. Liquid helium at 4.5K will be transported to the crab cavities in the 3 GeV transport line with a dedicated cryogenic distribution system similar to the existing Tevatron transfer line. Components of the cryogenic distribution system contain cryogenic control and isolation valves, cryogenic instrumentation, safety valves, etc.

It is assumed that on the time scale of the Project X, a large portion of the Tevatron ancillary cryogenic components will be available for use by the project. These components include

cryogenic nitrogen and helium dewars, gas storage tanks, purifier compressors, cryogenic transfer line and parts of the inventory management system.

Approximately 300 (Update!) SRF cavities distributed over the 350 (Update!) m length of the linac are cooled by two-phase superfluid liquid helium. The cavities are grouped in 34 cryomodules of six different types, SSR-0, SSR-1, SSR-2, 650-low β, 650-high β, and 1300 MHz cryomodules. For cost estimating purposes, all cryomodules are divided into three cryogenic units. The cryogenic feed point is located between the first and second units. The first cryogenic unit consists of SSR-0, SSR-1, SSR-2, 650-low β and 650-high β, while the second unit contains eight (8) CW 1300 MHz cryomodules. The third unit consists of the pulsed 1300 MHz cryomodules.

The upstream unit is subdivided into four (4) distinct cryogenic segments. The first segment contains seven (7) cryomodules (one (1) SSR-0, two (2) SSR-1 and four (4) SSR-2 cryomodules). The second segment comprises of seven (7) 650 MHz Low β cryomodules. The third and fourth segments each contain six (6) 650 MHz High β cryomodules. A cryogenic transfer line runs along the first cryogenic unit and is used to distribute superfluid helium and helium gas for the thermal shields and intercepts to each segment.

The second unit contains a single segment of eight (8) 1300 MHz cryomodules. The TESLA concept for connecting cryomodules is utilized for the 2nd and 3rd unit cryogenic distribution.

Operation of Project X in a continuous wave mode results in very high dynamic heat loads to the cryogenic system. For SRF components, dynamic heat load (due to RF power dissipation) on average is an order of magnitude greater than the static heat load (due to conduction and thermal radiation).

A preliminary heat load estimate has been performed. For the design study, an additional 50% margin is applied to the estimated heat loads to ensure the system could meet all operational requirements. With this factor, the total equivalent design capacity at 4.5 K for the entire linac is approximately 41 kW. The physical size of a plant of this capacity is too large to house in a single cold box. As a result, two cold boxes are envisioned; one to support the superfluid loads and one to support the thermal shield loads.

A wide range of possible cryogenic plant design solutions that satisfy all requirements and constraints for Project X will be studied further. Combining effective use of the existing Fermilab infrastructure with commercially available components requires further study. The final solution will be based on a cycle with either cold compression alone or utilizing a hybrid approach (both cold and ambient temperature compression). Ease of operation, reliability, ability to operate efficiently over a wide range of loads, capital and operational costs, and other factors will be considered in selecting the technology for the Project X cryogenic plant.

A study will be performed to ensure that the Project X cavity operating temperature and segmentation layout are optimized to minimize the combined capital and operating cost while maintaining system reliability.

IV.6 **Instrumentation**

Various beam instrumentation and diagnostics systems are necessary to characterize the beam parameters and the performance in all Project X sub-accelerators. For startup and initial beam commissioning we need to provide, at a minimum, beam instruments in order to observe:

- Beam intensity
- Beam position / orbit
- Transverse beam profiles
- Beam phase / timing

The high beam intensity / power and the presence of superconducting technologies also require a reliable, fail safe machine protection system (MPS) to prevent quenches in cryogenic elements or damage due to an uncontrolled loss of the high power beam. This system will be based on beam loss monitors (BLM) and other beam intensity monitors (toroids).

Beside these core beam instrumentation systems, more specialized beam diagnostics need to be provided, e.g. to characterize the longitudinal bunch profile and tails, transverse beam halo, and more advanced beam emittance measures. Even though some types of beam monitors (e.g. BPMs, toroids, etc.) can be standardized for most areas, the H^- source, the synchrotron, and injection / ejection areas demand some dedicated beam diagnostics (Allison scanner, fast Faraday cup, e-beam scanner, vibrating-wire, etc.).

A complete set of "beam instrumentation requirements" has to be established. Each sub-accelerator (linac, transport lines, MI, Recycler) needs to address the operating modes with the nominal, as well as non-standard beam parameters, and all requirements for the different beam instruments (resolution, precision, dynamic range, etc.). We foresee the following general detectors and systems for beam instrumentation and diagnostics:

Beam Position Monitors

The beam orbit monitoring is the most fundamental measurement and the most powerful diagnostics tool in an accelerator. Project X requires a large number (~100) of new beam position monitors (BPM), thus makes it a complex and expensive measurement system. BPM pickups need high quality RF cables to transmit their low-power signals to the read-out hardware outside the accelerator tunnel. This requirment may impact the arrangement or layout of some conventional facilities. It is necessary to locate BPM pickups in cryogenic SCRF sections of the machine, which needs extra care to meet UHV, cryogenic and clean room requirements simultaneously.

Beam Monitoring in the SCRF linac

The beam monitoring within the cryogenic environment is probably limited to beam position detection. As beam profile and other beam monitors with moving parts cannot operate in a cryogenic environment, beam emittance and similar measurement systems would require a "warm" diagnostics section within the SCRF linac.

Beam Profile Monitors

Profile monitors are required in the transfer line for measuring emittance and matching between the linac and transfer line and the Recycler. Options for transverse

profile monitors are the standard multi-wire monitor and the newer laser profile monitor. The choice of technology has not been selected.

Beam Loss Monitors

Typical fast ionization chambers with a large dynamic range will be utilized for most loss measurements. However, there may be instances where measurements of thermal neutrons or machine activation during cooldown periods are desired. The loss monitors will be incorporated in a machine protection system.

Beam Current Monitors

An accurate measure of beam current throughout the linac, transfer line, injection straight is required to determine transport and injection efficiency.

Special Monitors

Several types of special beam monitors and diagnostic tools are required to verify the beam quality and minimize beam losses. These includes the monitoring of the transverse beam halo (OTR screens with micro-mirrors, vibrating wire, laser wire) and the detection of longitudinal tails using optical sampling techniques with mode-locked laser wires. A list of special beam monitors and diagnostic tools needs to be established.

Data Acquisition and Timing

Most beam monitoring systems will use digital signal conditioning and processing methods to extract the wanted beam parameter(s). The generated output data needs to be "time stamped" with respect to the beam event, so beam and other recorded data can be cross-correlated throughout the entire Project X complex. This cross correlation will simplify diagnostics and trouble-shooting on the day-to-day operation.

Internal calibration systems, as well as data acquisition and transport cannot make use of a long pause in the beam pulse (there is none in CW operation). The integration times of some of the measured parameters, e.g. beam intensity, and their time stamping has to be discussed in detail.

Sufficient physical space will be made available to accommodate the required beam detection elements. At some critical, real-estate limited locations, e.g. LEBT, MEBT, injection / extraction, and SRF areas, a compromise has to be worked out, which enables a decent way to sense the beam without compromising its quality in the diagnostic sections.

IV.7 **Controls**

The control system is responsible for control and monitoring of all accelerator equipment, machine configuration, timing and synchronization, diagnostics, data archiving, and machine protection. Its scope covers all hardware and software asociated with interface of equipment to

the control system, the timing and machine protection system, and control and monitoring applications. A single integrated control system should exist for the entire complex based on an evolution of the current Fermilab system augmented to support EPICS based subsystems. The CW nature of the linac would require the machine protection system, and any trajectory stabilization or other fast feedback systems, to operate in a continuous mode.

The scale of the control system is expected to be similar to that of the existing complex but with the Project X linac rather than the Tevatron. The system should support up to 1M device properties. Time stamping must be provided so that all data from the CW linac and the pulsed linac can be properly correlated. The control system should contribute less than 1% to the unavailability of the accelerator complex. The high beam power implies the need for a sophisticated machine protection system to avoid damage to the accelerator due to errant beam pulses. Furthermore, to minimize routine losses and minimize activation of accelerator components a fast feedback system will be required to stabilize beam trajectories.

At the time the Project X linac begins operation, the NOνA Upgrade will have been completed and the Recycler, Main Injector, and NUMI beam line operated for some years in that configuration. These elements will be controlled by an evolution of the current Fermilab Control System. This includes field equipment, the timing system, front-end computers, services, and applications. While some changes will be needed in these accelerator components for Project X, the control system hardware and software represents a large investment that could be difficult to replace by the start of Project X operation.

It is highly desirable to have a single control system operating the entire complex rather than separate systems for the new linac and older parts of the system. There should only be a single copy of core services such as alarms and data archiving. Software applications should be able to access any device in the system. This model simplifies development and operation and reduces long-term maintenance costs of the complex. The Fermilab control system will be updated for the NOνA upgrade and to support the HINS and NML test facilities for Project X. This upgrade will include modernizing the application software environment as well as replacing obsolete hardware. Upgraded timing and machine protection systems will be developed for the Project X linac that will accomodate legacy hardware in the existing parts of the complex. These systems as well as linac control software will be prototyped at HINS and NML.

It is recognized that some equipment will be developed outside of Fermilab by institutions with expertise in the EPICS control system. Also it may be appropriate in some cases to use commercial hardware that comes with EPICS software. It is planned to support integration of EPICS front-ends and some core applications into the Fermilab control system.

The control system will specify standard interfaces between its internal components as well as with technical equipment. This will make integration, testing, and software development easier and more reliable and reduce the long-term maintenance load. Also, standard interfaces allow parts of the system to be more easily upgraded if required for either improved performance or to replace obsolete technologies. Only portions of the system need be changed while the core architecture of the control system remains the same.

IV.8 **LLRF**

The Low Level RF system encompasses the programming and regulation of the cavity field amplitude and phase as required by longitudinal beam dynamics in the machine. It also controls or interfaces to the ancillary equipment that is involved in the generation of RF. Hardware and software modules includes Cavity Field Controllers, PZT Controllers, Master Oscillator, Phase Reference Line, LO distribution, transfer synchronization and the interfaces to interlocks, timing systems and the control system. This section will cover first the 2 GeV CW 325MHz and 1300MHz Linac followed by the 2-8 GeV 53 MHz RCS requirements and system description.

IV.8.1 **LLRF for the CW 3 GeV SRF LINAC**

The proposed high level RF configuration for the CW linac provides a single power amplifier for each of the cavities. While this increases the number of LLRF controllers it does not greatly increase the component count and reduces project risk by following a more traditional control scheme. The design beam current field gradients determine the loaded cavity Qs and the cavity bandwidths. Analysis of the 1mA beam current and cavity gradients show that loaded Qs may be kept down in the low 10^7 range where control of cavity microphonics will not create excessive RF power demands, nor large field disturbances. In addition, CW operation eliminates the dynamic effects of Lorentz force detuning and modulator droop. In many ways the CW linac will operate in a regime similar to the 12GeV upgrade of CEBAF. The largest disturbance to the cavity fields will be the beam structure produced by the beam chopper. The LLRF system will provide the chop pattern and will therefore have the information required for accurate beam loading compensation.

For cost savings and hardware simplicity, the LLRF controllers will be grouped into stations that will cover two cryomodules (nominal 16 cavities) and the associated RF equipment. Fermilab has been extensively involved in SRF LLRF Control Systems for the ILC and the varied ongoing SRF programs on site. Two types of digital controllers have been developed and are in use, each of which could be modified to meet ICD-2 requirements. RF and microwave hardware has also been developed for HINS and ILCTA that directly apply to Project X. Ongoing R&D will determine the details of the beam-based calibration and of the phase reference distribution system.

IV.8.2 **LLRF for the Pulsed Linac**

Talk to Brian Chase!

IV.9 **Safety and radiation shielding**

Operation of accelerators and beam transport lines at the significantly higher beam power envisioned for Project X RDR presents some new challenges. Simple extrapolation of the methods used at Fermilab to design existing, relatively low power accelerators will be not sufficient. Fortunately, techniques developed at megawatt power accelerators such as SNS can be readily applied to Project X. Such techniques are already being applied at Fermilab to enhance operation of existing accelerators and beam transport lines. It will be shown that radiation

protection can be realized for Project X through the straightforward process methods currently in use along with a supplemental machine protection or beam loss management system.

There are two basic requirements for radiation protection to be observed. First are the regulatory requirements from the Code of Federal Regulations, DOE Orders, and the State of Illinois that are enumerated in the Fermilab Radiological Controls Manual (FRCM). These requirements are related to health and safety of workers, the public, and the environment. Second are the practical machine control requirements that are necessary to protect machines from short term and long-term damage due to beam loss. Prevention of excessive losses improves machine reliability, reduces the frequency of breakdowns, and simplifies required maintenance due to the need for less complex radiation protection procedures. While the methods for achieving these radiation protection requirements may be overlapping, the requirements for personnel and environment protection methods tend to be more rigorous and prescriptive than those required for meeting machine protection requirements. Controls designed primarily for machine protection may not be sufficiently rigorous for the regulatory mandated personnel and environmental protection. However, a machine protection system installed throughout the complex will be of utmost importance in order to prevent catastrophic failures. The details for the manner in which such as system is implemented (e.g., a safety system or controls system) will need to be addressed.

An electronic berm system has been considered. The E-berm systems that have been conceptualized to date are capable of detecting a 1 to 2% beam loss. Since many parts of accelerator complex are rated for 2 MW or higher beam power, this means a 20 to 40 KW beam loss could persist without detection by an E-berm system until some permanent damage occurs to otherwise disable the accelerator complex. In order to protect the Project X accelerator complex, a more sensitive and pervasive beam loss monitoring system will be required to be installed in accelerator and beam transport enclosures. A continuous argon-filled heliax cable acting as an ion chamber installed, for example, at the ceiling of accelerator/beam transport line enclosures could be used to not only identify that a loss condition exists but also pinpoint the location of the loss. Such systems have been considered for other high power accelerators.

IV.9.1 **Prompt radiation shielding**

Earth shielding for accelerator/beam transport enclosures can be easily determined for when the expected beam power loss is defined. It is possible to design the shield so that limits for uncontrolled access to berm surfaces could be allowed under conditions of full beam power loss. For example (see Table IV-17), for a 3 GeV, 3 MW beam loss in an enclosure with a distance of 5 feet from an accelerating cavity to tunnel ceiling, the shielding required to limit radiation levels at the surface to 1 mRem/hr is approximately 28.3 feet.

Beam enclosure	Cossairt Criteria	Beam energy	Beam Power	Component to ceiling distance	Required shielding
3 GeV linac	1a	3 GeV	3 MW	5	28.3 feet
Recycler/MI	1a	8 GeV	340 KW	1	27.1 feet

Recycler/MI	1a	120 GeV	2.1 MW	5	27.2 feet

Table IV-17: Shielding requirements for several beam power/enclosure geometries

It is feasible, for example, to build the 3 GeV linac enclosure with a 28.3 foot earth shield. However, if such an accident condition were to occur, catastrophic damage would result to an accelerating structure, beam pipe, or magnet. It will be possible to develop a plausible beam power loss strategy that could be used as a basis for the final shield design for the 3 GeV linac as well as the remainder of the complex.

A machine protection system or beam loss management system which is capable of detecting low power beam loss and interrupting beam operation will be required for a number of purposes, some of which are described further below. Such a system could be used as a basis to establish shielding criteria.

IV.9.2 Collimation systems to control beam losses

Collimation systems are a fundamental requirement for high power accelerators, beam transport lines, and the ion stripping injection region used in Project X. Multiple stage collimation systems are designed and strategically placed to remove beam halo in controlled, shielded locations. With proper optics and orbit control following collimation systems, beam losses in accelerators, in transport lines and at injection/extraction regions become relatively small, permitting high power operation in conjunction with a relatively safe working environment for beam enclosure maintenance related activities. Collimation systems have been incorporated upstream in the MI8 line and in the Main Injector accelerator with the remarkable result that residual radiation levels in the associated accelerator and beam line enclosures have decreased while beam power has increased. Collimation systems have also been used at the SNS with similar result. An H^- stripping foil/collimation system will also be included in the Recycler injection system. Collimation systems must be designed with shielding to allow personnel access for maintenance and to prevent excessive air, ground and surface water activation. While collimation systems are designed to meet machine protection requirements, they also provide intrinsic radiation protection necessary for feasible operation of high power accelerators and beam lines.

IV.9.3 Electronic berm

The existing passive shielding for the Recycler Ring and Main Injector enclosure may not be sufficient for operation at 2 MW (a soil equivalent shielding thickness of 24.5 ft). High intensity losses might be tolerated by devices such as Lambertson magnets at injection or extraction regions that could lead to excessive radiation dose rates on the shielding surface. An electronic berm could be used to compare beam intensity injected into Recycler Ring with that extracted from the Main Injector. A 1 to 2% difference could be detected on a pulse-to-pulse basis which would lead to a beam inhibit. Other controls such as radiation fences, radiation postings, and entry controls may also be a feasible alternative radiation protection option. Finally, a machine protection system could be considered for the Recycler/MI enclosure, which could provide an even more sensitive level of control.

IV.9.4 Accelerator component activation and residual radiation levels in accelerator/beam line enclosures

Residual radiation levels in beam transport lines and accelerators due to operational beam losses must be controlled in order to conduct maintenance activities while keeping personnel radiation exposure as low as reasonably achievable (ALARA). For 2-3 MW beam power, small fractions of a percent loss will result in very high residual radiation levels which would render beam enclosure access difficult and maintenance at loss points extraordinarily difficult. A sensitive machine protection system which inhibits beam operation when significant losses are present will be required to allow access and maintenance activity modes historically enjoyed at Fermilab.

For design purposes, a loss rate of 3 to 10 watts/meter results in a dose rate of about 100 mR/hr at one foot from beam line components such as magnets and accelerating cavities following a 30 day irradiation period and 1 day of cool down. A loss of 0.25 watts/meter results in a dose rate of about 100 mR/hr at one foot from low mass components such as beam pipes for the same irradiation/cooling period. Radiation levels are typically at least a factor of 5 less than these levels. For example, for a typical magnet beam loss location at 2 watts per meter, the fractional beam power loss is 1 ppm. A sensitive machine protection system will be required to quickly identify and suspend operation in the event such losses occur.

IV.9.5 Surface and ground water activation and air activation

IV.9.5.1 3 GeV Linac, Experimental Halls, Pulsed Linac, and Transfer Line to Recycler Enclosures

The site chosen for these enclosures is presently at the center of the Tevatron beam enclosure. In order to evaluate ground water activation, a geological survey (core borings) will be required to understand ground water migration rates at this site since no data presently exists. It would be prudent to begin characterization of the proposed site in order to confirm its suitability. In addition, the results of such characterization will be required in order to proceed with design of collimation system shielding and enclosure elevation determination.

Surface water and air activation must also be characterized. In order to calculate surface water and air activation, it will be necessary to know what type of machine protection system will be employed so that limits for surface water discharge can be understood. That is, the machine protection system will serve to limit the total beam loss that would also determine the level of surface water and air activation. Integration of these activation levels over the projected operating period would yield an estimate of annual surface water and air activity to be released from the facility. This estimate is necessary in order to ensure compliance with regulatory discharge permit limits for surface water and air.

IV.9.5.2 Recycler Ring and Main Injector Enclosures

Surface water, ground water, and air activation have been studied for the existing Recycler/Main Injector rings. Scaling from existing conditions and assuming the use of additional controls (e.g., E-berm or machine protection system) to limit uncontrolled losses in the Recycler and Main Injector machines, the surface water activation, ground water activation and air activation should remain well within acceptable limits. The design for the Recycler/MI

machine protection system will need to be understood in order to actually evaluate air, surface water, and ground water activation.

IV.10 Conventional Facilities

This Chapter outlines the conventional facilities required to house and support the proposed 3-GeV superconducting H^- linac and 8 GeV pulsed linac. Civil construction for the proposed facility includes all below-grade beam-line enclosures. All above-grade buildings, roads, parking, utilities and services to accommodate the equipment for the operation of the linac on the Fermilab site are also included.

Construction of the below-grade linac and beam transport lines as well as the above-grade service buildings are similar to previously utilized and proven construction methods previously executed at Fermilab. Construction of all below-grade enclosures consists of conventional open-cut type construction techniques. The architectural style of the new buildings reflects, and is harmonious with, the existing buildings. Currently, the layout has been optimized for the accelerator requirements. Future layouts will consider existing topography, sustainability, watersheds, vegetation, natural habitat, and wetlands. All the aspects will be thoroughly addressed in the Environmental Assessment for this project.

Site Construction

1. Site work
    a. Site Drainage will be controlled by ditches and culverts, preserving the existing watershed characteristics both during construction and subsequent operation.
    b. Road Construction includes a new temporary construction road providing access to Butterfield Road. This road will provide direct access for construction traffic during construction only – roadway will be restored to original condition upon completion of the project. New Service Road will provide permanent access to all service buildings and utility corridor.
    c. Landscaping includes the restoration of disturbed areas. Construction yards and stockpile areas will be removed after completion of the construction phase of the project. All disturbed areas will be returned to a natural state or landscaped in a similar manner as found at other Fermilab experimental sites. Erosion control will be maintained during all phases of construction.
    d. Wetlands Mitigation includes the avoidance or minimization of adverse impacts to wetlands in the project area. Environmental consultants would delineate wetlands, and a Clean Water Act permit application prepared for submittal to U.S. Army Corps of Engineers for impacts that cannot be completely avoided. Compensatory mitigation would be provided according to terms and conditions of the permit. This may be in the form of purchased wetland bank credits, restoration or enhancement of existing wetlands on site, or creation of new wetland areas. The permit would dictate the amount and type of mitigation, which must be in place prior to the initiation of construction. A

Floodplain/Wetland Assessment pursuant to 10 CFR 1022 would be incorporated into the Environmental Assessment.

2. Utilities

The following utilities are required to support the operation of the facility. The list incorporates current assumptions and will require further refinement as the design process progresses.

a. Electrical Power includes new duct banks and utilization of existing duct banks from two sources including Kautz Road Substation (KRS) and Master Substation (MSS). Separate high-voltage feeders with backup will be provided for conventional, machine and cryogenic power.
b. Communications include new duct banks tied into the existing communication network along Kautz Road.
c. Chilled Water (CHW & CHWR) for machine and building cooling will be supplied via new supply and return lines from the existing Central Utility Building (CUB).
d. Low Conductivity Water (LCW) for machine cooling will be supplied via new supply and make-up water from the existing Main Injector ring LCW system.
e. Industrial Cooling Water (ICW) for fire protection will be supplied via new supply and return lines from the existing D-0 Utility Corridor.
f. Domestic Water Supply (DWS) for potable water and facilities will be supplied via new supply line from the existing D-0 Utility Corridor.
g. Sanitary Sewer (SAN) for facilities will be supplied via new sewer main and lift station from to the existing D-0 Utility Corridor.
h. Natural Gas (NGS) for building heating will be supplied via new supply lines from the existing D-0 Utility Corridor.

3. Facilities Construction

Conventional facilities will be constructed with future upgrade capabilities considered in the initial design phase. Equipment galleries, enclosures and surface buildings will be designed to accommodate future expansion of the technical components of the facility. See Figure IV-24 for a site map and facilities locations. The major elements for the conventional facilities are as follows:

a) Below-Grade Construction
   Item 1 – 3 GeV Continuous Wave (CW) Linac Enclosure
   Item 2 – Experimental Area Switchyard
   Item 3 - Linac Beam Dump Enclosure
b) Above-Grade Construction
   Item 4 - Upstream Service Building
   Item 5 - Linac Gallery
   Item 6 – Typical Linac Service Building
   Item 7 - Cryogenic Service Building
   Item 8 - Center Service Building
c) Below-Grade Construction
   Item 9 – 3 – 8 GeV Pulsed Linac Enclosure

Item 10 – Proton Transport Line Enclosure

d) Above-Grade Construction

Item 11 – Klystron gallery

Item 12 – Linac Service Building

Item 13 – Linac Beam Absorber

Item 14 – Momentum Beam Absorber

Item 15 – Debuncher Service Building

Item 16 – Future Experimental Halls

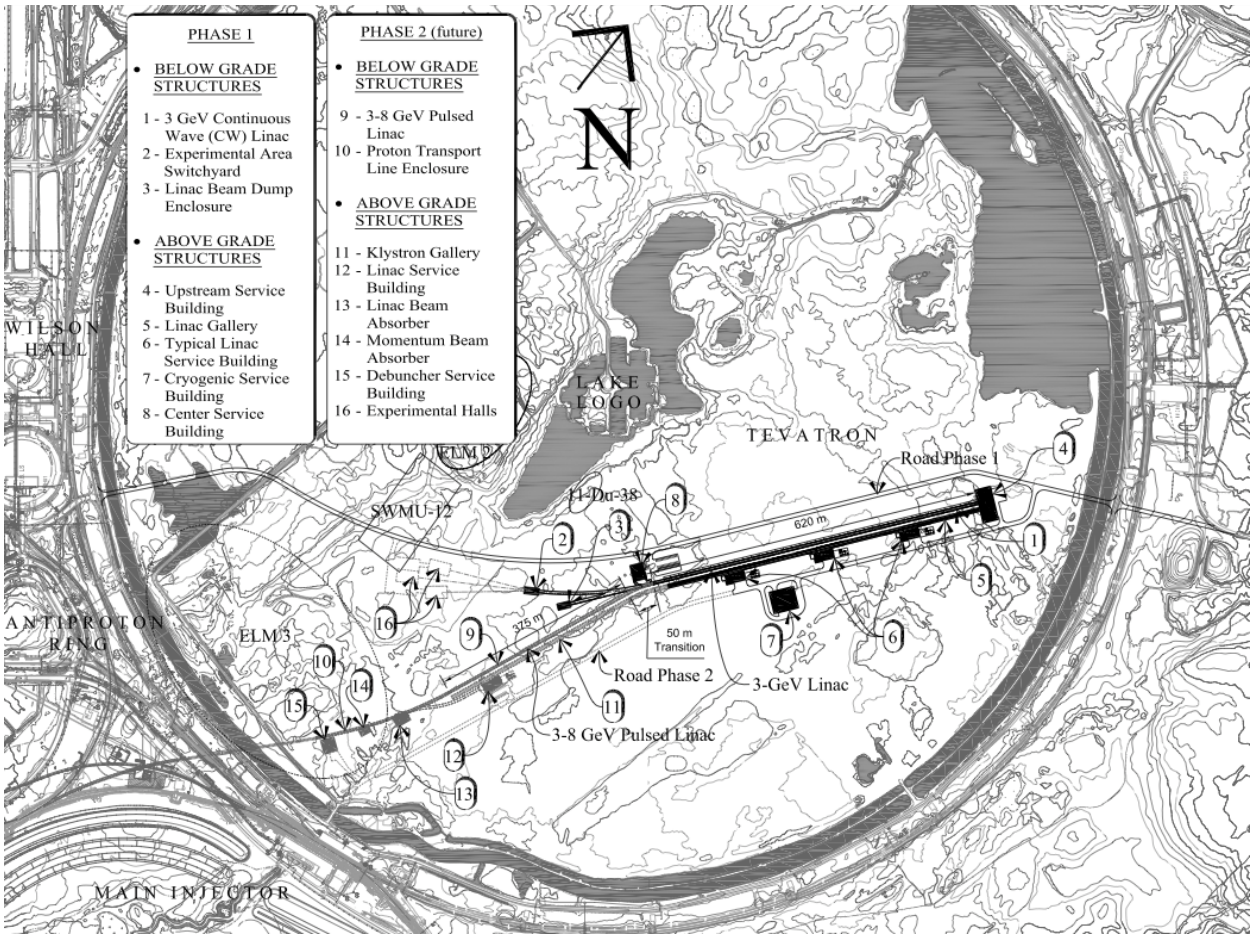

Figure IV-24: Site layout

V Appendix A: Longitudinal Beam Motion in a Flat-Bottom Potential Well

The equation of motion is

$$\ddot{\phi} + \Omega_{s0}{}^2 F(\phi,\phi_0) = 0\,, \quad \Omega_{s0} = \omega_0 \sqrt{\frac{eV_0 q\eta}{2\pi mc^2\gamma\beta^2}}\,, \tag{A.1}$$

where q is the harmonic number, η is the slip factor, ω_0 is the revolution frequency, e, m, γ and β are the particle charge, mass and relativistic factors, V_0 is the voltage of the first harmonic RF system, and ϕ_0 is the accelerating phase of the first harmonic RF system. In a general case of the two harmonic RF system the function $F(\phi,\phi_0)$ can be presented in the following form

$$F(\phi,\phi_0) = \sin\phi - \sin\phi_0 - \mathrm{v}_s \sin(2(\phi-\phi_0)) - \mathrm{v}_c \cos(2(\phi-\phi_0)) + \mathrm{v}_c \quad , \tag{A.2}$$

which was constructed so that it would satisfy $F(\phi_0,\phi_0) = 0$. The flat bottom potential well is determined by requirements of zeroing the first two derivatives:

$$dF(\phi,\phi_0)/d\phi\big|_{\phi=\phi_0} = d^2F(\phi,\phi_0)/d\phi^2\big|_{\phi=\phi_0} = 0 \quad . \tag{A.3}$$

It results in

$$\mathrm{v}_s = \frac{\cos\phi_0}{2}\,, \quad \mathrm{v}_c = \frac{\sin\phi_0}{4} \quad . \tag{A.4}$$

Consequently, the total and accelerating voltages of the second harmonic RF system are:

$$\begin{aligned} V_1 &= V_0\sqrt{\mathrm{v}_s{}^2 + \mathrm{v}_c{}^2} = \frac{V_0}{4}\sqrt{1+3\cos^2\phi_0}\,, \\ V_{a1} &= -V_0\mathrm{v}_c = -\frac{V_0}{4}\sin\phi_0\,. \end{aligned} \tag{A.5}$$

One can see that for the case $\phi_0 = 0$ (no acceleration) $V_1 = V_0 / 2$ and both the first and second harmonic RF systems do not transfer energy to the beam. In the case of beam acceleration the second harmonic decelerates the beam with decelerating voltage equal to ¼ of the voltage of the first harmonic RF system. Thus the one quarter of the power transferred to the beam from the first harmonic RF is transferred back to the second harmonic RF system.

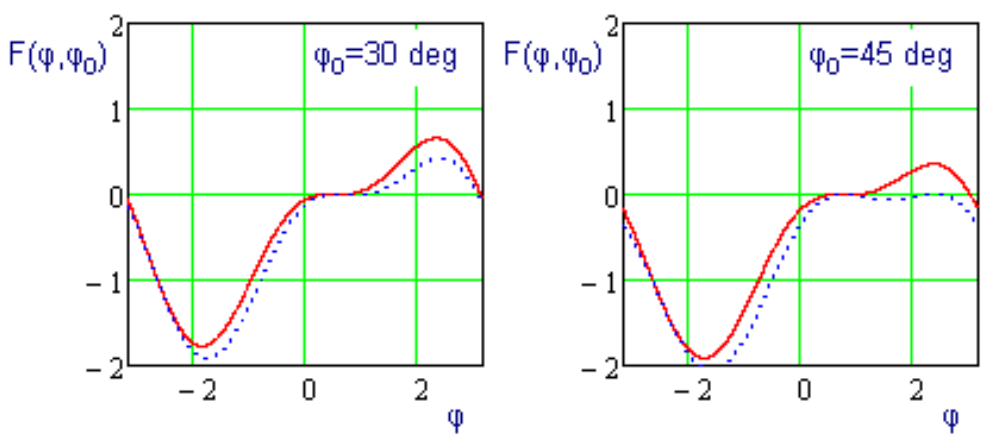

Figure A1.1. Dependence of $F(\phi,\phi_0)$ on ϕ for ϕ_0 = 30 and 45 deg and for the cases of the flat bottom potential well (red solid line) and the case of $\mathrm{v}_c = 0$ (blue dashed line).

To avoid the beam deceleration by the second harmonic RF system, use the requirements of zero derivative (first Eq. (A.3)) and $v_c = 0$. This situation is similar to the flat bottom case that results in $v_s = \cos\phi_0 / 2$. In this case, for small values of accelerating phase, the bottom of the well is still sufficiently flat. In contrast to the flat bottom case, such a scheme makes the bucket of finite size for $\phi_0 < \pi / 4$ only (see Figure A.1.1.)

The total area of the RF bucket is:

$$\varepsilon_L \equiv \oint p(s)ds = \frac{8mcC}{\pi q\beta}\sqrt{\frac{eV_0\gamma\beta^2}{2\pi mc^2 q\eta}}\Phi(\phi_0) \quad . \tag{A.6}$$

The form factors $\Phi(\phi_0)$ were computed by numerical integration for the cases of (1) the single harmonic acceleration, (2) the flat bottom well, and (3) the case of $v_s = \cos\phi_0 / 2$ and $v_c = 0$. Corresponding plots are presented in Figure A1.2. The dependences can be also approximated by the following equations:

$$\Phi(\phi_0) \approx 1.145\frac{1-\sin\phi_0}{\left(1+\frac{1}{2}\sin\phi\right)^2} \quad , \tag{A.7}$$

$$\Phi(\phi_0) \approx 1.145\frac{\left(1-\frac{2}{\pi}\phi_0\right)^{1.8}}{1-\frac{1}{4}\phi_0^{\,6}} \quad , \tag{A.8}$$

$$\Phi(\phi_0) \approx 1.145\left(1-\frac{2}{\pi}\phi_0\right) \quad . \tag{A.9}$$

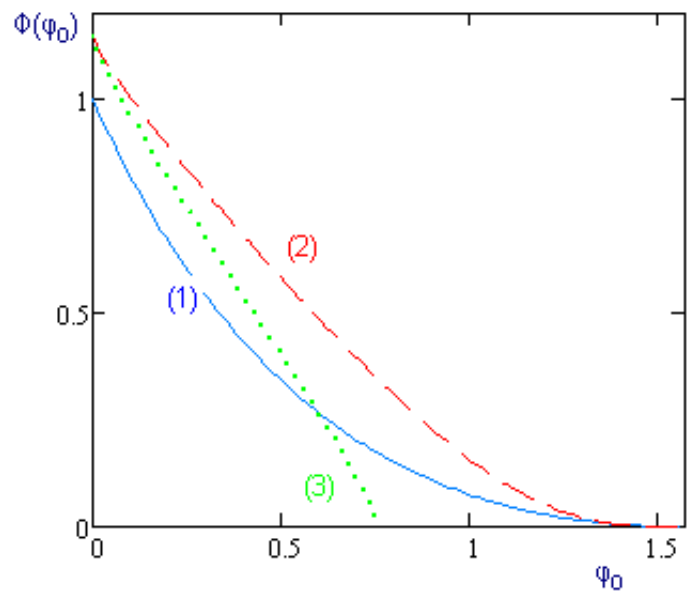

Figure A1.2. The form factors $\Phi(\phi_0)$ for the cases of (1) the single harmonic acceleration, (2) the flat bottom well, and (3) the case of $v_s = \cos\phi_0 / 2$ and $v_c = 0$.